DER MATERIALS QUARTERLY PROGRESS REPORT

For the Period
January 1, 2004 to March 31, 2004

Prepared by:

David P. Stinton, Manager, and
Roxanne A. Raschke
DER Materials Research
Oak Ridge National Laboratory

For:

Department of Energy
Office of Distributed Energy

DER MATERIALS QUARTERLY PROGRESS REPORT

January—March 2004

TABLE OF CONTENTS

Introduction

RECUPERATORS

Recuperator Alloys – Composition Optimization for Corrosion Resistance
B. A. Pint
Oak Ridge National Laboratory, Oak Ridge, Tennessee

Recuperator Materials Testing and Evaluation
E. Lara-Curzio
Oak Ridge National Laboratory, Oak Ridge, Tennessee

Advanced Alloys for High Temperature Recuperators
P. J. Maziasz, B. A. Pint, R. W. Swindeman, K. L. More, and M. L. Santella
Oak Ridge National Laboratory, Oak Ridge, Tennessee

CERAMIC RELIABILITY FOR MICROTURBINE HOT-SECTION COMPONENTS

Reliability Evaluation of Microturbine Components
H-T Lin, M. K. Ferber, and T. P. Kirkland
Oak Ridge National Laboratory, Oak Ridge, Tennessee

Development and Characterization of Advanced Materials for Microturbine Applications
M. K. Ferber and H-T Lin
Oak Ridge National Laboratory, Oak Ridge, Tennessee

Reliability Analysis of Microturbine Components
S. F. Duffy, E. H. Baker and J. L. Palko
Connecticut Reserve Technologies, LLC

NDE Technology Development for Microturbines
W. A. Ellingson, E. R. Koehl, A. Parikh, and J. Stainbrook
Argonne National Laboratory, Argonne, Illinois

CHARACTERIZATION OF ADVANCED CERAMICS FOR INDUSTRIAL GAS TURBINE/MICROTURBINE APPLICATIONS

Oxidation/Corrosion Characterization of Microturbine Materials
K. L. More and P. F. Tortorelli
Oak Ridge National Laboratory, Oak Ridge, Tennessee

Mechanical Characterization of Monolithic Silicon Nitride Si_3N_4
R. R. Wills, S. Hilton, and S. Goodrich
University of Dayton Research Institute, Dayton, Ohio

Microstructural Characterization of CFCCs and Protective Coatings
K. L. More
Oak Ridge National Laboratory, Oak Ridge, Tennessee

DEVELOPMENT OF MONOLITHIC CERAMICS AND HIGH-TEMPERATURE COATINGS

Kennametal's Hot-Section Materials Development
R. Yeckley
Kennametal, Inc., Latrobe, Pennsylvania

Saint-Gobain Hot Section Materials Development
R. H. Licht
Saint-Gobain Ceramics & Plastics, Inc., Northboro, Massachusetts

Environmental Protection Systems for Ceramics in Microturbines and Industrial Gas Turbine Applications, Part A: Conversion Coatings
S. D. Nunn and R. A. Lowden
Oak Ridge National Laboratory, Oak Ridge, Tennessee

Environmental Protection Systems for Ceramics in Microturbines and Industrial Gas Turbine Applications, Part B: Slurry Coatings and Surface Alloying
B. L. Armstrong, K. M. Cooley, M. P. Brady, H-T Lin, and J. A. Haynes
Oak Ridge National Laboratory, Oak Ridge, Tennessee

Polymer Derived EBC for Monolithic Silicon Nitride
R. Raj
University of Colorado at Boulder
Boulder, Colorado

Failure Mechanisms in Coatings
J. P. Singh, Kedar Sharma, and P. S. Shankar
Argonne National Laboratory, Argonne, Illinois

High-Temperature Diffusion Barriers for Ni-Base Superalloys
B. A. Pint, J. A. Haynes, K. L. More, and I. G. Wright
Oak Ridge National Laboratory, Oak Ridge, Tennessee

POWER ELECTRONICS

High Temperature Heat Exchanger
E. Lara-Curzio
Oak Ridge National Laboratory, Oak Ridge, Tennessee

Heat Exchange Concepts Utilizing Porous Carbon Foam
B. E. Thompson and A. G. Straatman
University of Western Ontario, London, Ontario, Canada

MATERIALS FOR ADVANCED RECIPROCATING ENGINES

Spark Plug Erosion and Failure

M. P. Brady, H. T. Lin, J. H. Whealton, R. K. Richards, and J. B. Andriulli
Oak Ridge National Laboratory, Oak Ridge, Tennessee

Advanced Materials for Exhaust Components of Reciprocating Engines
P. J. Maziasz
Oak Ridge National Laboratory, Oak Ridge, Tennessee

Development of Catalytically Selective Electrodes for NOx and Ammonia Sensors
T. R. Armstrong
Oak Ridge National Laboratory, Oak Ridge, Tennessee

Recuperator Alloys – Composition Optimization for Corrosion Resistance

B. A. Pint
Metals and Ceramics Division
Oak Ridge National Laboratory
Oak Ridge, TN 37831-6156
Phone: (865) 576-2897, E-mail: pintba@ornl.gov

Objective

In order to provide a clear, fundamental understanding of alloy composition effects on corrosion resistance of stainless steel components used in recuperators, the oxidation behavior of model alloys is being studied. The first phase of this study narrowed the range of Cr and Ni contents required to minimize the accelerated corrosion attack caused by water vapor at 650°-800°C. Other factors that continue to be investigated include the effects of temperature, alloy grain size, phase composition and minor alloy additions. These composition and microstructure effects also will provide data for life-prediction models and may suggest a mechanistic explanation for the effect of water vapor on the oxidation of steels. This information will be used to select cost-effective alloys for higher temperature recuperators.

Highlights

The oxidation behavior of commercial alloy foils and model alloys are being evaluated in order to better understand the role of alloy composition on the accelerated attack (AA) observed in exhaust gas at 650°-700°C. Long-term testing to 10,000h has been performed on a variety of commercial and experimental foil specimens in order to study their behavior. However, the mass gain data obtained from these specimens does not reflect the extent of reaction due to the combination of mass gain from oxidation and mass loss from evaporation

Technical Progress

Experimental Procedure

As outlined in previous reports, foil of commercial alloys was obtained for testing or rolled from thicker product at ORNL. Foil specimens (≈12mm x 17mm x0.1mm) were tested in the as-rolled condition without additional surface preparation. The oxidation tests were done in air + 10 vol.% water vapor with 100h cycles at 650°, 700°·or 800°C. After oxidation, selected specimens were Cu-plated, sectioned and polished to examine the oxide scale.

Results of oxidation testing

Testing at 650°C to 10,000h has been completed on a number of foil materials, Figure 1. Commercial type 347 foil showed AA between 1,000 and 2,000h under these conditions. Four modifications of type 347 foil also were tested and showed superior performance. The third modification began to show AA at 8,000h but the other three compositions did not show AA after 10,000h. Higher alloyed commercial alloys also were tested, Figure 1. These alloys showed low mass gains or mass losses likely due to volatilization of $CrO_2(OH)_2$. However, the specimen of Fe-20Cr-25Ni+Nb (rolled from NF709 or 20/25Nb) showed increased mass gain during the last 2,000h of testing. The specimen of

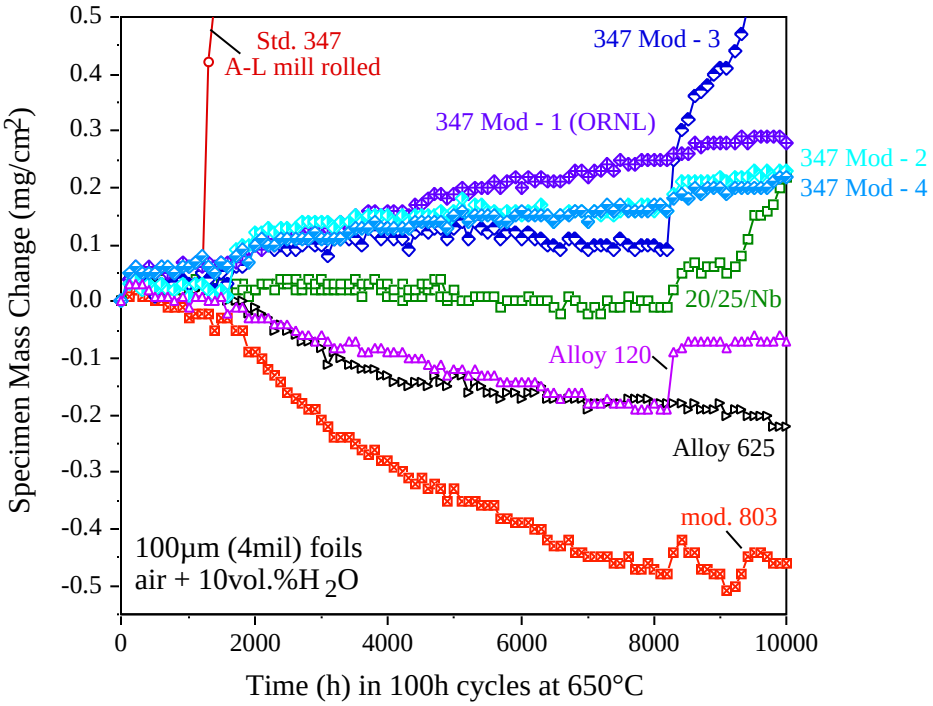

Figure 1. Specimen mass gains for various foil (100µm thick) materials during 100h cycles in humid air at 650°C.

alloy 120 (Fe-25Cr-35Ni) also showed an increase at one point but did not continue to gain afterwards. Specimens of alloy 625 and a modified 803 composition also showed fairly continuous mass losses during the test.

Figure 2 shows specimen mass gain results for foils tested at 700°C for up to 10,000h. Low mass gains and/or mass losses reflect a slow oxidation rate and some evaporation. An increase was noted for 20/25/Nb foil after ≈8,500h. Similar mass change results were found for mill-rolled and ORNL-rolled alloy 120 foils. After a significant incubation period (≈7,500h), a mill-rolled foil specimen of type 347 foil showed AA. The incubation time before AA was much longer than at 650°C. The longer incubation period may be related to the faster scale growth rate at 700°C. A longer period of time may be needed to start AA when a thicker surface oxide forms. Also shown in Figure 2 are results for two specimens of a ORNL-rolled Fe-20Cr-20Ni-4Mn foil. This composition is the first attempt to develop a low-cost creep- and corrosion resistant stainless steel. The higher mass gain for this foil compared to some of the other compositions is not attributed to AA but instead to its higher Mn content (compared to 1-2% in the other alloys). The high Mn content leads to excessive incorporation of Mn in the scale and a faster oxidation rate. As mentioned in prior reports, Mn can be beneficial in preventing AA but in a thin foil, increasing the metal consumption rate can be detrimental to its lifetime.

Figure 3 shows the results for foils tested at 800°C in air + 10%H_2O. Only the foil specimen of alloy 120 was run to 10,000h. This specimen showed a larger mass gain for the last 2,000h of the test. Whether this indicates the onset of AA will be determined by further characterization of the oxide scale and Cr content of this specimen. However, it was a relatively modest increase in mass compared to some of the other specimens. The foil specimen of alloy 625 was stopped at 6,000h for

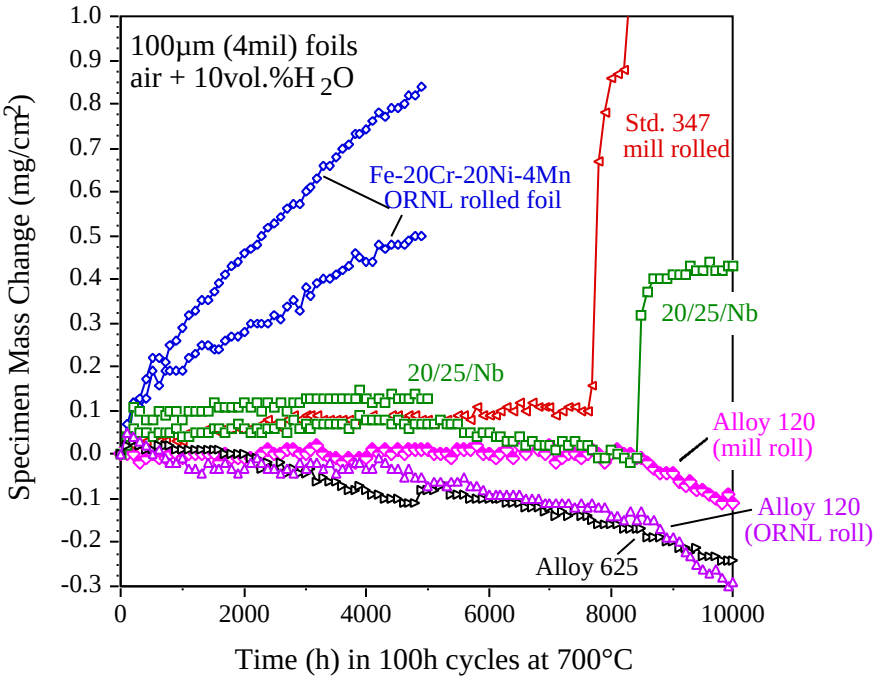

Figure 2. Specimen mass gains for various foil (100µm thick) materials during 100h cycles in humid air at 700°C.

characterization and did not show any signs of AA. The specimens of Fe-20Cr-25Ni+Nb were stopped at 5,000, 6,000 and 7,000h. For this composition, the latter two specimens showed signs of

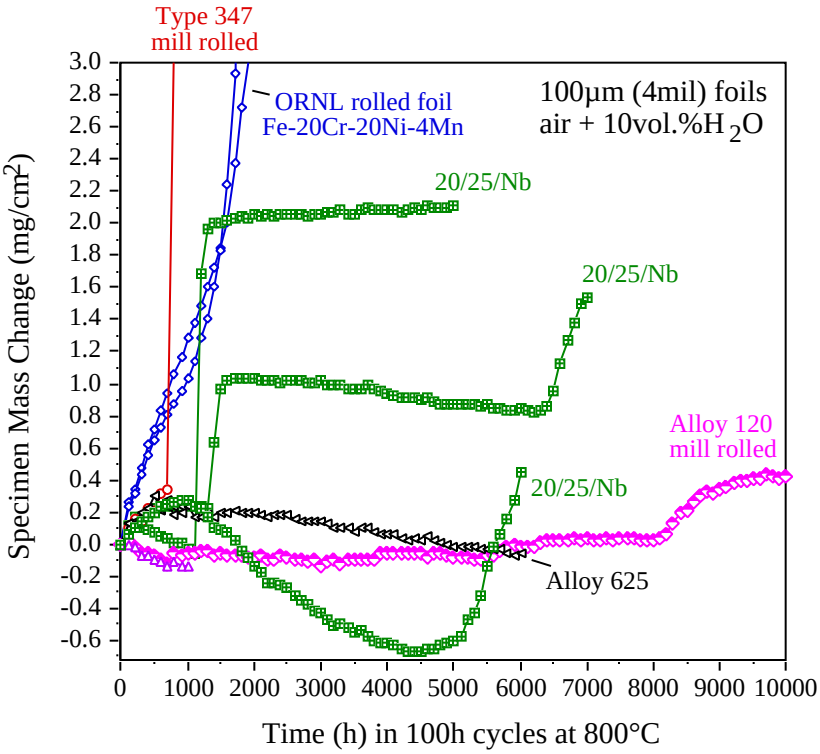

Figure 3. Specimen mass gains for various foil (100µm thick) materials during 100h cycles in humid air at 800°C.

AA when removed from the test due to their rapid mass gains. Foil specimens of Fe-20Cr-20Ni-4Mn were stopped after 2,000h due to excessive mass gain. These specimens outlasted commercial 347 foil which showed AA after less than 1,000h at 800°C, Figure 3. In general, the failure times for the various foils show the benefit of increasing Cr and Ni contents. The Fe-20Cr-25Ni+Nb foil specimens showed AA between 5,000 and 7,000h while alloy 120 only showed a modest increase in mass after 8,000h. The performance of the Fe-20Cr-20Ni-4Mn likely reflects the previously mentioned problem with the high Mn content. New laboratory scale heats with compositions based on Fe-20Cr-20Ni are being fabricated in an attempt to achieve better corrosion resistance.

Collecting data for 10,000h (100, 100h cycles) required more than 2 years. One goal of this program is to develop predictive models requiring less experimental work. However, one important issue that has become clear from these results is that specimen mass gain data is not providing sufficient information for such a model. Figures 4 and 5 illustrate the problem. Figure 4 shows the specimen mass gain data for two foil specimens tested at 800°C in humid air and Figure 5 shows the cross-sections of the oxide scales formed on these specimens. The scale thicknesses observed should have produced a mass gain of ≈0.7mg/cm^2 (marked in Figure 4) assuming that the scale is mostly Cr_2O_3. For alloy 625, a mass loss was measured, while for the Fe-20Cr-25Ni+Nb foil specimen a higher mass gain was observed. Most of the large mass gain occurred during 1 or 2 cycles and is likely due to some AA at the specimen edge or imperfections in the laboratory made foil. In neither case did the mass gain give an accurate reflection of the corrosion product. In general, this is because the specimen mass change is the net result of several general phenomena:

$$\Delta M_{specimen} = \Delta M_{oxide\ growth} - \Delta M_{evaporation} - \Delta M_{spallation} \qquad (1)$$

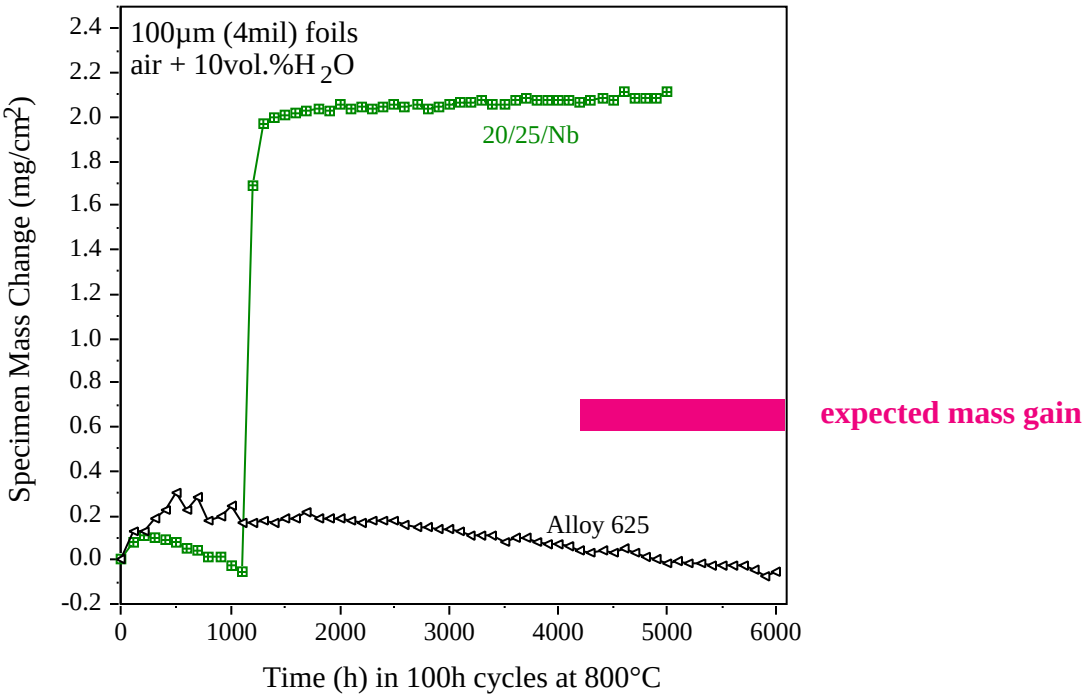

Figure 4. Specimen mass gains for two 100µm thick foil specimens during 100h cycles in humid air at 800°C compared to the predicted mass gain based on the scale thickness after the test.

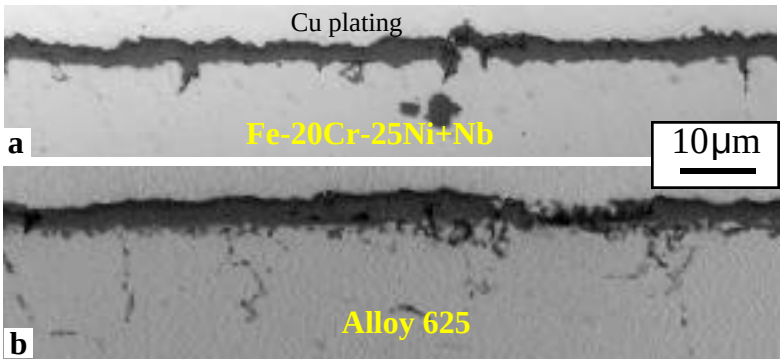

Figure 5. Light microscopy of scale cross-section for the foils in Figure 4 exposed in humid air at 800°C. (a) Fe-20Cr-25Ni+Nb after 5,000h and (b) alloy 625 after 6,000h.

No spallation has been observed from these specimens. Thus, in the case of the alloy 625 foil specimen in Figure 4 and 5b, the mass loss observed is attributed to volatilization of $CrO_2(OH)_2$.and significant Cr depletion in this specimen has been reported previously. A similar explanation would explain the low mass gains or mass losses for the specimens of alloy 625, alloy 120 and Fe-20Cr-25Ni+Nb at lower test temperatures, Figures 1 and 2. Therefore, rather than a model based on mass change, a model is being developed based on Cr consumption which should produce a more accurate lifetime prediction. For new or untested alloys, testing a series of foil specimens for different times over several thousand hours should provide a Cr consumption rate that could then be used to predict long-term behavior. These 10,000h specimens will provide important Cr consumption results for developing this model and the Cr depletion profiles for these specimens will be reported in subsequent reports.

Status of Milestones

Fabricate foil material of two most promising compositions for creep and corrosion testing that simulate conditions in a recuperator.
(March 2004) COMPLETED - fabricated two batches of foil for testing.

Industry Interactions

Discussed oxidation data with W. Matthews of Capstone in January 2004

Discussed materials selection issues with Williams International in March 2004.

Discussed results of NACE conference paper with several members of the audience, March 2004.

Problems Encountered

None.

Publications/Presentations

Presented paper “The Long-Term Performance of Model Austenitic Alloys in Humid Air,” (NACE Paper 04-530, Houston, TX) presented at NACE Corrosion 2004, New Orleans, La, March 2004.

Recuperator Materials Testing and Evaluation

Edgar Lara-Curzio, Rosa Trejo and K. L. More
Metals and Ceramics Division
Oak Ridge National Laboratory
P.O. Box 2008, Oak Ridge, TN 37831-6069
Phone: (865) 574-1749, E-mail: laracurzioe@ornl.gov

Objective

The objective of this sub-task is to screen and evaluate candidate materials for the next generation of advanced microturbine recuperators. To attain this objective, a commercially available microturbine was acquired and in coordination and collaboration with its manufacturer, it was modified to operate at recuperator inlet temperatures as high as 843°C. The durability of candidate recuperator materials will be determined by placing test specimens at a location upstream of the recuperator, followed by determination of the evolution of the material's physical and mechanical properties as a function of time of exposure. During exposure tests inside the microturbine, it will be possible to subject test specimens to various levels of mechanical stress by using a specially designed sample holder and pressurized air. The selection of materials to be evaluated in the modified microturbine will be made in coordination and collaboration with other tasks of this program and with manufacturers of microturbines and recuperators.

Highlights

A 500-hr test campaign was completed to evaluate Haynes 120® alloy.

Technical progress

In this document we report the results from the evaluation and characterization of foils of Haynes 120® alloy after a 500-hr test campaign in ORNL's recuperator testing facility. This alloy has been considered a potential candidate material for the manufacture of advanced microturbine recuperators[1] because it "combines excellent high-temperature strength and oxidation resistance[2]". Tables I and II list the composition and tensile properties of Haynes 120®.

Table I. Composition of Haynes 120® alloy (wt. %)[2]

Element	Concentration	Element	Concentration	Element	Concentration
Ni	37	Mo	2.5 (max)	Al	0.1
Cr	25	Mn	0.7	C	0.05
W	2.5 (max)	Si	0.6	Cb	0.7
Co	3 (max)	Fe	33 (balance)	B	0.004
N	0.2				

[1] Omatete, O., O., Maziasz, P. J., Pint, A. B., and Stinton, D. P., "Assessment of Recuperator Materials for Microturbines," ORNL TM-2000/304
[2] Haynes International, Kokomo, IN 46904

Table II. Tensile Properties of Haynes 120® alloy[2]

Yield strength (MPa)	Tensile strength (MPa)	Elongation (%)
375	735	50

Evaluation of baseline properties of Haynes 120® alloy foils.
The foil materials used in this investigation were supplied by Capstone Turbine Corporation in the form of 20.3-cm wide rolls with thicknesses of 0.089 mm.

Miniature dog-bone shaped test specimens, with their principal axis aligned parallel to the rolling direction, were obtained from the foil rolls by electric discharge machining (Figure 1). The tensile behavior of the miniature test specimens was determined at ambient conditions using a procedure that has been described in detail elsewhere[3]. The tensile tests were carried out at a constant crosshead displacement rate and both the load and crosshead displacement were recorded during the test. Because of the small dimensions of the test specimens it was not possible to measure directly the tensile strain of the test specimens, but values of strain were determined from the crosshead displacement data after applying a correction for the compliance of the load train.

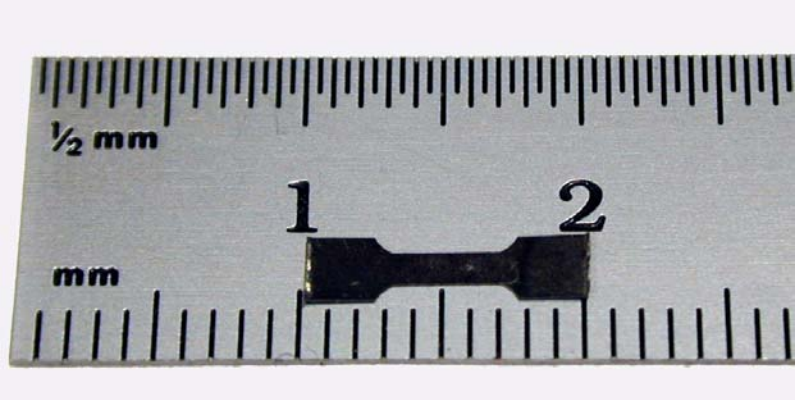

Figure 1. Miniature test specimen used for determination of tensile properties of Haynes 120® alloy.

Figure 2 shows stress versus strain curves obtained from the tensile evaluation of miniature test specimens. The tensile stress-strain curves are characterized by a linear region associated with elastic deformation, a well-defined transition to plastic deformation at a high yield stress and failure strains near 40%.

Table III summarizes the results of these tests and lists values for the 0.2% yield strength, ultimate tensile strength and strain at failure, which are consistent with those reported by the alloy manufacturer[2] (See Table II).

[3] E. Lara-Curzio, "Recuperator Materials Testing and Evaluation" in DER Materials Program Quarterly Report, June-September, 2003

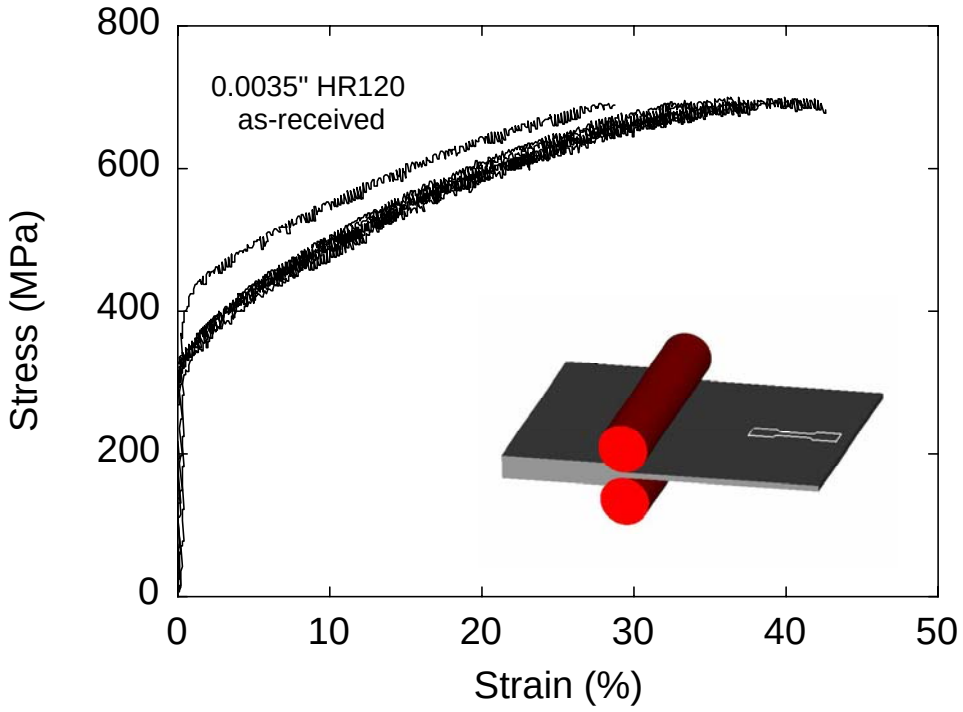

Figure 2. Stress-strain curves obtained from the tensile evaluation of miniature test specimens of 0.089-mm thick specimens of Haynes 120® alloy with their main axis parallel to the rolling direction.

Table III. Summary of tensile results for as-processed 0.089-mm thick foils of Haynes HR-120® alloy.

Haynes 120® alloy	0.2% Yield Strength (MPa)	Ultimate Tensile Strength (MPa)	Failure Strain (%)
|| to rolling direction	373 ± 31	697 ± 4	37 ± 5

Evaluation of Haynes 120® alloy foils in ORNL's microturbine test facility.
Foil strips 75-mm long and 14-mm wide were e-beam-welded onto a Haynes 230® alloy sample holder as described in detail elsewhere[3]. The diameter of the sample holder onto which the foils were welded was 23.1 mm.

The sample holder was internally pressurized using plant air at 60 psi and subjected to a 500-hour exposure in ORNL's modified microturbine operating with the settings listed in Table IV. The temperature of each foil was monitored during the test using type-K thermocouples that had been placed inside the sample holder.

Table IV. Microturbine settings for 500-hr test.

Engine Speed	45,000 RPM
Turbine Exit Temperature	800°C
Fuel	natural gas

In addition to the magnitude of air pressure inside the sample holder, the temperature of the four foils and the turbine exit temperature were recorded during the test, as illustrated by the temperature history in Figure 3. The maximum and minimum temperatures were 745°C and 632°C, respectively.

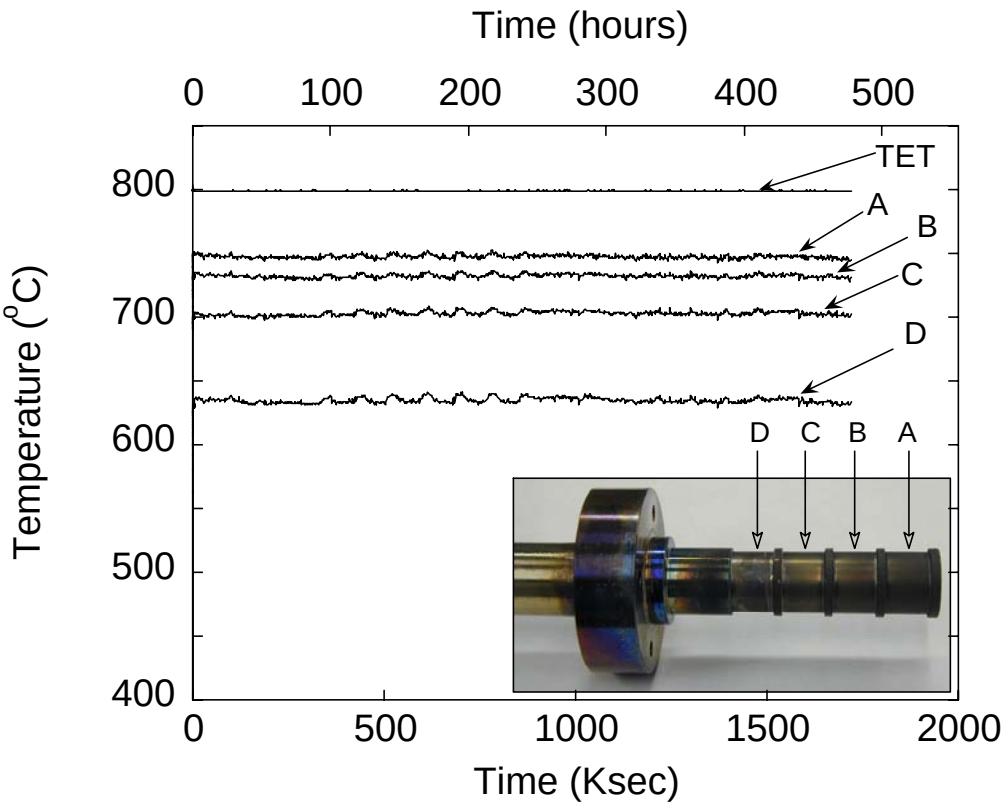

Figure 3. Temperature history for 500-hr test to evaluate the behavior of 0.089-mm thick foils of Haynes 120® alloy.

Post-test analysis

Figure 4 shows the sample holder and Haynes 120® foils at the end of the 500-hr exposure. The foils were removed from the sample holder using a lathe and a diamond tool. About 14 miniature test specimens were obtained from each foil by electric discharge machining for subsequent tensile evaluation and microstructural characterization.

Figure 4. Photographs of sample holder with 0.089-mm thick Haynes 120® foils after 500-hr test at TET=800°C and internal pressure of 60 psi.

Figures 5-8 present the stress versus strain curves obtained from the tensile evaluation of the miniature test specimens. It was found that the ultimate tensile strength and ductility of Haynes 120® alloy decreased by 15% and 50%, respectively, after 500 hours exposure at 745°C. At the lowest exposure temperature of 632°C the ultimate tensile strength and ductility decreased by 10% and 23%, respectively. Table V summarizes the tensile results.

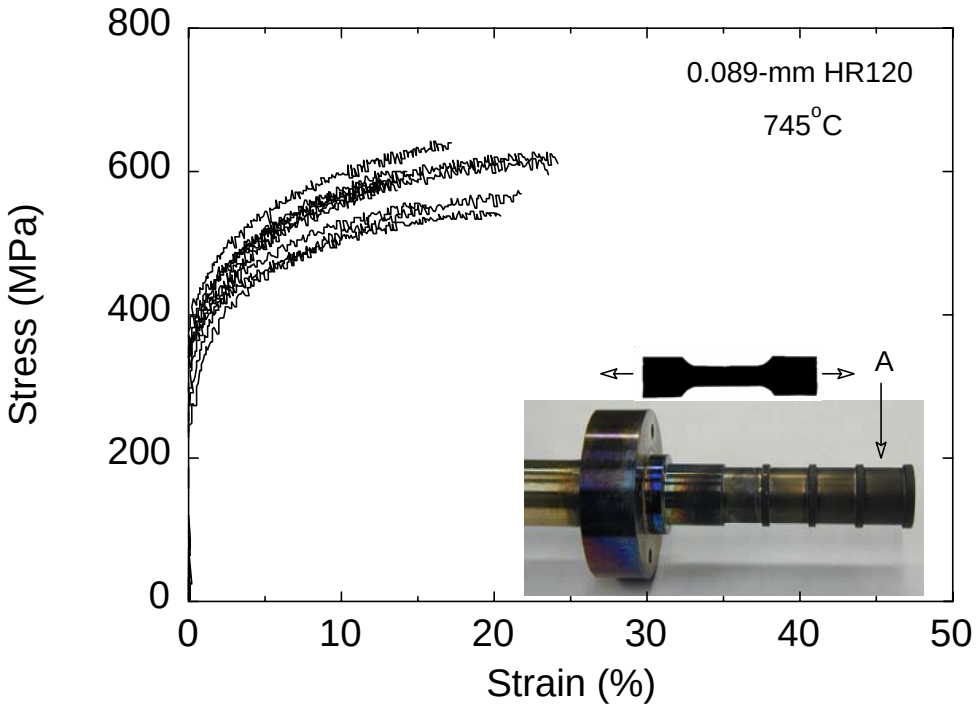

Figure 5. Stress versus strain curves obtained from the tensile evaluation of miniature test specimens obtained from 0.089-mm thick Haynes 120® alloy exposed at 752°C for 500 hours.

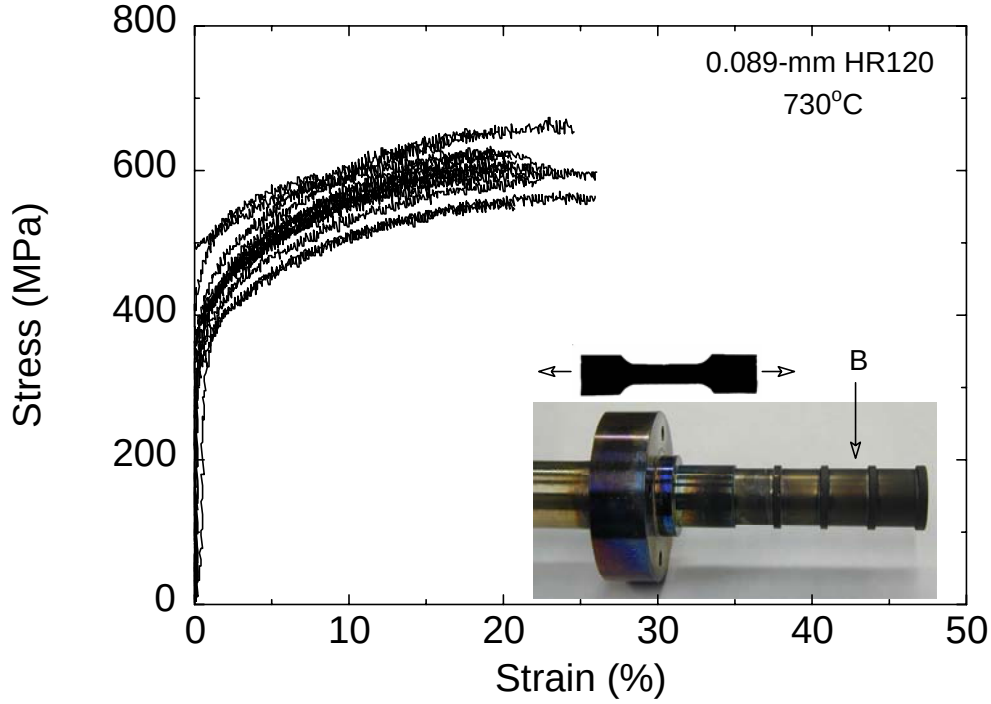

Figure 6. Stress versus strain curves obtained from the tensile evaluation of miniature test specimens obtained from 0.089-mm thick Haynes 120® alloy exposed at 736°C for 500 hours.

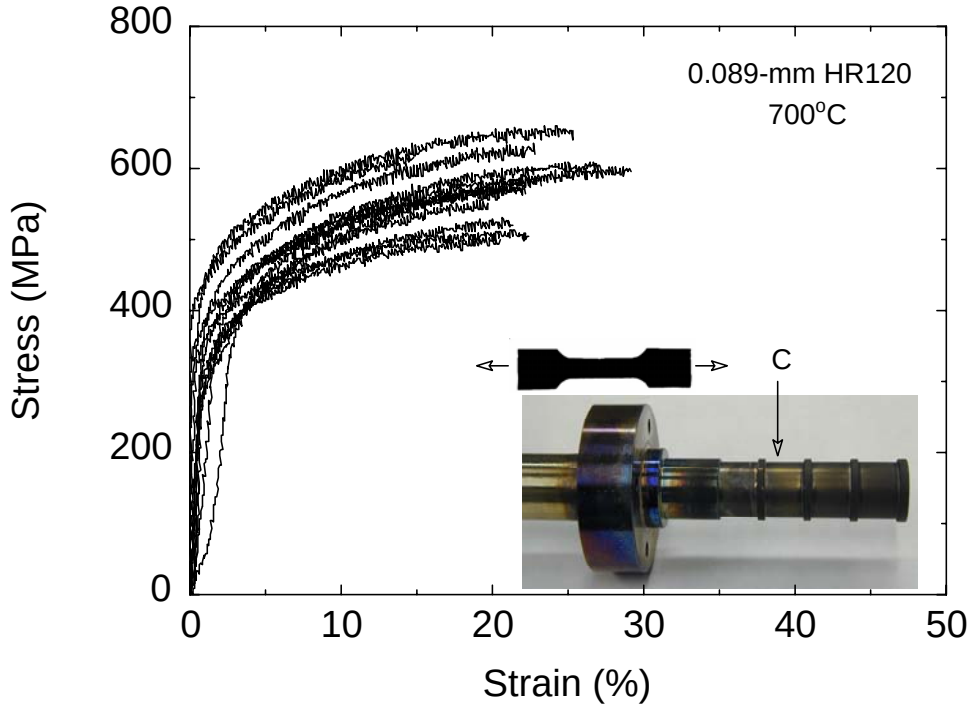

Figure 7. Stress versus strain curves obtained from the tensile evaluation of miniature test specimens obtained from 0.089-mm thick Haynes 120® alloy exposed at 700°C for 500 hours.

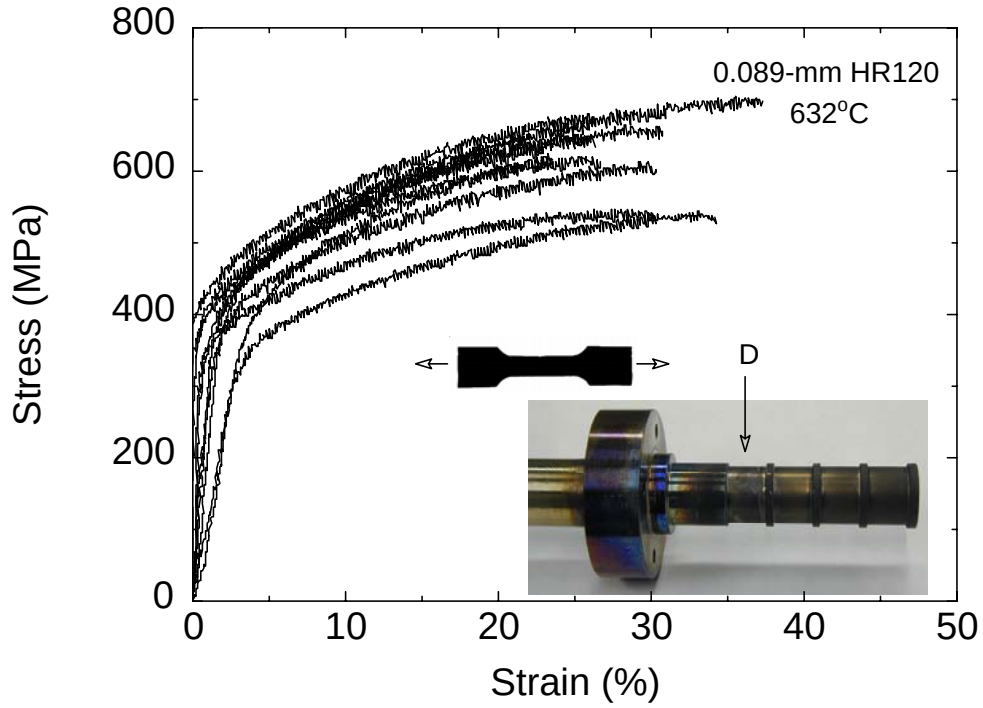

Figure 8. Stress versus strain curves obtained from the tensile evaluation of miniature test specimens obtained from 0.089-mm thick Haynes 120® alloy exposed at 679°C for 500 hours.

Table V. Summary of tensile results for Haynes 120® alloy.

Foil	T (°C)	0.2% σ_y (MPa)	UTS (MPa)	Failure strain (%)
1	745	388 ± 35	594 ± 32	18.0 ± 4.4
2	730	421 ± 37	615 ± 30	21.0 ± 4.4
3	700	408 ± 39	582 ± 48	23.0 ± 4.7
4	632	407 ± 27	631 ± 53	29.0 ± 4.7

Figure 9 shows the normalized ultimate tensile strength of HR120® alloy foils as a function of exposure temperature. The symbols represent the average value of 12-14 tests, while the error bars correspond to one standard deviation with respect to the mean. Also included is a correlation of the form:

HR120®
$$\frac{\sigma}{\sigma_o} = \left(1 - \frac{T}{1000}\right)^6 \qquad (1)$$

where T is the exposure temperature in degrees Centigrade and σ_o is the tensile strength at 20°C. Figure 10 compares these results with those previously published for 347 stainless steel[3] and HR230®[4].

[4] E. Lara-Curzio, "Recuperator Materials Testing and Evaluation" in DER Materials Program Quarterly Report, October-December, 2003

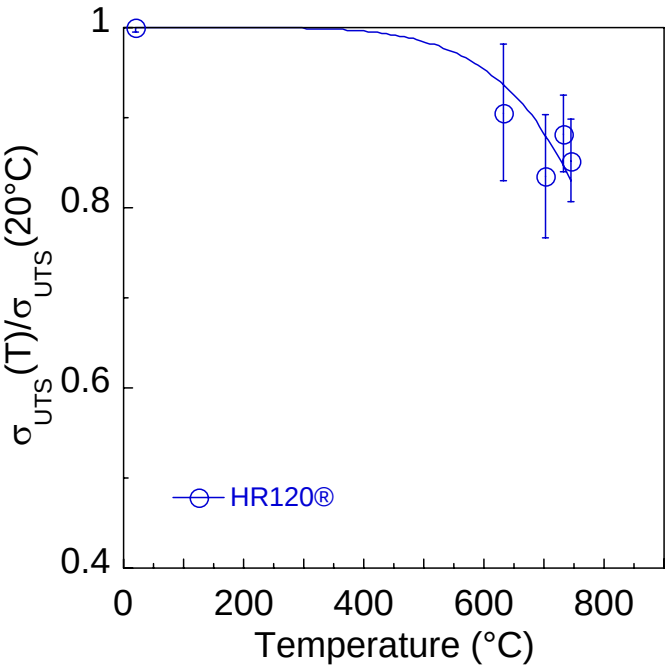

Figure 9. Normalized ultimate tensile strength of HR-122® alloy foils as a function of 500-hr exposure temperature. Error bars correspond to one standard deviation about the mean value.

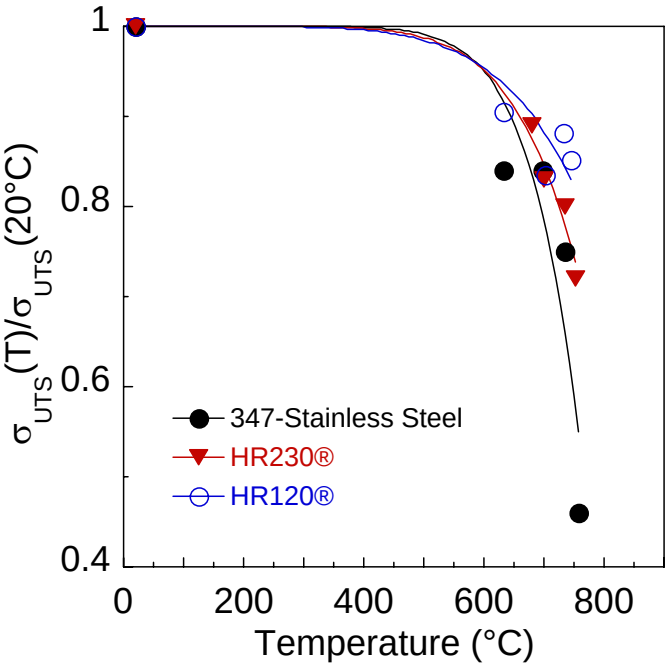

Figure 10. Comparison of ultimate tensile strength of 347-stainless steel, HR-230® alloy and HR-120® alloy foils as a function of temperature for 500-hr exposure.

It was found that among the three alloys, HR120® exhibits the best resistance to exposure to microturbine exhaust gases, followed by HR230® and 347 stainless steel. For the latter two materials, the following correlations were found to provide a good description of the dependence of their ultimate tensile strength with exposure temperature.

HR230®

$$\frac{\sigma}{\sigma_o} = \left(1 - \frac{T}{900}\right)^{7.5} \tag{2}$$

347 stainless steel

$$\frac{\sigma}{\sigma_o} = \left(1 - \frac{T}{825}\right)^{9.4} \tag{3}$$

While there are no fundamental basis behind the form of these correlations, it is interesting to observe that larger "normalizing temperature" and smaller exponent are associated with increasing resistance to exposure to microturbine exhaust gases.

Figure 11 presents scanning electron micrographs of cross-sections obtained from HR-120®foils after 500-hr microturbine exposure. It was found that only a very thin multilayered oxide scale had formed and that it was thicker on the surface exposed to the exhaust gases. A chemical analysis (Figure 12) revealed that the grain boundaries closest to the surface exposed to the exhaust gases had been depleted of chromium but that they were rich in nickel. The depletion of chromium from grain boundaries close to the metal-oxide interface has been found to be a common feature in all three materials examined to date. In the case of HR120® alloy foils, the oxide scale possesses a multilayered structure consisting of mixed oxides of silicon, chromium and iron.

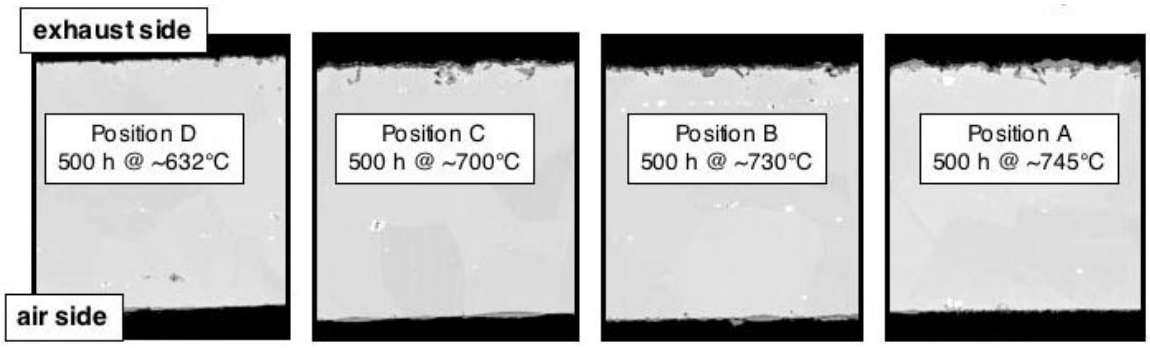

Figure 11. Scanning electron micrograph of cross-section obtained from 0.089-mm thick Haynes 120® alloy foil after 500-hr exposure at 745°C. The lower surface in the micrograph had been exposed to the microturbine exhaust gases.

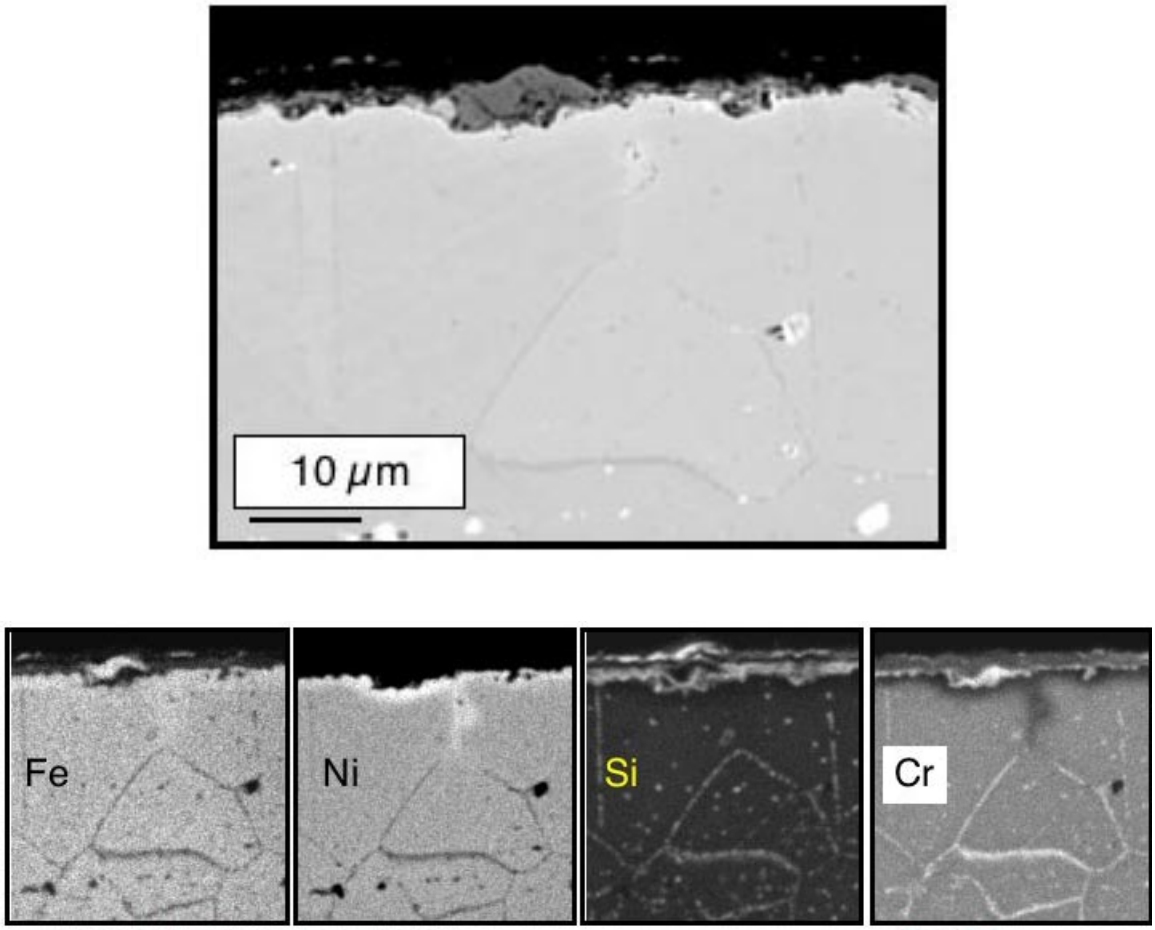

Figure 12. Scanning electron micrograph of cross-sectional area of 0.089-mm thick Haynes 120® alloy foil that had been exposed for 500 hours at 745°C. The upper surface in the micrograph had been exposed to the microturbine exhaust gases. Atomic composition maps of the area in the inset are included.

Analysis of the fracture surfaces of miniature tensile test specimens obtained from foils that had been exposed to the highest temperature (745°C) for 500 hours (Figure 13) revealed intergranular mode of failure. Dimples, which are associated with ductility and plastic deformation and were prevalent on the fracture surface of test specimens of 347 stainless steel and HR230® alloy, were not evident on the fracture surfaces of test specimens of HR120®. However, there was evidence of the existence of sub-micron size particles rich in Fe, Cr and Ni on the fracture surfaces.

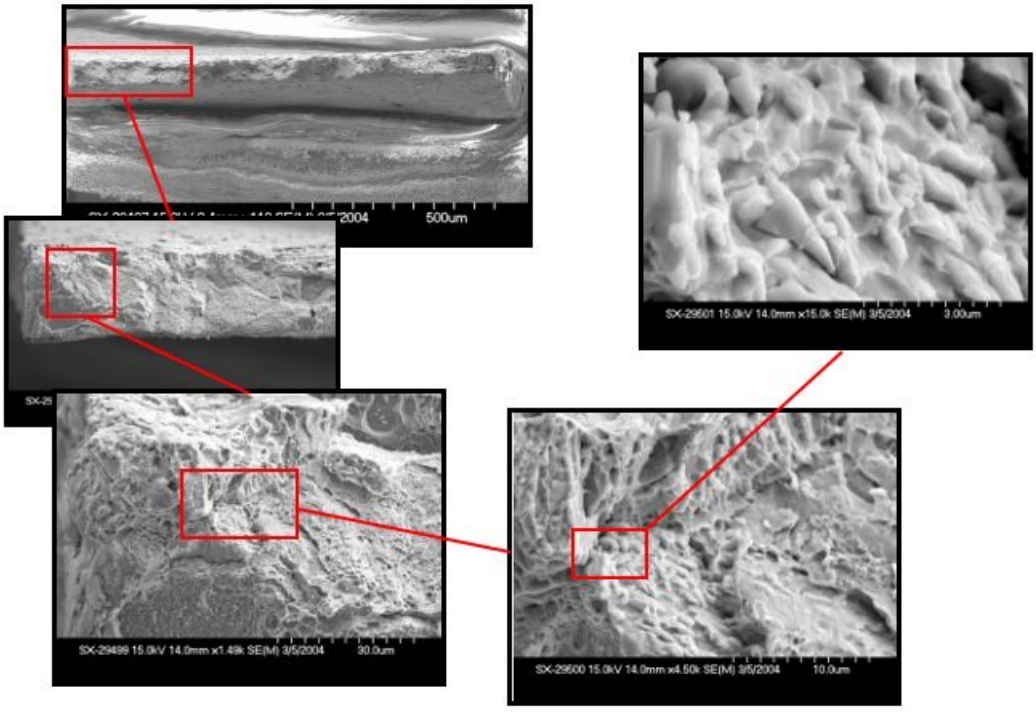

Figure 13. Fracture surface of 0.089-mm thick miniature tensile specimen of HR120® alloy obtained from foil exposed at 745°C for 500 hours. Fracture appears to be intergranular with particulates rich in Cr, Ni and Fe.

Status of Milestones

On schedule

Industry Interactions

Capstone Turbine Corporation provided the foils used in this investigation.

Problems encountered

The Power Distribution Module of the Engine Control Module failed and had to be replaced.

Publications/Presentations

None

Advanced Alloys for High-Temperature Recuperators

P. J. Maziasz, B. A. Pint, K. L. More,
J. P. Shingledecker, and N. D. Evans
Metals and Ceramics Division
Oak Ridge National Laboratory
P.O. Box 2008, Oak Ridge, TN 37831-6115
Phone: (865) 574-5082, E-mail: maziaszpj@ornl.gov

Objective

The main objective of this program is to work with commercial materials suppliers (foil and thin sheet) and recuperator manufacturers to enable manufacture and evaluation of upgraded recuperators from cost effective alloys with improved performance and temperature capability. The near term goal is better performance to or above 704°C (1300°F), and the longer-term goal is reliable performance at 760°C (1400°F) and higher.

Highlights

Materials for use to about 704°C (1300°F)

While severe moisture-enhanced oxidation occurs in standard 347 steel after only 1000-1500h at 650-700°C, new ORNL modified 347 steels with added Mn and N, and the more oxidation-resistant commercial alloys like HR120, NF709 and alloy 625, all show much better resistance to moisture enhanced oxidation after similar testing. A new joint project between ORNL and Allegheny-Ludlum (AL) was initiated this quarter to produce a range of commercial foils and sheet for recuperator manufacturing of their new AL 20-25+Nb stainless alloy with a composition of Fe-20%CR-25%Ni+Nb.

Materials for use to 760°C (1400°F) or higher

Foils of commercial alloys (0.003-0.005 in.) HR120, NF709 and alloy 625 all show good creep rupture resistance at 750°C and 100 MPa. Commercial recuperator sheet (0.010 in.) of alloy 625 was obtained from Ingersoll Rand Energy Systems last quarter, and shows outstanding creep resistance with no rupture after about 2,300 at 750°C. Testing will continue next quarter.

Technical Progress

Recuperator Component Analysis

Different microturbine OEMs have provided pieces of fresh and engine-tested PFR and PSR recuperators made from standard 347 stainless steel for analysis, testing, and characterization, which was completed previously. ORNL continued expanded analysis of PFR recuperator air cells and related manufacturing process specimens with Ingersoll Rand Energy Systems this quarter.

Detailed component analyses data are only reported to each of the OEMs. Collaborative efforts between ORNL and the recuperator makers to provide or characterize advanced

alloys (i.e. HR120, 20-25Nb or alloy 625) with more temperature capability and reliability continued this quarter.

Selection and Commercial Scale-Up of Advanced Recuperator Materials:
a) Materials for use to about 704°C (1300°F)

Testing of standard 347 steel with modified commercial processing for improved creep rupture resistance as sheet and foil was completed by ORNL and Allegheny Ludlum (AL). AL has made this material commercially available as AL347HP, and commercial quantities appropriate for recuperator air cell manufacturing have been supplied to Capstone Turbines and Ingersoll Rand Energy Systems.

Last quarter creep testing of specimens from plate stock was completed to measure improvements of the initial series of ORNL modified 347 stainless steels relative to standard 347 steel. Both the mod. 2 and mod. 4 ORNL modified 347 steels have significantly longer rupture life and lower secondary creep rates than standard 347 stainless steel creep tested previously at 750°C.

Previous oxidation testing in 10% water vapor at 650-750°C continued this quarter. That testing shows a significant benefit for the ORNL modified 347 steels that contain Mn and N additions relative to standard 347 steel, particularly the mod. 4 steel. Detailed microanalysis using analytical electron microscopy of the modified 347 (mod. 4) steel specimen shows complex surface oxides rich in Mn and Cr on top of a thinner chromia layer at the metal-oxide scale interface. There is a clear role of Mn that helps form a protective oxide to resist moisture-enhanced oxidation, in addition to its role in improved creep resistance. Tests at 650°C continued beyond 10,000 h this quarter.

b) Materials for use at 760°C (1400°F) or higher

HR 120 (Fe-25Cr-35Ni) is one of the more promising commercially available materials which has significantly better creep-resistance and corrosion-resistance in this temperature range at 3-4 times the cost of 347 stainless steel. Commercial 3.5 mil foil of HR120 was obtained by ORNL from Elgiloy Specialty Metals (Elgin, IL) and creep-tested at 704°C/152 MPa, and at 750°C/100 MPa. The HR 120 foil lasted 900h at 704°C, and lasted for 3300 h at 750°C, both with good rupture ductility. The creep resistance of HR 120 at 750°C is about 13 times better than standard 347 steel foil with standard commercial processing (Fig. 1). Creep data is also included for NF709 (Fe-20Cr-25Ni, Nb, N), from boiler tubing that was split and rolled into foil at ORNL. The NF709 shows about 50% longer rupture life than HR120. Alloys 625 foil shows roughly similar creep rupture life, but a much lower creep rate.

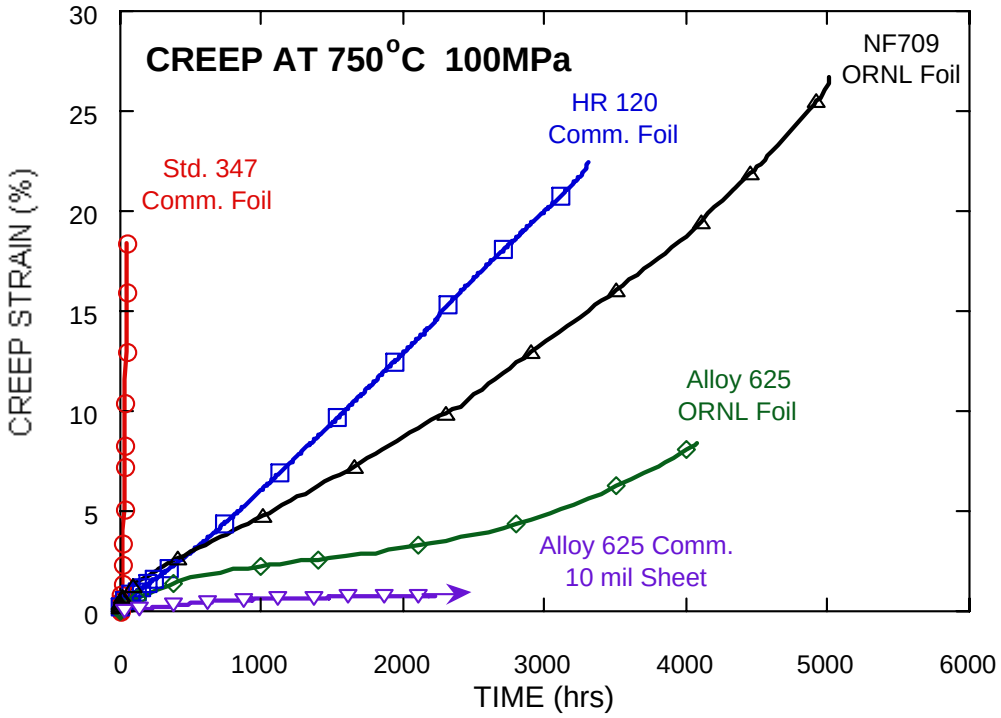

Figure 1 – Comparison of creep rupture curves for testing of commercial or ORNL processing of 4 mil foils of high performance alloys at 750°C and 100 MPa (14.5 ksi). Foils include prior data on commercial HR120, and ORNL processed foils of NF709, alloy 625, and new data on commercial 10 mil sheet of alloy 625.

This quarter, new samples of commercial 10 mil sheet of alloy 625 used for manufacturing PFR recuperator aircells were placed into creep tests at 704 and 750oC, and tests continue to about 2,300 h with no rupture. Fig. 1 shows that the 10 mil sheet shows even better creep resistance than the 4 mil foil, most likely due to difference in grain size and processing. Creep testing will continue next quarter, and microcharacterization will be done after the specimens rupture.

The commercial HR 120 foil and ORNL foils of alloy 625 and NF709 have also been incorporated into the oxidation testing matrix, and at 650-750°C are resistant to water-vapor enhanced oxidation, at least to about 8000 h. Oxidation testing will continue next quarter, and many of these steels and alloys will also be incorporated into the ORNL recuperator testing facility next quarter.

Status of Milestones

FY2004 – In collaboration with Allegheny Ludlum, process a 5000 lb commercial heat of corrosion-resistant 20/25 Nb alloy into foils and sheet for high-temperature recuperators (August 2004). (On-Schedule)

Industry Interactions

Microturbine OEM Ingersoll-Rand Energy Systems sent ORNL a sample of commercial 10 mil sheet of alloy 625, used for PFR aircell manufacturing, for creep and corrosion testing. ORNL and Ingersoll Rand continued the braze alloy studies in support of their advanced PFR recuperator manufacturing efforts. ORNL and AL initiated a new joint project effort to produce the new AL 20-25+Nb stainless alloy that has shown significantly better oxidation and creep resistance relative to standard 347 steel in their preliminary testing. The DOE milestone related to this joint project is on schedule. Tenative agreement was obtained from Capstone Turbines, Inc. and Ingersoll-Rand Energy Systems to participate in this project and take the appropriate commercial foils and sheet of AL 20-25+Nb to assess recuperator aircell manufacturing behavior.

Problems Encountered

None

Publications/Presentations

P. J. Maziasz, P. A. Bint, J. P. Shingledecker, K. L. More, N. D. Evans, and E. Lara-Curzio, "Austenitic Stainless Steels and Alloys with Improved High-Temperature Performance for Advanced Microturbine Recuperators," paper GT2004-54239 was written and accepted for presentation and publication at the ASME Turbo Expo 2004, to be held 14-17 June, 2004 in Vienna, Austria.

CERAMIC RELIABILITY FOR MICROTURBINE HOT-SECTION COMPONENTS

Reliability Evaluation of Microturbine Components

H. T. Lin, M. K. Ferber, and T. P. Kirkland
Oak Ridge National Laboratory
Oak Ridge, TN 37831-6068
Phone: (865) 576-8857, E-mail: linh@ornl.gov

Objective

Evaluate and document the long-term mechanical properties of very small specimens machined from ceramic components (e.g., blades, nozzles, vanes, and rotors) in as processed and after engine testing at ambient and elevated temperatures under various controlled environments. This work will allow microturbine companies to verify mechanical properties of components and apply the generated database in probabilistic component design and lifetime prediction methodologies. The work also provides a critical insight into how the microturbine environments influence the microstructure and chemistry, thus mechanical performance of materials.

Highlights

Studies of mechanical properties of biaxial discs machined from airfoils of SN282 silicon nitride integral vane ring (Kyocera Industrial Ceramic Corp., Vancouver, WA) was completed. The SN282 silicon nitride integral vane ring, acquired from UTRC, was designed for UTRC ST5+ advanced microturbine system (Fig. 1). Biaxial discs (7 mm in diameter x 0.5 mm in thickness) were machined from airfoils. Ball-on-ring test was carried out at room temperature with the as-processed surface under tension. Database generated has been provided to Kyocera for processing refinement, and also to UTRC for its probabilistic component design and life prediction effort.

Figure 1. Photos of UTRC SN282 silicon nitride integral vane ring designed for ST5+ advanced microturbine system.

Development and Characterization of Advanced Materials for Microturbine Applications

M. K. Ferber and H-T Lin
Metals and Ceramics Division
Oak Ridge National Laboratory
P.O. Box 2008, Oak Ridge, TN 37831-6069
Phone: (865) 576-0818, E-mail: ferberk@ornl.gov

Objective

The primary objective of this project is to evaluate the long-term mechanical and chemical stability of advanced materials of interest to the DER program. Currently the project is evaluating (1) structural ceramic, which are being considered for use as hot-section components in microturbines and (2) thick thermal barrier coatings (TTBCs) being developed for thermal management in combustor liners used in industrial gas turbines. The structural ceramics effort focuses on the development and utilization of test facilities for evaluating the influence of high-pressure and high-temperature water vapor upon the long-term mechanical behavior of monolithic ceramics having environmental barrier coatings. In the case of the TTBCs, the primary focus is on the evaluation of changes in microstructure and thermal properties arising from long-term aging tests.

A secondary objective of the program is to develop and characterize the toughened silicon nitride ceramics with the following attributes:

- Fracture toughness $\geq$ 10 MPa•$m^{1/2}$ with fracture strengths > 1 GPa, and
- High mechanical reliability at low and intermediate temperatures coupled with creep resistance at the desired operating temperatures,
- Enhanced resistance to elevated temperature environmental damage, and
- Higher thermal expansion coefficients to better match the expansion of promising environmental barrier coating (EBC) systems.

Highlights

A program to graphically illustrate component reliability for selected structural ceramics was developed. This program utilizes strength/stress versus temperature plots to compare finite element results for a specific component with the strength-temperature data for a number of commercial silicon nitride ceramics. The strength is adjusted to account for both slow crack growth and creep. The effect of recession is simulated by increasing the finite element stresses as the material is lost.

Technical Progress

The steam injection system (Figure 1) described in the previous quarterly report was used to evaluate the temperature sensitivity of recession of the SN282 silicon nitride by exposing three specimens at 1100, 1200, and 1300°C. The recession was evaluated as a function of time by

interrupting each test periodically and measuring the change in the gage diameter using a coordinate measuring machine. The maximum loss in gage diameter was taken as the appropriate measure of surface recession. The mid-span profiles of the specimens exposed for 884 h are shown in Figure 2. These data were subsequently used to calculate recession as a function of angle measured with respect to the injection direction (Figure 3). Although the maximum reduction in gage diameter for the specimen exposed at 1200°C was slightly larger than that at 1300°C, the total amount of material loss was much larger for the specimen exposed at 1300°C. The recession of the 1300°C specimen was also more asymmetric in that the recession along one side (angle = 90°) was much greater than that along the opposing side. These differences were attributed to variability in the geometries of the alumina injection tubes. As shown in Figure 4, the gap of the injection tube used with the specimen exposed at 1200°C was very well matched to the gage diameter (6.35 mm). In the case of the injection tube used with the specimen exposed at 1300°C, the gap (6.98 mm) was significantly larger that the gage diameter indicating that it was less effective at restricting the steam flow. One would expect that the local velocity would be smaller for this case.

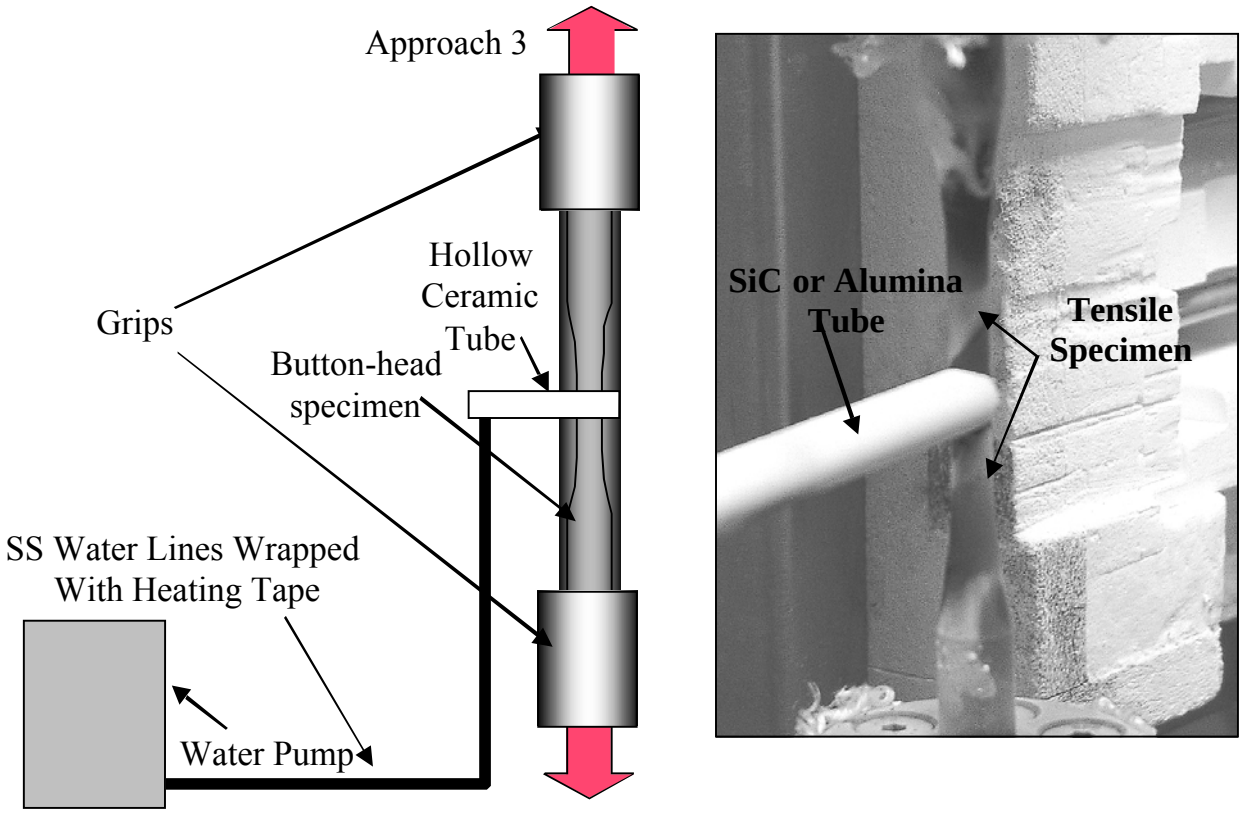

Figure 1: Direct Steam Injection System.

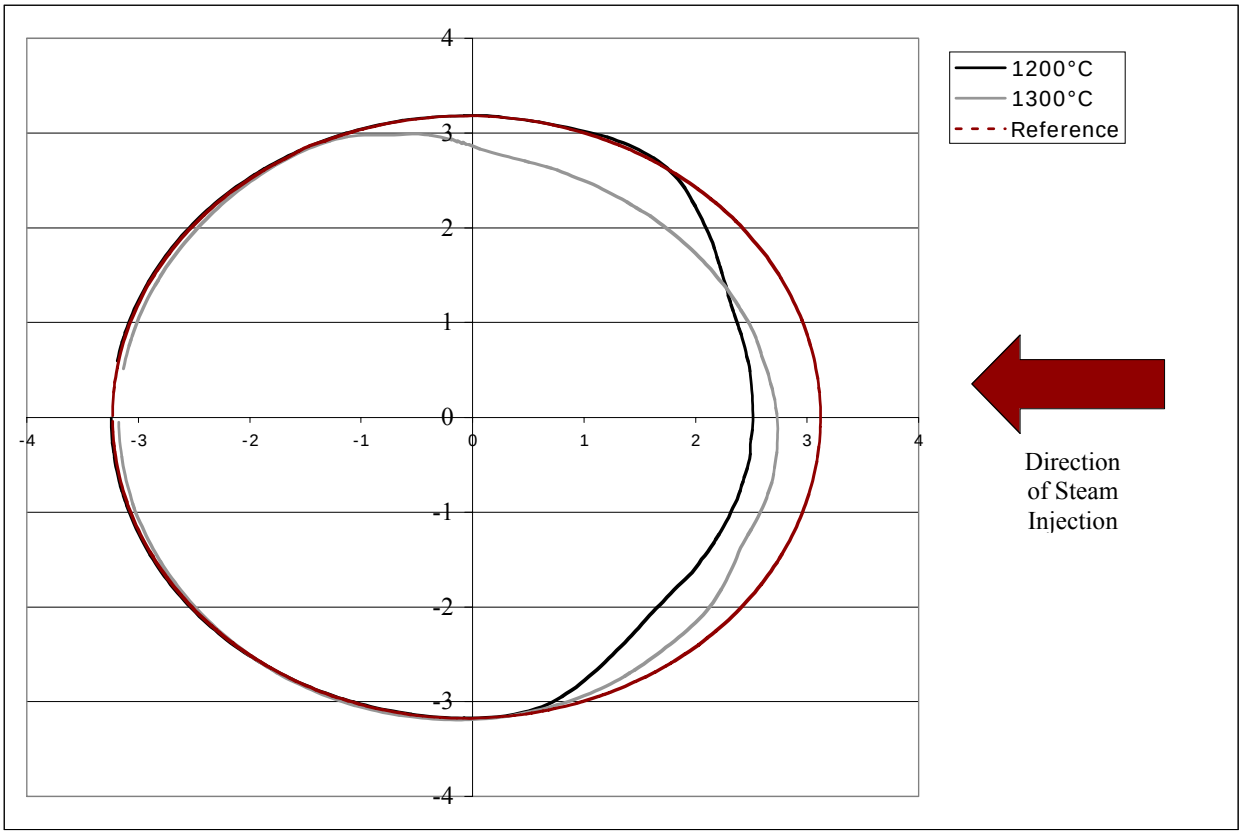

Figure 2: Surface profiles for specimens exposed at 1200 and 1300°C.

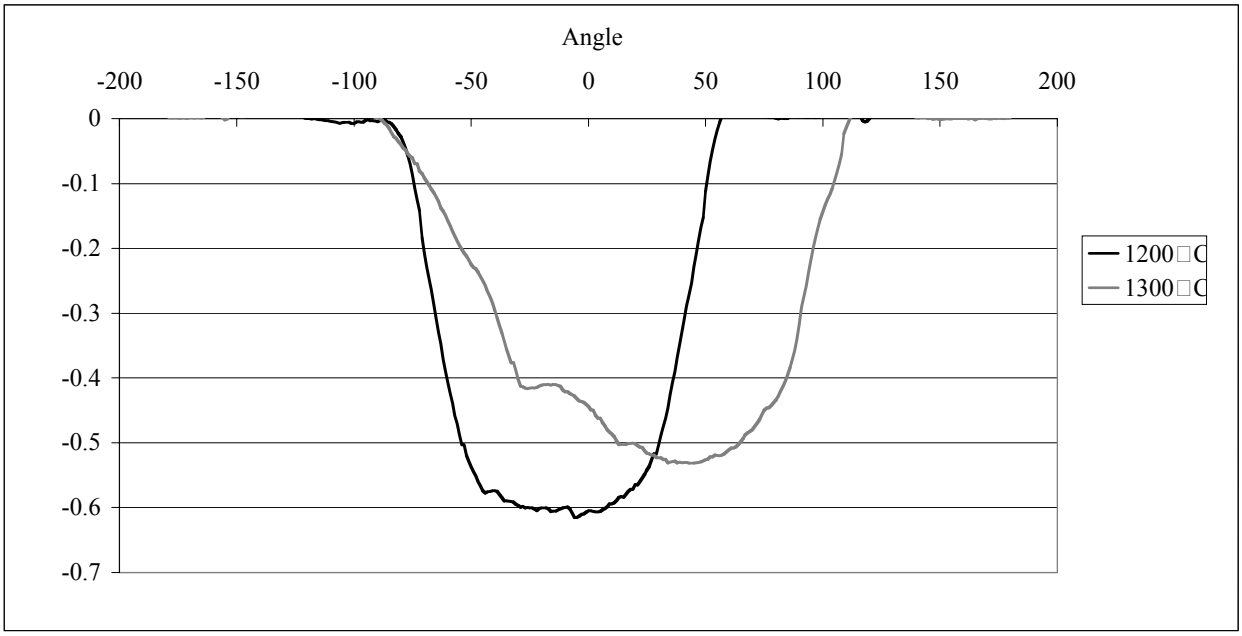

Figure 3: Extent of recession as a function of angle measured with respect injection direction.

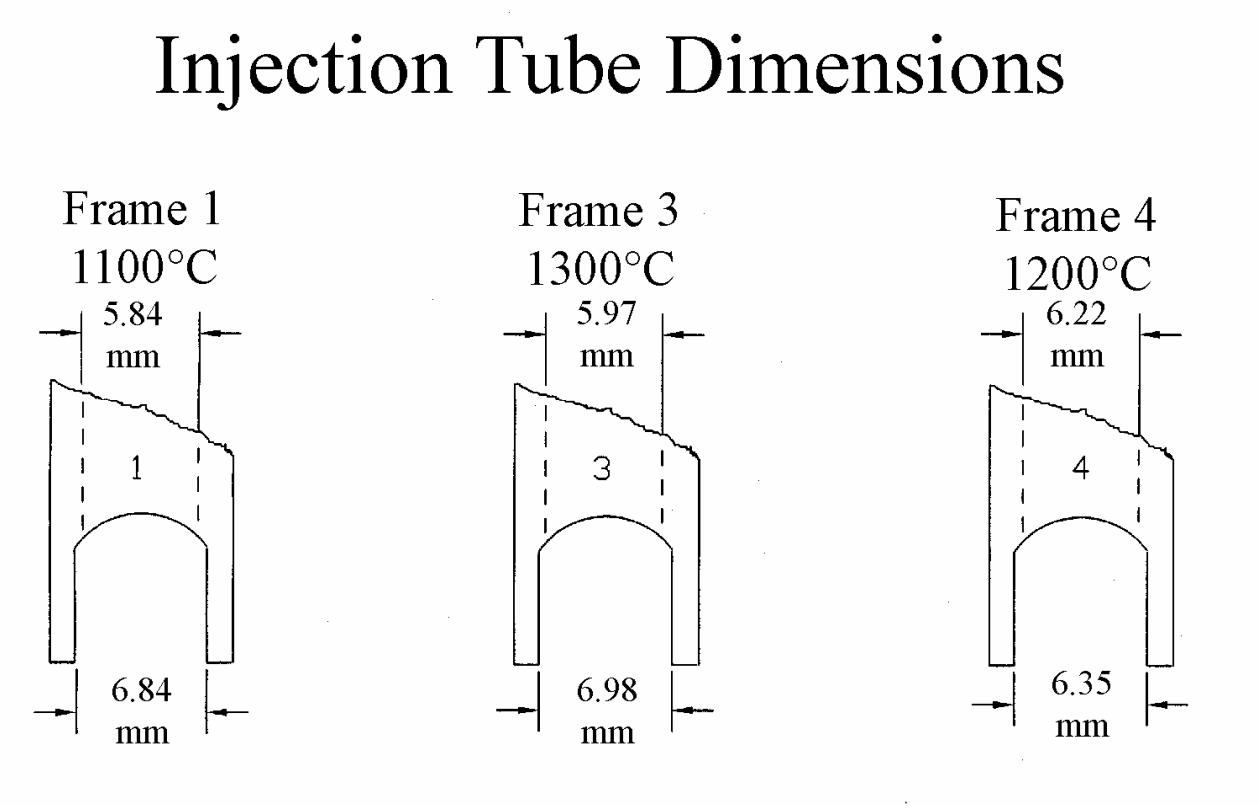

Figure 4: Geometry of the alumina injection tubes.

Status of Milestones

(1) Complete the characterization of thick thermal barrier coatings (supplied by Solar Turbines) aged for periods up to 5000 and issue report-March 2004 Completed

(2) Complete mechanical property assessment of toughened silicon nitride ceramics and incorporate into database-October 2004

(3) Complete the characterization of commercially available environmental barrier coatings and issue report-March 2005.

Industry Interactions

Teleconferences were held Jay Morrison of Siemens to discuss the characterization of their alumina composites and thermal barrier coatings.

Problems Encountered

None

Publications

None

References

None

Technical Progress

Studies of dynamic fatigue properties for SiAlON ceramics (Kennametal Inc., PA) were continued during this reporting period. Kennametal was awarded by DOE under Microturbine Materials Program to develop SiAlON ceramics for hot-section components for advanced microturbines. The SiAlON ceramics due to their superior wear resistance have been developed for metal cutting tool applications, and might have great potential for structural applications in microturbine systems. The purpose of this study is to generate a database for down-selecting the candidate composition(s) and also for probabilistic component design and life prediction efforts carried out by microturbine companies. All of the materials, sintered with different chemical compositions, i.e., rare earth oxide content, contain a mixture of α- and β-SiAlON grain microstructure. The SiAlON ceramics were fabricated under the Phase I contract, and MOR bars were longitudinally machined per the revised ASTM C116 standard with 600 grit surface finish. The dynamic fatigue tests were carried out at 20 and 1204°C and at stressing rate of 30 and 0.003 MPa/s in air per ASTM C1465. The 30 MPa/s is used to evaluate the inert characteristic strength as a function of temperature, and 0.003 MPa/s is applied to measure the slow crack growth (SCG) susceptibility at high temperatures.

Test results at 20°C and 30 MPa/s showed that all of the SiAlON materials exhibited comparable relatively low Weibull modulus with respect to commercially available silicon nitride ceramics evaluated and reported previously (Table 1 and Fig. 2-7). Preliminary fractography examinations indicated the low Weibull moduli obtained for all of the SiAlON materials evaluated might result from the metal contamination during processing. Also, results showed that the values of the inert characteristic strength of SiAlON strongly depended on the size and content of elongated β-SiAlON grains. For instance, the material contained fine α-SiAlON matrix plus a relative high content of β-SiAlON grains (e.g., AB832 and AB832) exhibited higher characteristic strengths than those with more equiaxed microstructure (e.g., AB582 and AB532). The effect of β-SiAlON elongated grain size and content on the measured mechanical strength is consistent with those previously reported for silicon nitride ceramics. On the other hand, results showed there was minor change in inert characteristic strength accompanied with a high fatigue exponent for 2308E material when tested at 20°C and 0.003 MPa/s (Fig. 8 and 9). Note that the 2308E material showed a 20% degradation in strength with a low fatigue exponent (~36) when tested at 1204°C (Table 1), indicative of high susceptibility to SCG at temperature. Dynamic fatigue tests at 1204°C will be carried out for these SiAlON materials and results will be discussed in the next quarterly report.

Table 1. Summary of uncensored Weibull and strength distributions for Kennametal SiAlON ceramic specimens with as-machined surface (longitudinally machined per the revised ASTM C1161 standard).

Material	# of Spmns. Tested	Stressing Rate (MPa/s)	Temp. (°C)	Uncens. Weibull Modulus	± 95% Uncens. Weibull Modulus	Uncens. Chrctstic Strength (MPa)	± 95% Uncens. Chrctstic Strength (MPa)
2308A	15	30	20	5.92	3.80, 8.55	651	589, 715
2308E	15	30	20	6.06	3.91, 8.73	783	710, 858
2308E	12	0.003	20	6.62	4.06, 9.90	807	729, 887
AB132	15	30	20	6.39	4.16, 9.14	878	801, 958
AB531	15	30	20	10.65	6.75, 15.55	801	757, 844
AB532	15	30	20	8.47	5.27, 12.65	721	673, 771
AB582	15	30	20	7.21	4.65, 10.34	567	523, 613
AB831	15	30	20	8.45	5.42, 12.29	960	894, 1025
AB832	15	30	20	10.70	6.83, 15.57	1029	973, 1084
2308A	15	30	1204	9.79	6.52, 13.62	393	370, 415
2308E	15	30	1204	7.45	4.67, 11.05	540	489, 582
2308A	15	0.003	1204	10.68	6.87, 15.38	415	392, 437
2308E	14	0.003	1204	3.37	2.29, 4.55	440	369, 522

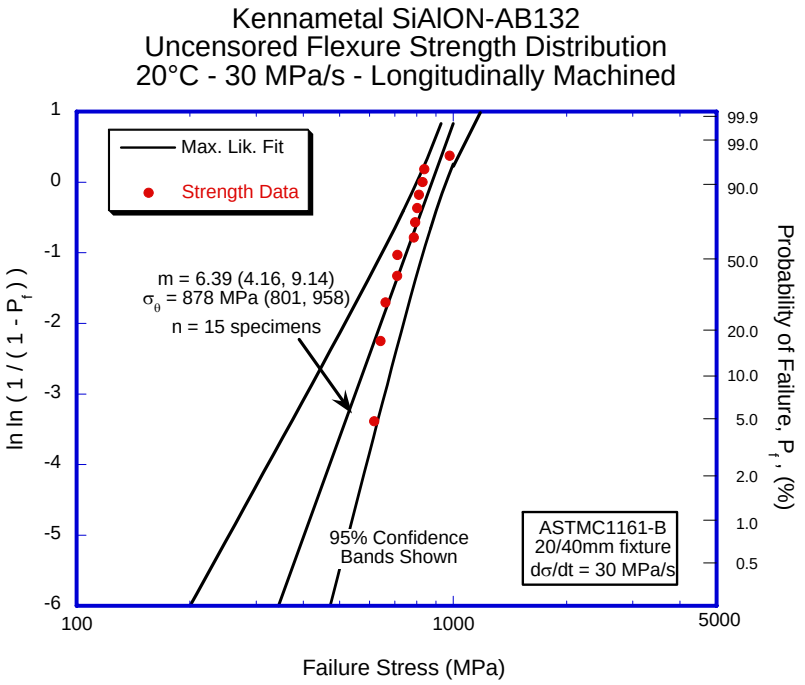

Figure 2. Uncensored flexure strength distribution at 20°C and 30 MPa/s of SiAlON-AB132 ceramic with as-machined surface (bulk material).

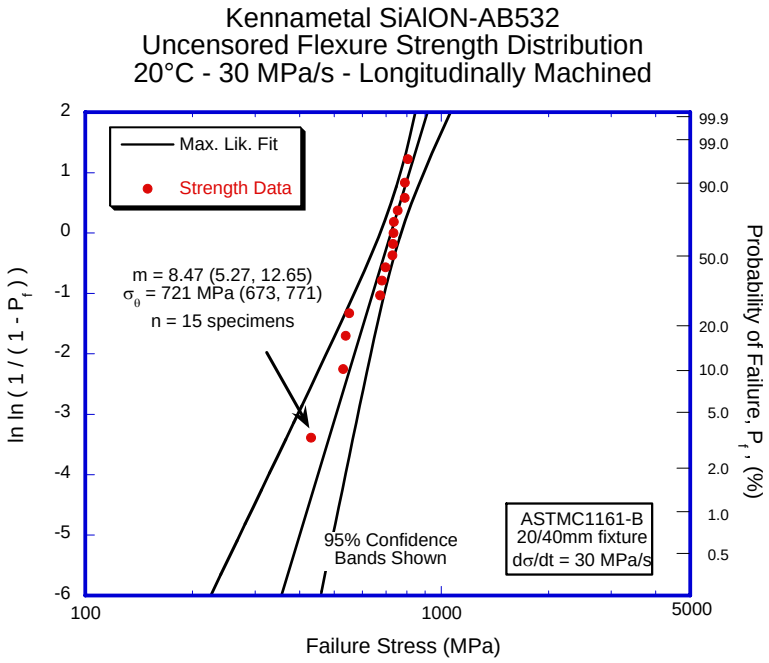

Figure 3. Uncensored flexure strength distribution at 20°C and 30 MPa/s of SiAlON-AB531 ceramic with as-machined surface (bulk material).

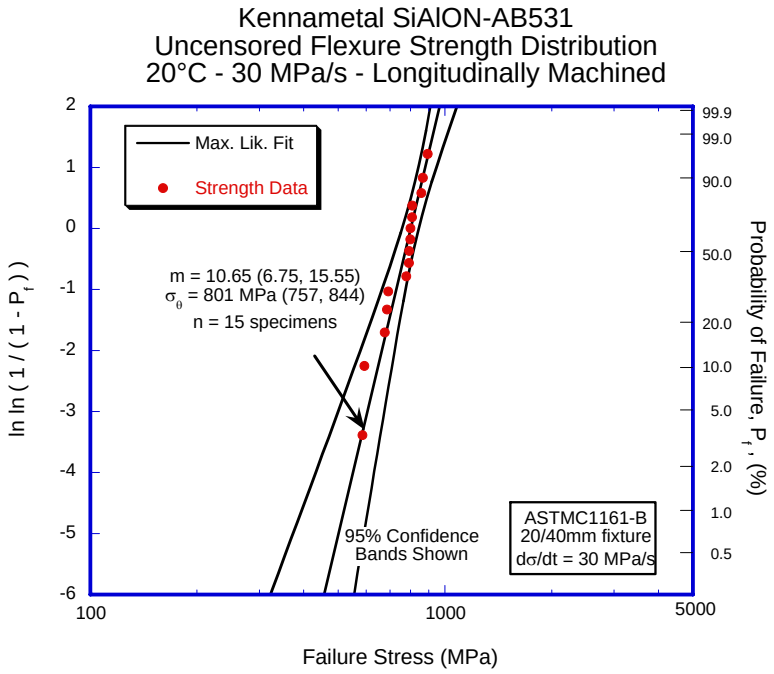

Figure 4. Uncensored flexure strength distribution at 20°C and 30 MPa/s of SiAlON-AB532 ceramic with as-machined surface (bulk material).

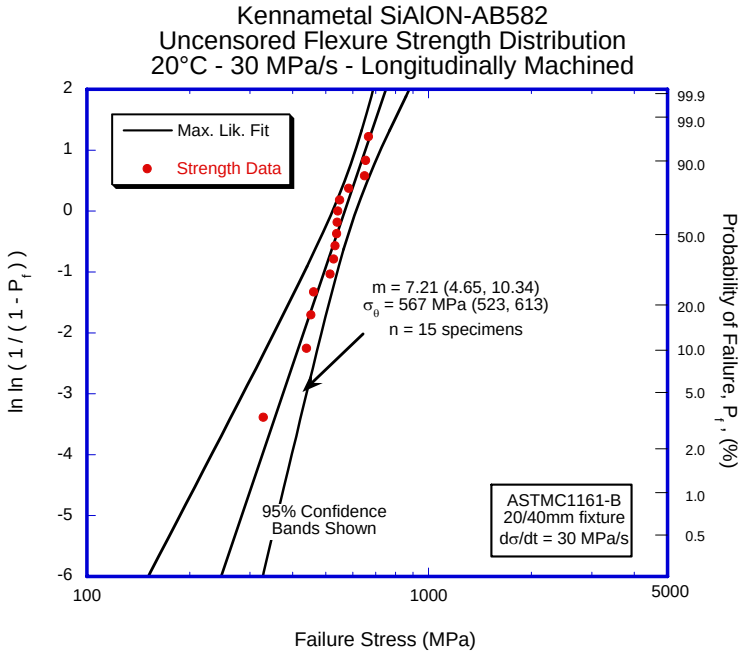

Figure 5. Uncensored flexure strength distribution at 1204°C and 30 MPa/s of SiAlON-AB582 ceramic with as-machined surface (bulk material).

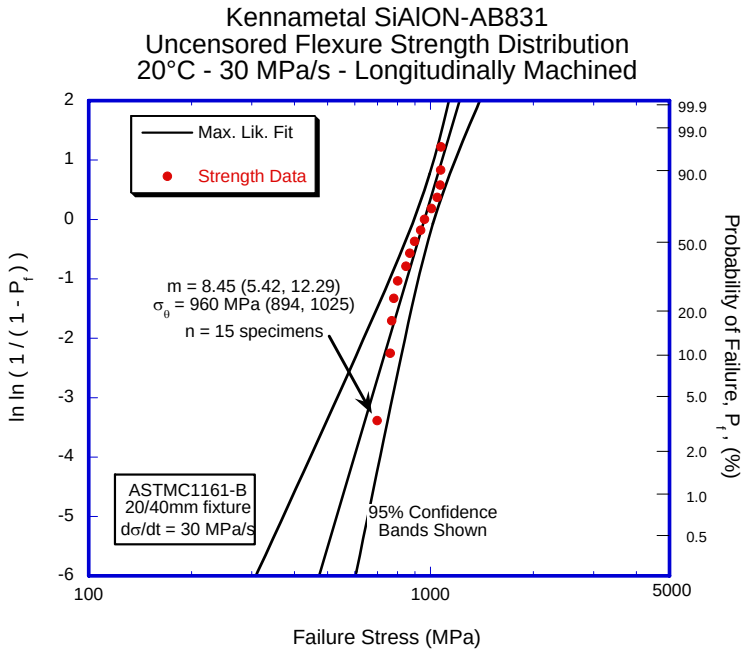

Figure 6. Uncensored flexure strength distribution at 1204°C and 30 MPa/s of SiAlON-AB831 ceramic with as-machined surface (bulk material).

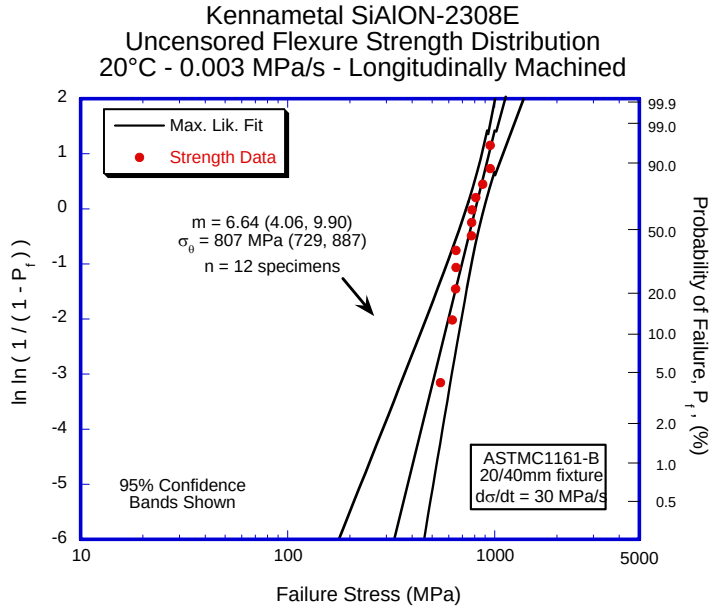

Figure 7. Uncensored flexure strength distribution at 20°C and 30 MPa/s of SiAlON-AB832 ceramic with as-machined surface (bulk material).

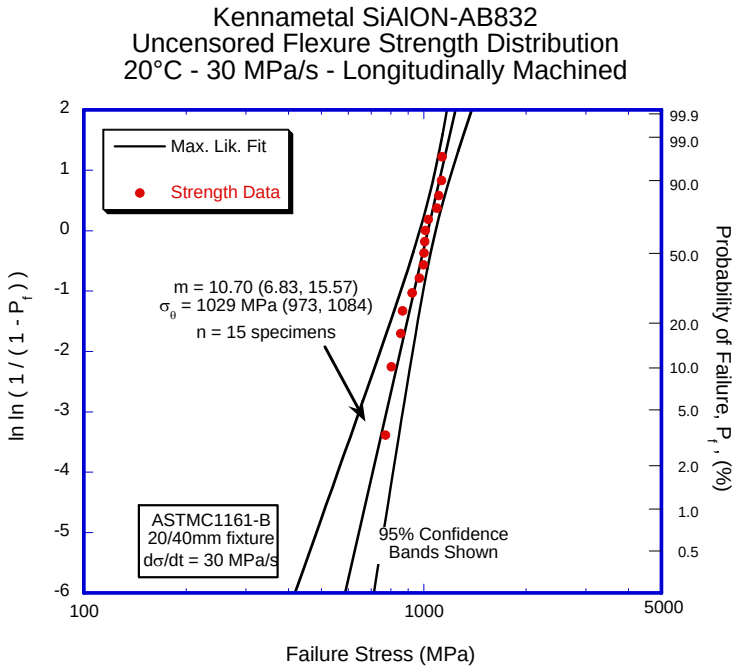

Figure 8. Uncensored flexure strength distribution at 20°C and 0.003 MPa/s of SiAlON-2308E ceramic with as-machined surface (bulk material).

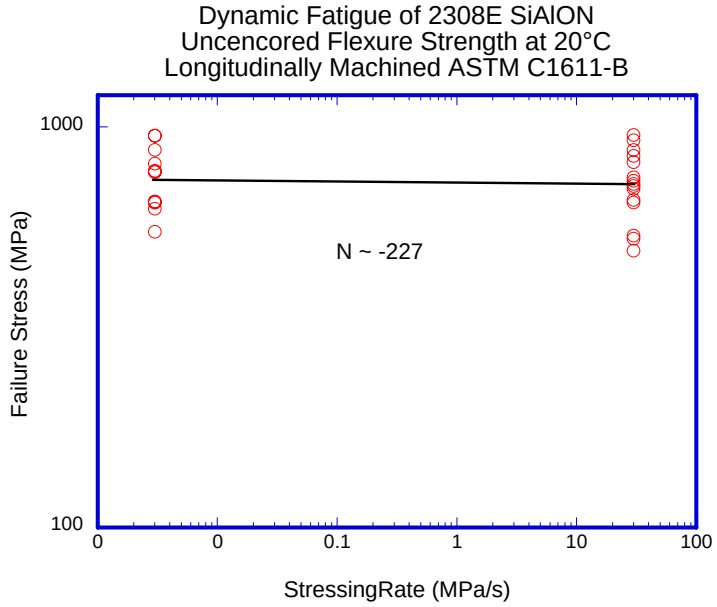

Figure 9. Flexure strength versus stressing rate for SiAlON-2308E with as-machined surface (bulk material) tested at 20°C.

An Ingersoll-Rand type NT154 silicon nitride microturbine rotor, similar to Kyocera SN237 rotor, has been received from Saint-Gobain Ceramics & Plastics (Fig. 10). Biaxial discs will be machined from airfoils for mechanical strength evaluation using

ball-on-ring method at room temperature. Test results will be provided to Saint-Gobain for processing optimization and to microturbine companies for their probabilistic component design and life prediction.

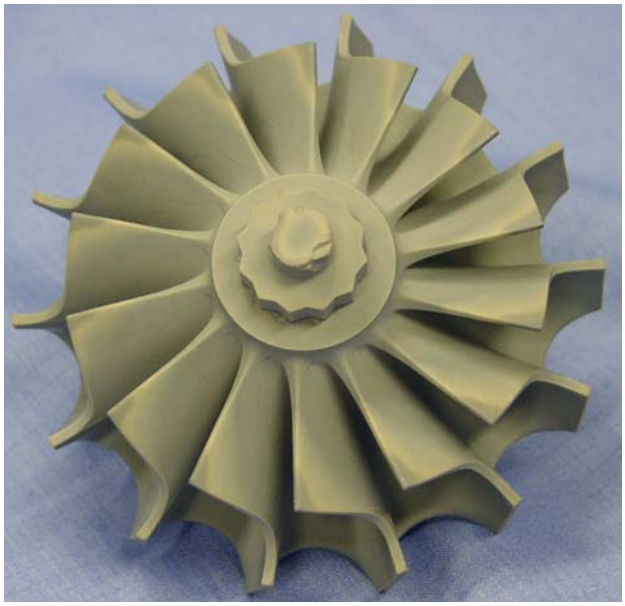

Figure 10. Photo of NT154 silicon nitride microturbine rotor manufactured by Saint-Gobain.

Status of Milestones

1. Complete evaluation of next generation Si_3N_4 with EBC from SMRC, Japan after long-term steam jet testing. September 2004. On schedule.

Industry Interactions

Communication with John Holowczak, Venkata Vedula, and Jun Shih at UTRC to discuss the mechanical results of SN282 integral vane ring.

Communication with Vimal Pujari and Ara Vartabedian at Saint-Gobain Ceramics & Plastics on the updates of the testing status and results for NT154 silicon nitride materials manufactured during Task II effort under Phase I contract, and also the preparation status for NT154 microturbine rotor.

Communication with Russ Yeckley at Kennemetal on the dynamic fatigue test results of SiAlON ceramics manufactured during Task I effort.

Communication with Professor Rishi Raj at University of Colorado on the testing and evaluation of SiCN EBC materials under steam environments.

Problems Encountered

None

Publications/Presentations

H. T. Lin and M. K. Ferber, "Evaluation Methodology for Mechanical Property of Complex-Shaped Ceramic Components." Presented at International Cocoa Beach Conference & Exposition on Advanced Ceramics & Composites, Cocoa Beach, FL, January 25-30, 2004

M. K. Ferber, H. T. Lin, S. F. Duffy, J. K. Kesseli, and M. Costen, "Characterization of a Ceramic Rotor Developed for the IR Power Works Microturbine," Presented at International Cocoa Beach Conference & Exposition on Advanced Ceramics & Composites, Cocoa Beach, FL, January 25-30, 2004.

Reliability Analysis of Microturbine Components

S.F. Duffy, E.H. Baker & J.L. Palko
Connecticut Reserve Technologies, LLC
2997 Sussex Court
Stow, Ohio 44224
Phone: 330-678-7328 E-mail: sduffy@crtechnologies.com

Objective

The current objectives of this project are as follows:

- Connecticut Reserve Technologies, LLC (CRT) will create the ability whereby an end user generates output in the form of unitless area- or volume- (or both) loading factors (k_A and k_V, respectively) as a function of Weibull modulus. Additional output will include the discrete area and volume that are used in the calculation of effective areas and effective volumes (i.e., report 6 values: k_A, k_V, A, V, $k_A \bullet A$, and $k_V \bullet V$). This will allow users of the software to conduct nonstandard parameter estimation analyses assuming the existence of either surface flaw populations, volume flaw populations, or a concurrent combination of the two.

- In addition, CRT will continue work supported by the NASA MEMS program that began 3 years ago and focus on implementing an edge recognition capability in the CARES program. At the present time the CARES interface to ANSYS, entitled ANSCARES, will recognize and compute edge stresses for a handful of ANSYS elements. However, the algorithm to compute a probability failure due to edge defects for a component is missing from within CARES. CRT will consult with researchers at ORNL to ascertain which elements should be included from the ANSYS library of elements in the ANSCARES interface. Then CRT will begin the process of updating the CARES code to compute a component probability of failure due to edge defects.

- Create a capability in *CARES* to estimate "allowable" effective stress in a component when a specific failure probability is known or desired, and calculate effective stress "ranges" about the desired effective allowable stress value that are associated with any desired confidence level.

- Update *CARES* so that it interfaces with *ANSYS 8.0.*

- Create a capability to pool censored data (for the most common test specimen geometries and for user-specified loading factors or effective-areas or effective-volumes).

- Create a capability to determine confidence bounds about pooled censored data.

- Create a capability to determine confidence bounds about predicted reliability of a component.

- Create a capability to determine confidence bounds about predicted reliability of a proof-tested component.

- Update interfaces between *WeibPar* and *CARES*.

Highlights

Connecticut Reserve Technologies, LLC (CRT) is currently developing and enhancing a method to determine Weibull distribution metrics for the Ingersol Rand microturbine rotor. The combination of service stress state and a requisite probability of survival for a Si_3N_4 microturbine rotor are being used to determine Weibull modulus - characteristic strength pairs for any arbitrary Si_3N_4 scaled to standard mechanical test coupons and test methods.

CRT has also developed the ability to compute effective area, effective volumes, and reliability prediction confidence bounds using the *CARES* algorithm and the *WeibPar* software for arbitrary component geometries.

Technical Progress

The finite element model of the IR rotor originally provided to CRT had the surface geometry removed at some point in the creation of the model. CRT has modified an ANSYS macro designed to extract surface information (stress states and geometry) for elements that were attached to areas created in the solid modeling phase. The original rotor is depicted in Figure 1.

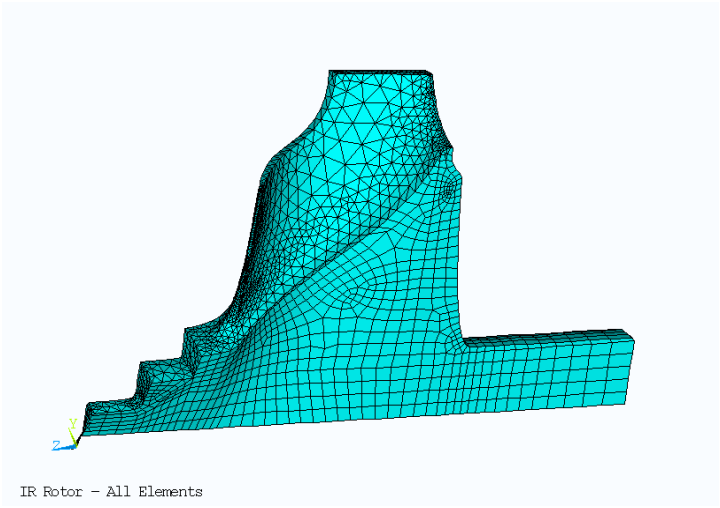

Figure 1 Entire mesh - Ingersoll Rand rotor

In extensively modifying an existing surface macro CRT was able to identify elements from within the mesh that have an element surface coincident with the surface of the rotor. These selected elements are depicted in Figure 2. Note that for elements with surfaces coincident with the surface of the rotor the entire element is shown, not just the face of the element coincident with the surface of the rotor.

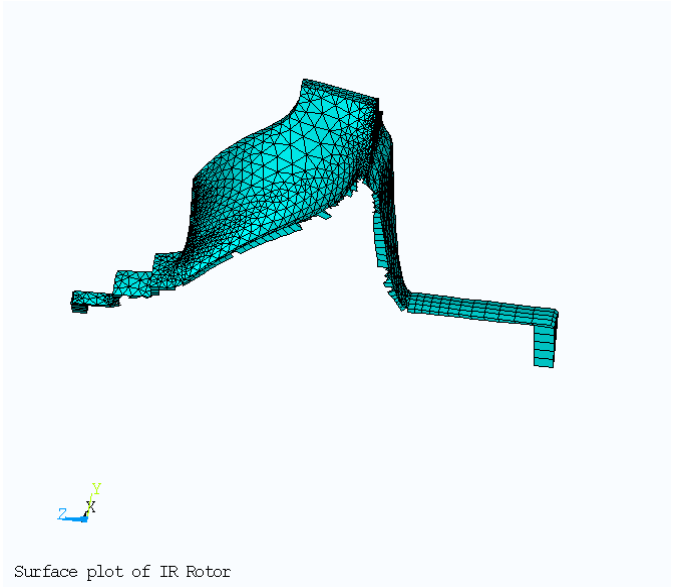

Figure 2 Elements with surfaces coincident with the surface of the IR rotos

With this information CRT can now generate Weibull metrics relative to a surface flaw analysis. The results of this endeavor will be reported on in an upcoming quarterly report.

As indicated above CRT has developed an ability to compute bounds on component reliability using bootstrap techniques. In an upcoming report CRT will provide figures similar to those depicted in Figures 3 and 4 relative to the IR rotor. In Figure 3 a relationship has been established between the effective area of a component and the Weibull modulus of the material used to fabricate the component.

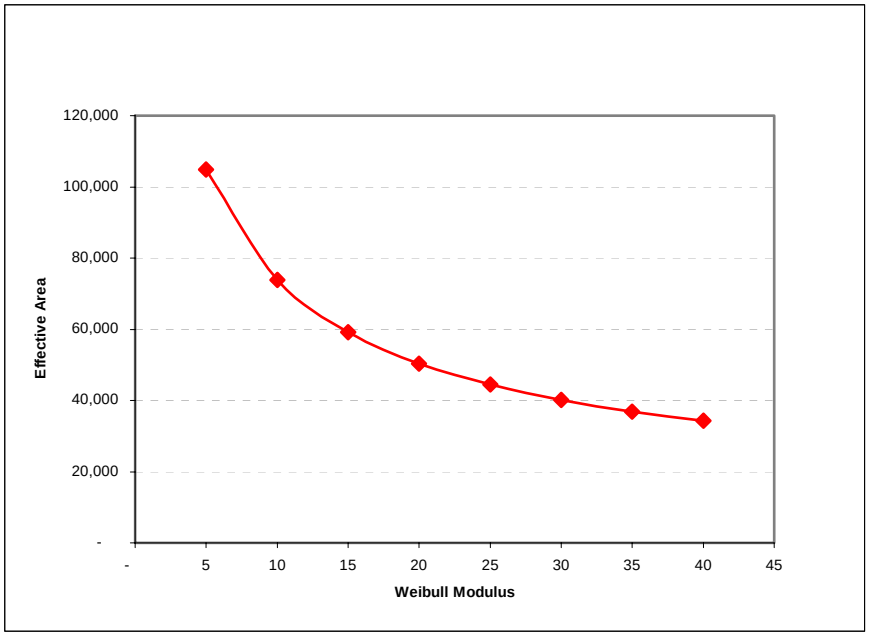

Figure 3 – Component effective area as a function of Weibull modulus

Figure 4 depicts the bounds on component reliability based on the size of the data set used to generate the Weibull parameters and the information if Figure 3. The blue diamond is the component probability of failure given the biased maximum likelihood Weibull parameters. The extreme two data points (circles) are the 5% and 95% confidence bounds. One is 90% certain that the actual component reliability falls between these two points. The open circle is the mean probability of failure. This point is the unbiased probability of failure.

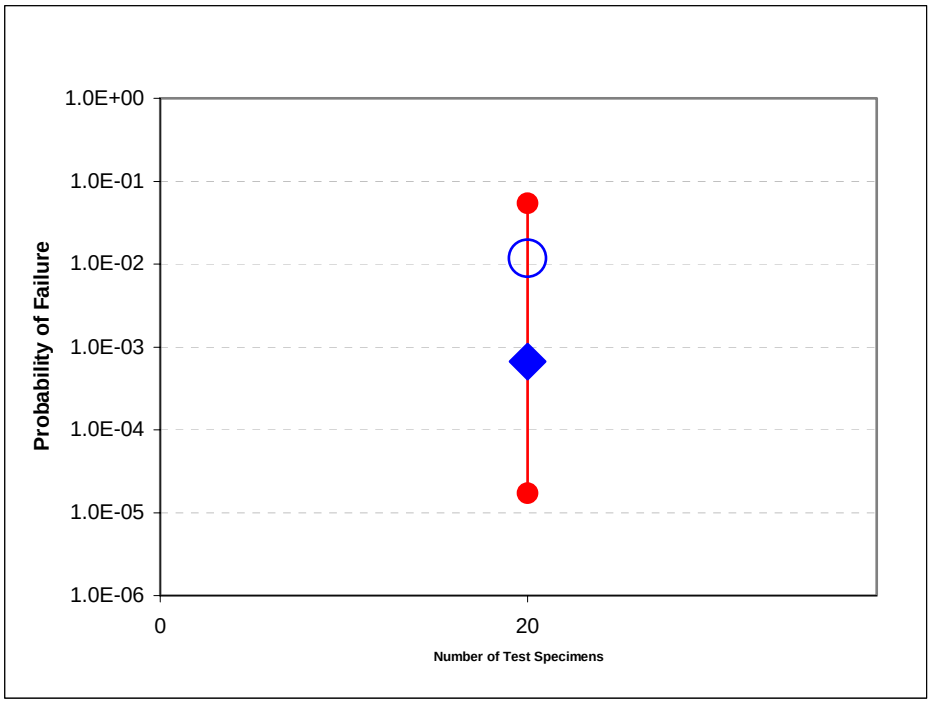

Figure 4 – Confidence bounds on component reliability

Status of Milestones

Determine characteristic strength - Weibull modulus "maps" for both surface- and volume-based flaws that limit strength in ASTM C1161B and ASTM C1161C bend bars and ASTM C1273 Button-head tensile specimen geometries. Use the stress state of the Ingersol-Rand rotor to direct those calculations and compose and submit a publication-ready ORNL/TM Report summarizing those methods and results. [30Sep04] *On schedule.*

Provide ORNL with latest versions of CARES and WeibPar. [30Sep04] *On schedule*

Industry and Research Interactions

None this reporting period.

Publications

None this reporting period

Conference Presentations

"Life Prediction of Structural Components," **S. F. Duffy**, LA Janosik, A. A. Wereszczak, B. Schenk, A. Suzuki, J. Lamon, and D. J. Thomas, Presented at the 28th Annual Cocoa Beach Conference and Exposition on Advanced Ceramics and Composites Ceramics & Components in Energy Conversion Systems Symposium Session: "Ceramic Materials and Component Characterization for Gas Turbines," January 28, 2004

NDE Technology Development for Microturbines

W. A. Ellingson, R. Visher, C. Deemer, E. R. Koehl, and Z. Metzger
Argonne National Laboratory
9700 South Cass Avenue
Argonne, IL 60439
Phone: (630) 252-5058, E-mail: Ellingson@anl.gov

Objective

The objective of this project is development of low-cost, reliable nondestructive evaluation/characterization (NDE/C) technologies for: (1) evaluating low-cost monolithic ceramics for hot section components of microturbines or industrial gas turbines, (2) evaluating environmental barrier coatings (EBCs) for monolithic ceramics and ceramic matrix composites, and (3) evaluating other materials which are part of the technology to advance the programs for the Office of Distributed Energy. The project is directly coupled to other Office of Distributed Energy projects focused on materials developments.

Highlights

There are two highlights this period. First, we more fully explored the use of the Optical Coherence Tomography (OCT) system for characterizing EBCs and second, we successfully completed the addition of more nodes, now up to 44 nodes, to the Beowolf cluster for high speed X-ray computed tomographic (CT) image reconstruction .

Technical progress

Technical work this period focused on 3 areas: (1) developments towards volumetric, 3D, X-ray imaging for improving the reliability and processing methods of low-cost monolithic ceramic materials, (2) work on oxide-based ceramic composites, and (3) work to establish characteristics of new EBCs.

Characterization of EBCs using Optical Coherence Tomography(OCT)

Work this period on OCT has focused in two areas. The first is continuing to understand the theory behind the technique so as to better apply it to EBC materials. Second, efforts have continued to improve the OCT system itself.

Volumetric Visualization of Flaws in Ceramic Rotors
High Speed Image Reconstructions using the Beowulf Computer cluster

The advances in the area of large area, high resolution flat panel X-ray detectors has enabled X-ray computed tomography (CT) to detect features much smaller in real components then were previously possible. However, the lager size and high resolution of these detectors, such as the RID 1620 detector (17" square with a 200 μm Pixel size) used at ANL, causes the time for data reconstruction to increase dramatically. The number of calculation required to compute a CT reconstruction is on the order of magnitude of N^3, where N is the number of columns in the data set. For the RID 1620, the floating point operations (FLOPs) required for reconstruction is on

the order of 100 GigaFLOPs. For a detector with half the resolution, only 10 GigaFLOPs would be required.

In a cooperative effort with the Basic Sciences Division-Materials (BSD-M) at ANL, a massively parallelized computer architecture (called a Beowulf cluster) has been developed. Using computer code developed at ANL, this cluster is capable of significantly reducing the time required for CT data reconstruction. The cluster has been specifically designed for very high speed 3D X-ray image reconstructions using the massive data sets that are being collected from the large area flat panel X-ray detectors (as large as 22 GB for a single data set on the RID 1620).

In its current configuration, the cluster the cluster contains 17 PIII 450 MHz Intel processors and three P4 2.2 GHz Intel processors. A benchmark on the reconstruction code was obtained using a typical data set. Figure 1 shows the reconstruction time as a function of the number of processors (i.e. nodes) used to perform

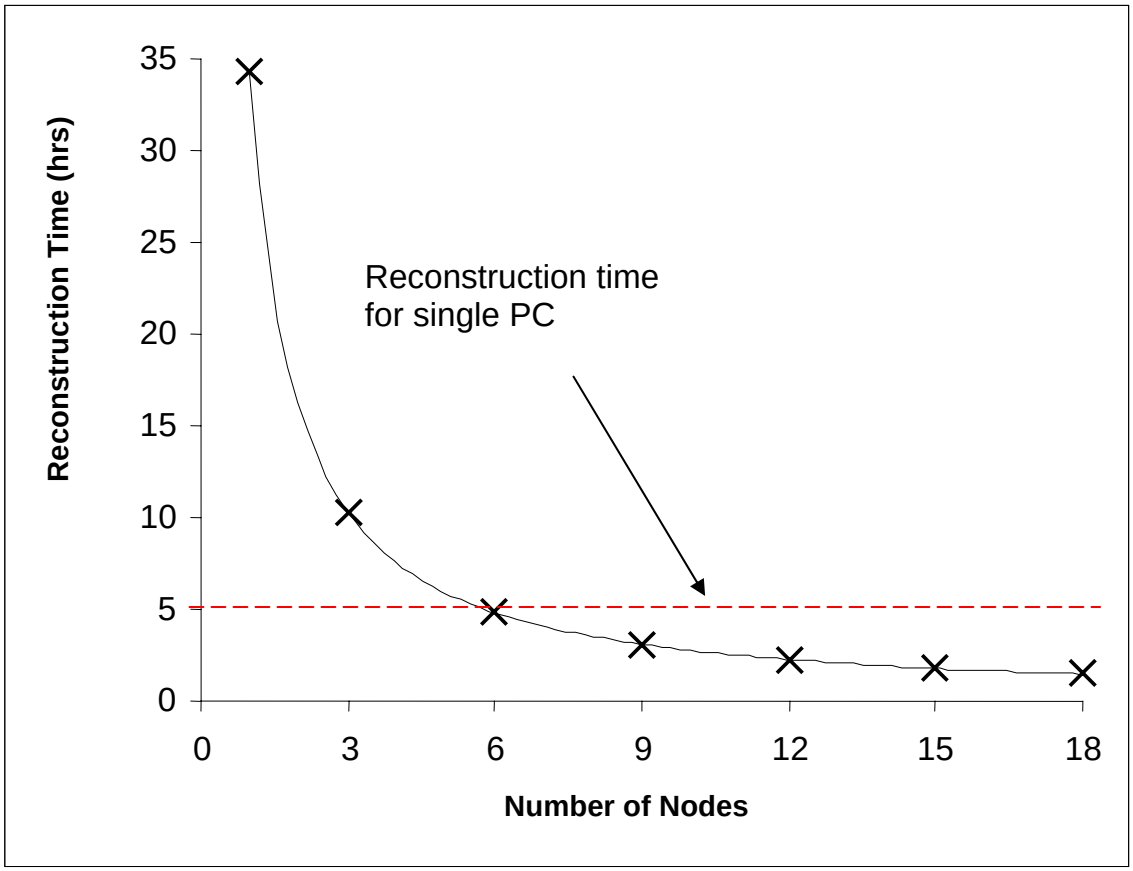

Figure 1: Plot showing the Beowulf reconstruction benchmark

the calculations. As indicated by the red line in Figure 1, a single PC workstation using dual Intel Xeon processors performs the reconstruction in approximately 5 hours. Using 18 nodes, the Beowulf cluster performs this same reconstruction in 3.5 hours, a 30 % reduction in computational time. It is important to note that the reconstruction code has yet to be optimized. Thus, the reconstruction time can be further reduced.

We added new nodes to bring the cluster up to 44 nodes and plans now are to go to 50. After the addition of each new node, the amount of savings in reconstruction time is observed. These new nodes will be based on the Intel Pentium 4 (P4) processor and have 512 MB of memory each. Once the new nodes have been added, the original 18 nodes will be upgraded to match the specifications of the new nodes. Currently, the first 3 new nodes have been added to the cluster. A "new" node (using the Intel P4 processor) can perform approximately 3 times the number of calculations than an "old" node (using the Intel PIII processor). The original cluster benchmark was performed with these additional nodes, and the calculation time was reduced by a factor of 2 when using all 21 nodes as compared to the original 18. The new benchmark curve is shown in Figure 2. It is expected, that the cluster will contain 50 P4 2.2 GHz processors by July of 2004.

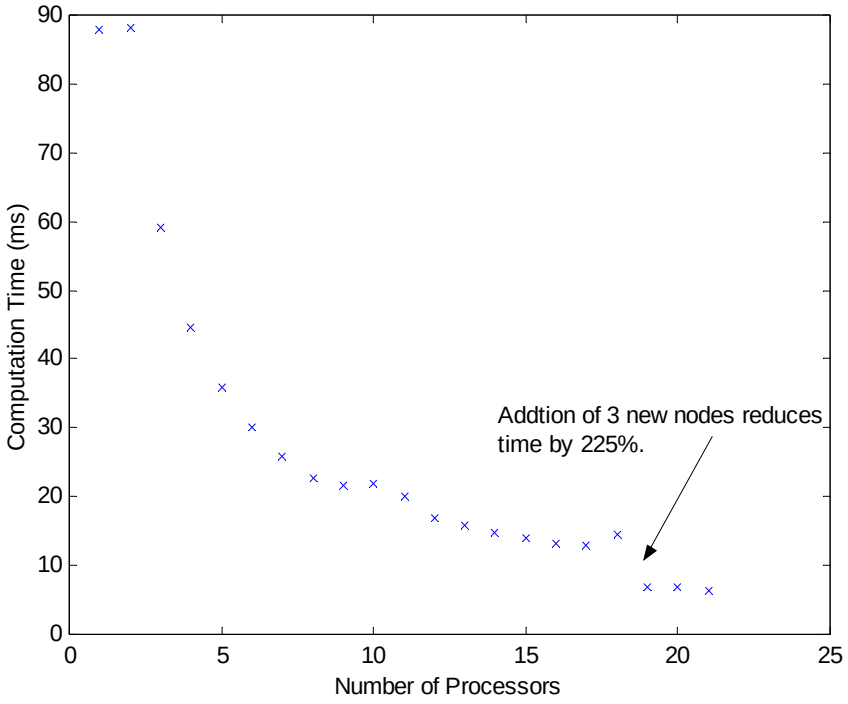

Figure 2: Beowulf cluster performance benchmark—Pi calculation.

To further investigate the capabilities of detection of flaws in monolithis ceramic mocroturbine components using new detectors, the gelcast Si_3N_4 AS800 rotor used previously was again used (see Fig 3). To again note the details, the three sections cut from the unbladed rotor had diameters of 67 mm, 112 mm, and 178 mm respectively. A series of three flat-bottom holes (having diameters of 0.4 mm, 0.6 mm, and 1.5 mm) were machined into each section using an ultrasonic drilling system. This time the detection study was done using the 450 kVp X-ray source (see 3rd Microturbine quarterly report from 2003) and two X-ray detectors were utilized; (1) an amorphous silicon flat panel area detector with a spatial resolution of 400 μm/ pixel, and (2) a linear CMOS based detector with a spatial resolution of 83 μm/ pixel. An example of a X-ray CT reconstruction from the CMOS linear detector is shown in Fig. 4. To quantify the detectability of the seeded defects using the two detectors, the relative 16-bit grey level from in the flat-bottom holes were compared to an undamaged region from each reconstruction. The grey scale difference was plotted and is shown in Fig. 5 for each flaw in each of the three sections. It is apparent that the flaw detectability of data from the high resolution CMOS detector is much better than the lower resolution area detector. It should be noted that the

RID1620 detector with 400 µm pixels could not resolve the 0.4 mm diameter hole in the 178 mm diameter section, but the CMOS detector was able to resolve this easily with a 7000 grey scale difference in the 16-bit image.

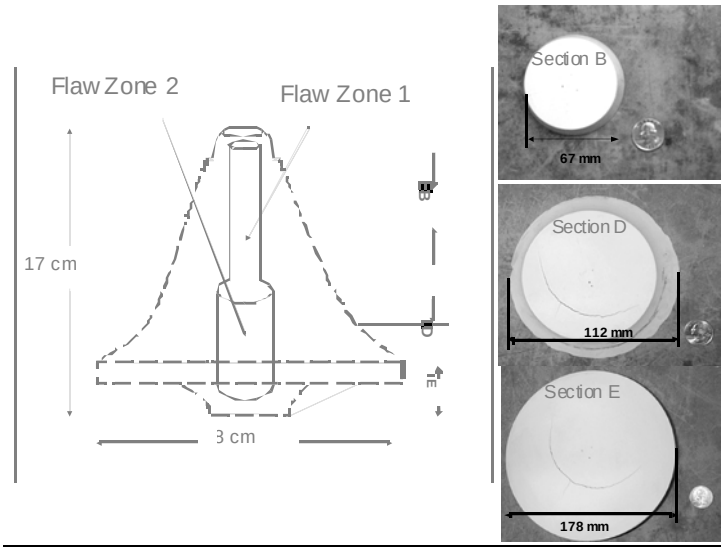

Fig. 3. Schematic diagram of unbladed gelcast AS800 microturbine rotor showing location of sections and digital photographs showing the seeded defects in sections.

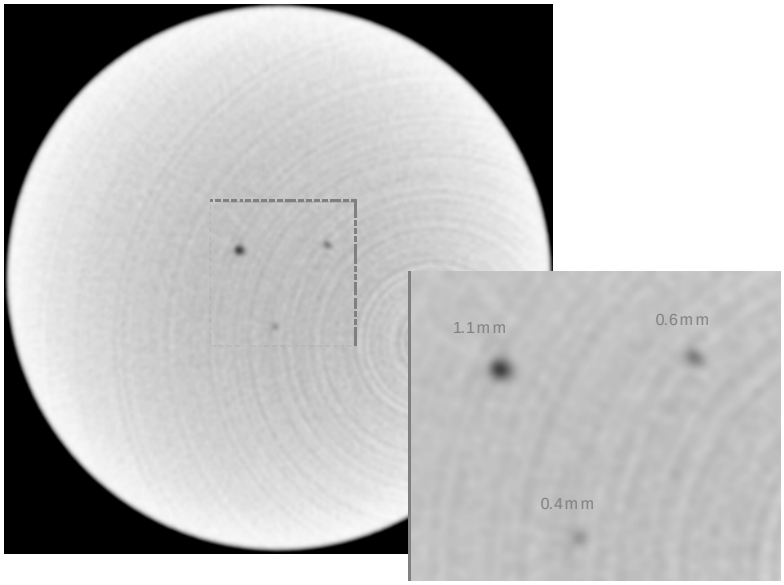

Fig. 4. CT reconstruction of the 67 mm diameter section showing the three seeded defects.

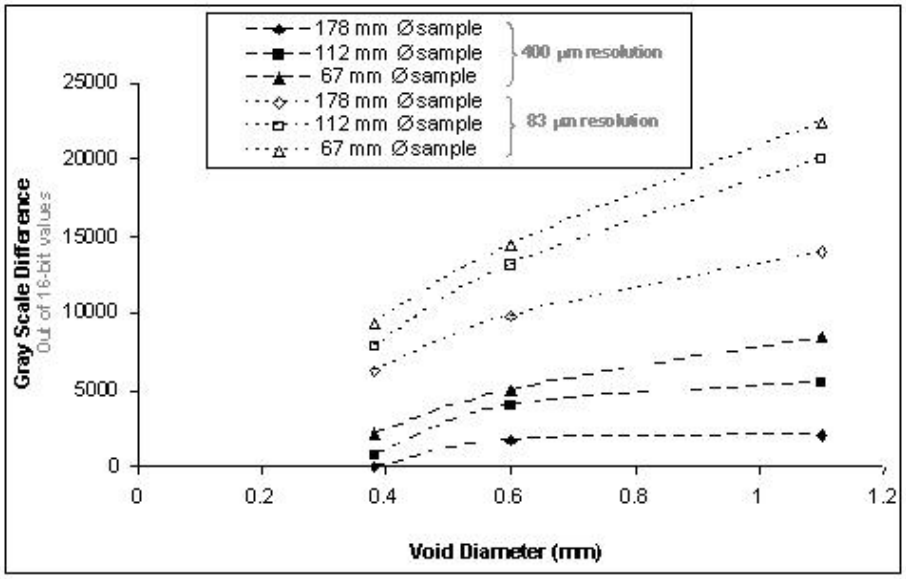

Fig. 5. Plot showing the resolution of the two detectors to identify the seeded defects

Status of milestones

A. Demonstrate high-speed 3D-X-ray computed tomography to detect critical sized flaws in full-sized monolithic rotors. The new CMOS 80µm detector has allowed detection of necessary flaws. However, speed of reconstruction for 3D volumes is still too slow and work is progressing with the Beowolf Cluster.

B. Complete installation of software for modeling laser scatter and demonstrate the ability to predict sensitivity of detection in EBCs. The software, Emflex, was installed on a Sun Blade 100 computer. The "field-solver" software, EMFlex, is now running and parameteric variables are now being added. The first reflection mode data set has been run. This allows comparison between the experiments and theory.

Industry/National Lab Interactions

1. Discussions took place with staff from Saint-Gobain Industrial Ceramics and Plastics as it was Saint-Gobain who provided the OCT system.
2. Discussions continued with staff of Solar Turbines , Siemens-Westinghouse and COI relative to oxide/oxide composites
3. Discussions also continued with staff of Northwestern University relative to EBCs for monolithic materials

Problems encountered/resolved

The RID1620 large area x-ray detector has now been returned to service and is working well after repair and modification. We have also now have excellent results with the new large length, 36-inches, CMOS linear array detector. The RID1620, with 200um square pixels, had to be returned to PerkinElmer for repair.

Trips/meetings

1. W.A. Ellingson attended the 28th International Cocoa Beach Conference and Exposition on Advanced Ceramics and Composites held January 25-30, 2004 in Cocoa Beach, FL.

2. C. Deemer attended the 28th International Cocoa Beach Conference and Exposition on Advanced Ceramics and Composites held January 25-30, 2004 in Cocoa Beach, FL. He gave a paper titled "Improved Reliability of High-Temperature Ceramic Microturbine Components through High-Speed X-ray Computed Tomography."

3. R. Visher attended the 28th International Cocoa Beach Conference and Exposition on Advanced Ceramics and Composites to be held January 25-30, 2004 in Cocoa Beach, FL. He presented a paper titled "Initial Investigation of Optical Coherence Tomography for Nondestructive Evaluation of Ceramic Coatings."

4. W. A. Ellingson plans to attend the International Gas Turbine Conference to be held in Vienna, Austria, June 13-17, 2004. He will present a paper titled" Optical Coherence Tomography as a Nondestructive Evaluation method for Ceramic Coatings."

CHARACTERIZATION OF ADVANCED CERAMICS FOR INDUSTRIAL GAS TURBINE/ MICROTURBINE APPLICATIONS

Mechanical Characterization of Monolithic Silicon Nitride Si_3N_4

R. R. Wills and S. Goodrich
University of Dayton Research Institute
300 College Park, KL-165, Dayton, OH 45469-0162
Phone: (927) 229-4341, E-mail: roger.wills@udri.udayton.edu

Objective

The objective of this project is to work closely with microturbine materials suppliers to characterize monolithic ceramics and provide the data obtained to microturbine manufacturers via a website database. User-friendly software, that will allow prospective users to readily compare different silicon nitrides, will also be developed. This project consists of the following four tasks.

Task 1: Evaluate Strength and Mechanical Properties of New Materials

This task is motivated by the materials needs of the microturbine manufacturers and the ceramic component suppliers. Consequently, Task 1 will focus on the generation of key mechanical property data for these materials with emphasis on strength, strength distribution, time-dependent failure, elastic properties, and fracture toughness. In particular, the effects of water vapor are very important.

Continued testing and evaluation of SN281/282 at 1400°C will be conducted by dynamic stressing and creep in air and water vapor. Baseline mechanical property data will also be measured for materials supplied by Kennametal and Saint Gobain Advanced Ceramics as part of their materials development effort funded by ORNL. The initial focus will be on measuring creep flexure strength. For new materials and EBC systems the focus will be on determining other properties such as thermal expansion, thermal diffusivity, hardness, elastic modulus and fracture toughness. This type of data is needed to support finite elements analyses.

Task 2: Develop "User Friendly" Software for Searching Existing Mechanical Properties Database

UDRI has received a number of requests from microturbine manufacturers for strength and time-dependent mechanical property data for current silicon nitride and silicon carbide ceramics. The current database contains a number of searchable PDF files and an Excel database containing the individual strength and creep data points by material for different temperatures. Integration of the site, with the National Aeronautics and Space Administration (NASA) Glenn's Ceramics Analysis and Reliability Evaluation of Structures (CARES)/Life software, will allow the user to predict reliability and life of various advanced ceramic materials. This tool will aid designers in their search for application-appropriate advanced ceramic materials.

The CARES computer code has a specific input format, but the existing data format used in the website is not compatible with this format. This task will focus on generating these input files for all the existing data and for data generated on new materials. In addition, the website will be redesigned and given a new URL to facilitate easier access.

Task 3: Screening of Novel Oxidation Resistant and EBC Compatible Silicon Based Ceramics

Above 1100°C, the long-term reliability of structural ceramic components is limited by loss of material through water vapor enhancing the corrosion of silicon based structural ceramics. This has necessitated the development of multilayer environmental barrier coatings (EBCs) to protect the underlying structural ceramic. In this task, UDRI will screen potential new EBC coating materials such as the aluminum silicon carbides for which no or little data currently exists. The primary screening test will be oxidation in water vapor. For new materials and EBC systems, focus will also be on determining other properties such as thermal expansion, thermal diffusivity, hardness, elastic modulus and fracture toughness, which are needed to support design work using finite element analyses.

A second approach to solving this problem is not to coat the silicon nitride but to fabricate composite silicon nitrides that contain 10-30 mol % of an oxidation resistant second phase. Studies on silicon nitride-barium aluminosilicate ceramics have shown that good mechanical properties can be obtained despite the relatively high amount of second phase. This task will concentrate on the preparation and characterization of two-phase silicon nitrides containing alkali aluminosilicates. Emphasis will be on determining the oxidation behaviour of such composites in water vapor.

Task 4: Mechanical Properties and Failure Mechanisms of EBC Coated Materials

In this task, UDRI will use its capabilities and expertise to examine the mechanical properties of EBC coated structural ceramics to determine the adhesion and reliability of the coating under load at elevated temperature.

Highlights

Dynamic fatigue testing of Kyocera's SN281 silicon nitride at 1400 and 1500°C in saturated water vapor gave slow crack growth exponents of 61 and 43, both values being higher than found in an air environment. Oxidation of aluminum silicon carbide in air at 1500°C obeyed parabolic kinetics with a dual oxide layer being formed. The database website has been modified with input files for the CARES computer design code. Files for AS-800, SN88, NT154 and GS44, and GN-10 silicon nitrides have been added.

Technical Progress

Dynamic Fatigue of Kyocera SN-281 Silicon Nitride in Air /Water Vapor Atmosphere

A water generating system was set up to flow water vapor saturated air as the atmosphere around each specimen undergoing dynamic fatigue testing at 1400 and 1500°C. The system consisted of an air pump, a flowmeter, several water bubblers contained in a constant temperature water bath, and a hygrometer immediately before the furnace. The stainless steel tubing carrying the air/water vapor mixture to the furnace was heated to 150°C to prevent condensation of water prior to it entering the furnace surrounding the test specimen. The hygrometer reading was 60°C.

Dynamic fatigue testing at 1400 and 1500°C was conducted using stressing rates of 0.003 and 30 MPa/s. While fracture origins are frequently difficult to discern in this grade of silicon nitride, it appeared that fracture occurred at surface flaws based upon optical and scanning electron microscopy. Figures 1 and 2 compare the slow crack growth behaviour at 1400 and 1500°C in both ambient air and the air /water vapor atmosphere. All the graphs were calculated using regression analysis.

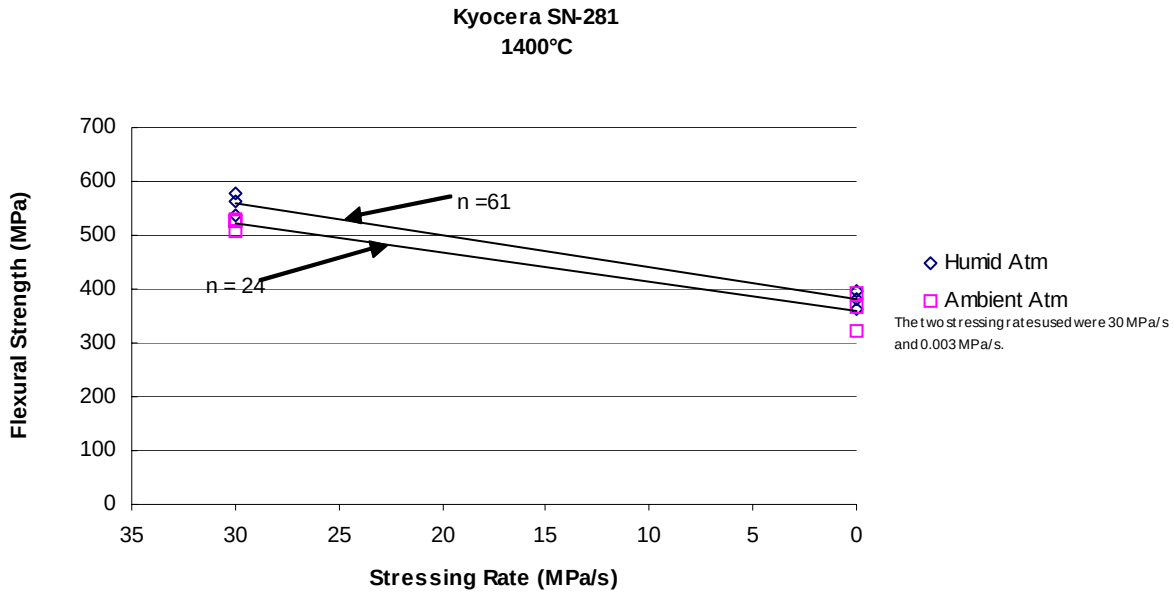

Figure 1. Dynamic Fatigue of SN281 in Air and Air/Water Vapor Atmospheres at 1400°C.

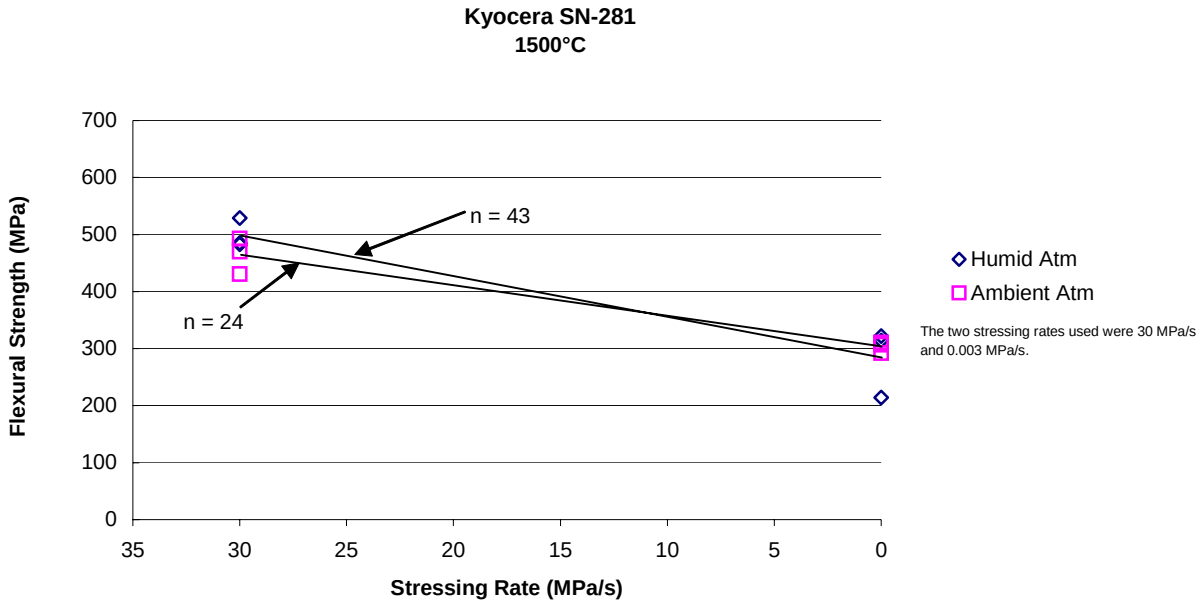

Figure 2. Dynamic Fatigue of SN281 in Air and Air/Water Vapor Atmospheres at 1500°C.

While the crack growth rates in air are identical (N=24) the addition of water vapor to the atmosphere reduces crack growth rates. This is consistent with a crack blunting mechanism due to oxidation of the silicon nitride during dynamic fatigue. Higher oxidation rates at the higher temperature in the air/water vapor atmosphere would also be expected to increase the crack growth exponent, but this is not what is observed. Rather the exponent dropped from 61 at 1400°C to 43 at 1500°C. In a water vapor saturated environment, the two principal chemical reactions occurring at the crack tip are oxidation of the silicon nitride to silica and volatilization of tetrahydroxysilane. One possible explanation for the change in slow crack growth exponent is that volatilization of material in front of the crack tip is occurring and that this is a more influential factor than oxide growth in governing crack tip velocity. Removal of local material in and around the crack tip would certainly enhance crack velocity.

Most silicon nitrides exhibit crack growth exponents in air that decrease with increasing temperature. For example, NT164 has n values of 159, 35 and 18 at 1038, 1150 and 1350°C. In contrast, SN 281 has a constant n of 24 in air at both 1400 and 1500°C. The classic explanation of slow crack growth invokes crack formation ahead of the main crack as a result of grain boundary sliding facilitated by a viscous grain boundary phase. Since the viscosity of the grain boundary phase decreases with increasing temperature, the value of n decreases. This mechanism does not appear to be operating in the SN281 silicon nitride. Rather, there appears to be some threshold based mechanism since an increase in temperature does not cause enhanced slow crack growth. Damping studies by Pezzotti, et al.[(1)] show that the lutetium silicate phases entrapped at multiple grain junctions lock grain motion and retard grain boundary sliding in this temperature regime. Grain boundary sliding and diffusional flow do not occur until >1620°C.

The most likely model to explain the above data would be one that assumes that a crack propagates along the grain boundary by a process of surface and grain boundary diffusion in which adjoining grains behave elastically. Chang[2] developed such a model and showed good agreement between theory and experiment with a set of creep crack growth data on several Si-Al-O-N samples.[3] In this model:

$$K/K_{min} = 1/2[(v/v_{min})^{1/2} + (v/v_{min})^{-1/2}] \quad (1)$$

where K is the stress intensity factor, $K_{min} = 1.69\ K_{ic}$ is the minimum K below which no crack growth is predicted, K_{ic} is the critical stress intensity factor, v is the crack tip velocity , and v_{min} is the minimum crack velocity for $K=K_{min}$.

It seems likely that slow crack growth in SN281 follows this model.

Upgrading the Website

The website has been modified so that users can see that CARES input files are being added to the site. Files for AS-800, SN88, NT154 and GS44, and GN-10 silicon nitrides have been added. These files include test conditions, specimen geometry, surface finish and failure stresses. The modified website can be viewed at http://www.udri.udayton.edu/design_data_files.

Aluminum Silicon Carbides: a Potential EBC

Aluminum containing ceramics generally possess good oxidation resistance and are thus worthy of consideration as EBCs. While many of these have been considered or are currently under investigation as potential EBCs, one group of aluminum containing ceramics that has received little attention to date is the aluminum silicon carbides. Although little property data exists for these materials, initial oxidation studies on Al_4SiC_4[4] indicate the formation of a thin protective oxide layer of alumina and mullite. The objective of the current task is to determine the oxidation resistance of these materials in water vapor and to determine some of their basic properties and, hence, ascertain whether or not these materials can be considered as viable EBC materials.

Small rectangular plates approximately 0.6 in x 0.3 in x 0.04 in were cut out of the hot pressed billet. After cleaning, the Al_4SiC_4 was subjected to oxidation at 1500°C in air. An initial sample was oxidized for 48 hours, and the oxidation kinetics were determined over 144 hours in air by weighing the sample at several intervals.

The data was examined for linear, parabolic and logarithmic kinetics. Excellent correlation with parabolic kinetics (see Figure 3) was found. This form of oxidation kinetics is also typically exhibited by silicon carbide and silicon nitride ceramics. Both samples showed two layers covering the Al_4SiC_4. Figure 4 shows these two layers formed after oxidation at 1500°C for 144 hours. The outer surface was rough and porous, as shown in Figure 5, and not what one would like to see for a protective oxide.

After 48 hours, the thicknesses of the inner and outer layer were 60 and 40 microns. After 144 hours, the inner layer is largely unchanged in thickness but the outer layer had grown to 75 microns. Based upon x-ray diffraction analysis and elemental mapping, the outer oxide layer is mainly alumina with some mullite and the inner layer a mullite layer. The difference in thermal expansion of these materials explains the delamination seen between these layers in some of the micrographs. The alumina grains are blocky and approximately 10 microns in size, whereas some acicular grains can be seen in the inner mullite layer.

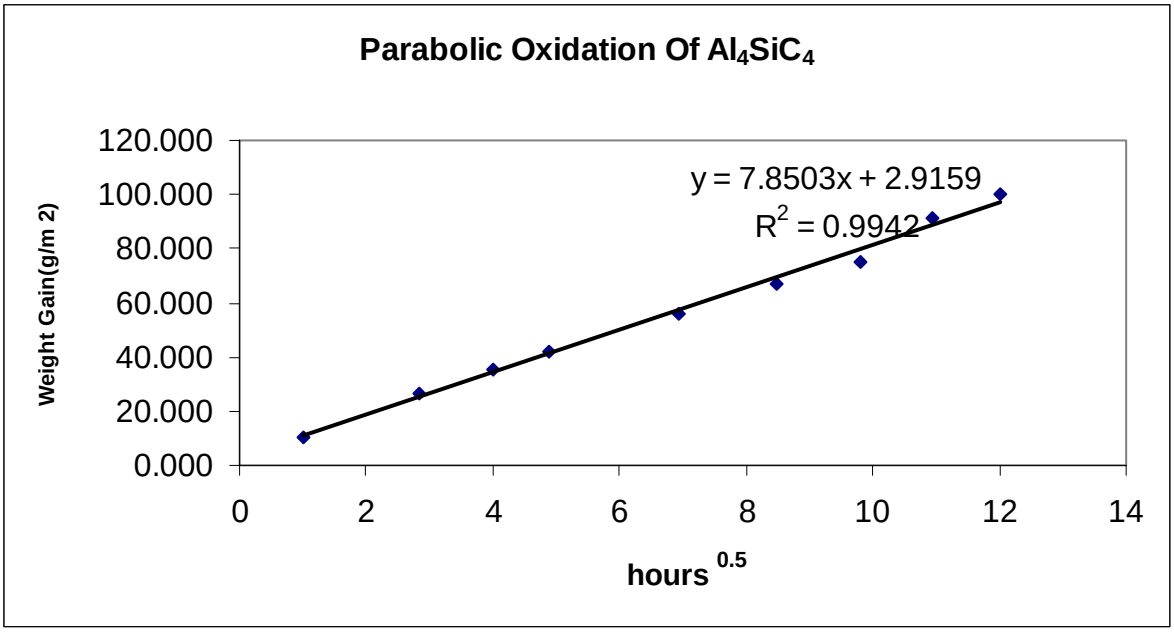

Figure 3. Parabolic Oxidation Kinetics of Al_4SiC_4 in Air at 1500°C.

Al_4SiC_4 Layer 1 Layer 2

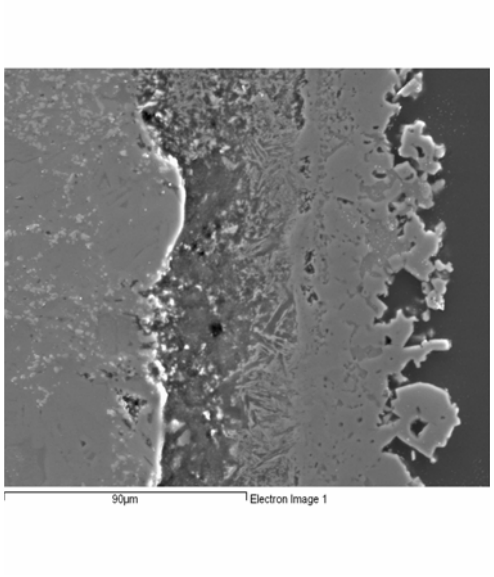

(a)

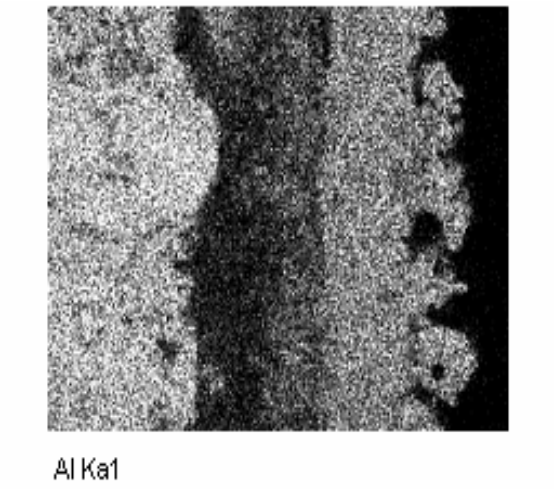

(b)

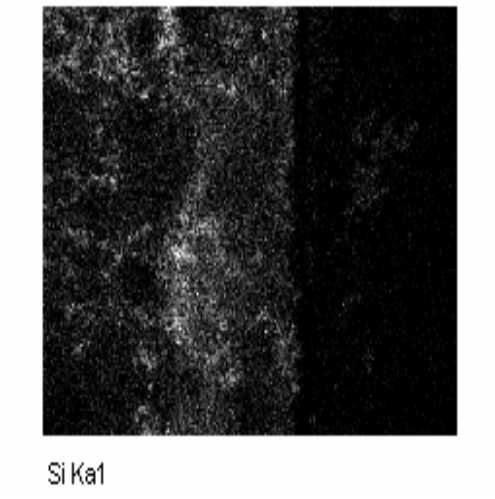

(c)

Figure 4. Cross Section of Two Surface Oxide Layers on Al_4SiC_4. (a) On the Al_4SiC_4 after exposure to air at 1500°C for 144 hours together with aluminum (b) and silicon (c) EDAX scans.

(Note: the inner oxide layer contains much less aluminum than either the substrate or the outer oxide layer.)

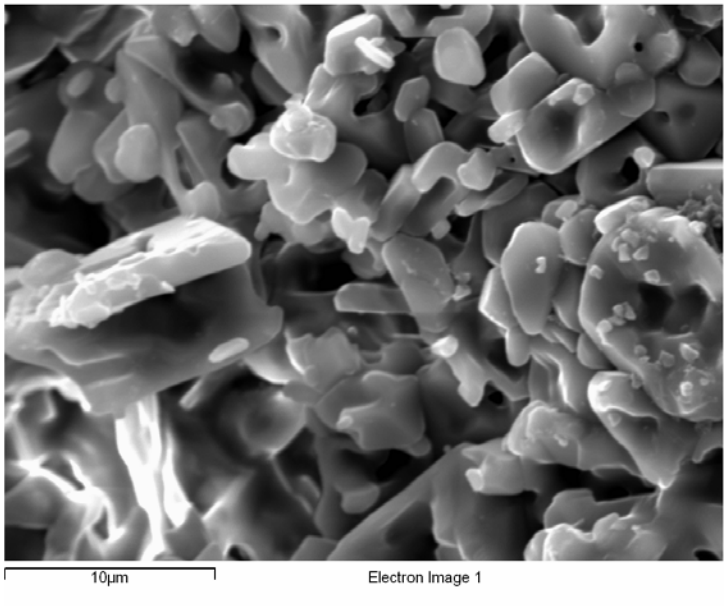

Figure 5. Microstructure of Surface Oxide Layer Showing Internal Porosity.

Status of Milestones

1) Testing and Evaluation of SN-281/282

Slow crack growth testing in both air and air/water vapor at 1400 and 1500°C has been completed.

2) Testing of Materials from Kennametal and St. Gobain

Heat capacity of NT154 has been completed.

3) Evaluation of Aluminum Silicon Carbide

Sample preparation and oxidation in air has been completed. Oxidation kinetics in water vapor and thermal properties need to be completed.

Industry and Research Interactions

A visit was made to Oak Ridge National Laboratory and a presentation given. A brief discussion was held with John Holowczak and Ellen Sun regarding oxidation of BSAS. One ORNL paper was reviewed.

Problems Encountered

None

Publications

None

References

1. G. Pezzotti, K. Ota, Y. Yamamoto, and Hua-Tay Lin, "Elementary Mechanisms behind the High Temperature Deformation Behaviour of Lutetium Doped Silicon Nitride," *J. Amer. Ceram. Soc.* 86(3), 471(2003).

2. T. Chang, "A Diffusive Crack Growth Model for Creep Fracture," *J. Amer. Ceram. Soc.* 65(2), 93 (1982).

3. M.H. Lewis and B.S.B. Karunaratne, "Determination of High Temperature K_1 –V Data for Si-Al-O-N Ceramics," pp 13-32 in Fracture Mechanics Methods for Ceramics, Rocks and Concrete. Edited by S.W. Freiman and E.R. Fuller, Jr., ASTM STP 745 (1981).

4. J. Schoennahl, B. Willer, and M. Daire, "Preparation and Properties of Sintered Materials in the Systems Si-Al-C and Si-Ti-C," p. 338 in Materials Science Monographs 4: Sintering- New Developments, Elsevier Science Publishing, Amsterdam (1979).

Microstructural Characterization of CFCCs and Protective Coatings

K. L. More and P. F. Tortorelli
Metals and Ceramics Division
Oak Ridge National Laboratory
Oak Ridge, Tennessee 37831-6064
Phone: (865) 574-7788, E-mail: koz@ornl.gov

Objectives

Characterization of CFCC materials and CFCC combustor liners after exposure to simulated (ORNL's Keiser Rig) and actual (engine tests) combustion environments

Exposures of candidate environmental barrier coatings (EBCs) to high water-vapor pressures (in Keiser Rig) to determine thermal stability and protective capability

Work with CFCC and coating suppliers/manufacturers to evaluate new/improved ceramic fibers, protective coatings, and composite materials

Highlights

During this quarter, a meeting was held at Solar Turbines on March 31 to determine an evaluation plan for two sets of CFCC/EBC combustor liners which were exposed at either the Chevron and Malden Mills engine test sites. Research staff from ORNL, UTRC, and Solar Turbines attended the meeting.

Technical Progress

Two sets of CFCC/EBC combustor liners have recently been removed from engine tests (conducted by Solar Turbines) and will be evaluated microstructurally and mechanically at ORNL. Details of the CFCC/EBC combustor liners and engine test conditions are as follows:

Chevron Test #6

Inner Liner –Hi-Nicalon fiber, melt-infiltrated (MI) SiC/SiC liner with a Si/BSAS EBC (no intermediate layer) – produced by Goodrich, Inc.

Outer Liner – enhanced SiC/SiC (CVI) liner with a Si/(Mullite+BSAS)/BSAS EBC – produced by GE Power Systems Composites

Inner liner ran for 5,135 hours, 43 starts. Outer liner was first refurbished liner that ran initially for 7,238 h, was refurbished, and ran an additional 5,135 h in Chevron Test #6. Only inner liner will be evaluated at ORNL (outer liner may be refurbished again for additional engine testing).

Malden Mills #3

Inner Liner – Tyranno fiber, MI SiC/SiC liner with a Si/SAS EBC – produced by GE Power Systems Composites

Outer Liner – Tyranno fiber, MI SiC/SiC liner with a Si/(Mullite+SAS)/SAS EBC – produced by GE Power Systems Composites

Inner and outer liner set ran for a total of 8,368 h and 32 starts (engine #2) before being removed from engine test due to extensive EBC loss on inner liner. Both inner and outer liners will be evaluated at ORNL.

All three of the liners to be evaluated were bulk cut at Solar Turbines and have been received at ORNL for additional sectioning into coupons for microstructural characterization and mechanical testing. These liners will provide for several unique characterization opportunities to add to an existing and extensive database on characteristics of engine-tested CFCC/EBC combustor liners. To date, the primary focus of the engine tests and subsequent characterization has been on evaluating the current state-of-the-art BSAS-based 3-layer EBC system applied to several different CFCC liners. Previous engine tests conducted at both Chevron (test #5) and Malden Mills (tests #1 and #2) had CFCC liners with the 3-layer BSAS-based EBC. Application of this EBC system to the gas-path surfaces of the CFCC liner increased the liner lifetimes significantly, however, significant volatilization of the BSAS top-coat was observed on these coated liners. The liners to be evaluated in this new study have different EBC systems; and inner liner with only a 2-layer Si/BSAS EBC and inner and outer liners with SAS-based EBCs.

Photographs of the gas path surfaces for each of the liners described above are shown in Figures 1, 2, and 3. Figure 1 shows the inner liner with a Si/BSAS 2-layer EBC from Chevron engine test #6. Extensive loss of the EBC was observed after only 5,135 h engine testing. Figure 2 shows the surface of the inner liner from Malden Mills engine test #3 which had a Si/SAS 2-layer EBC. Nearly the entire CFCC was exposed due to loss of the EBC. The outer liner from the Malden Mills engine test #3, Figure 3, exhibited minimal EBC loss.

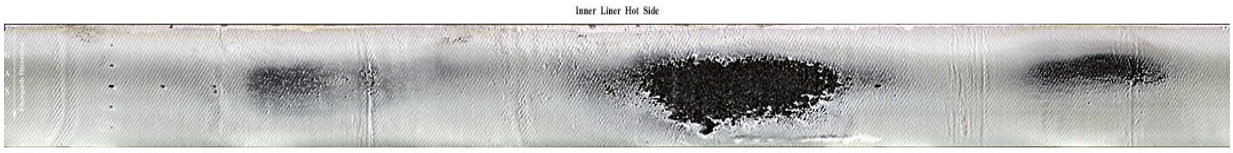

Figure 1. Gas-path surface of inner liner from Chevron engine test #6 showing localized loss of Si/BSAS EBC.

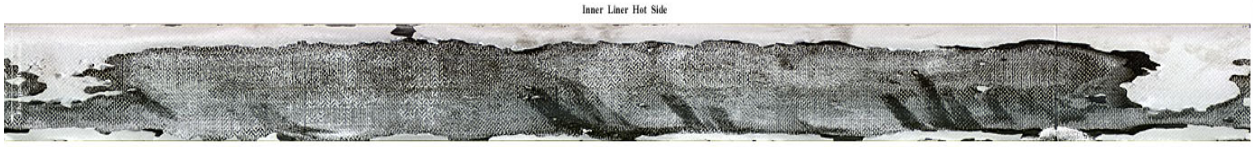

Figure 2. Gas-path surface of inner liner from Malden Mills engine test #3 showing extensive loss of Si/SAS EBC across entire surface.

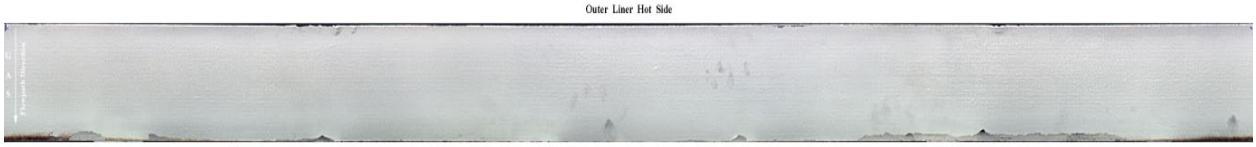

Figure 3. Gas-path surface of outer liner from Malden Mills engine test #3 showing minimal loss of Si/(Mullite+SAS)/SAS EBC.

Status of Milestones

06/04 Milestone — Prepare a report and present results on the evaluation of oxide/oxide composite materials exposed in the Keiser Rig for use as microturbine or stationary gas turbine combustor liners. (June 2004)

This milestone is in progress and will be completed on time. ATK-COI Ceramics, Inc. oxide/oxide composite material, A/N720, is currently being exposed under simulated microturbine exhaust conditions in ORNL's Keiser Rig at 1200°C for 3000 h. Results are completed for exposure of the same material for 3000 h @ 1135°C.

Industry Interactions

1. Study underway with Andy Szweda of ATK-COI Ceramics, Inc. to expose A/N720 oxide/oxide composites in the Keiser Rig at 1200°C for 3000 h in 1000 h increments. Post-exposure characterization (microstructural and mechanical) is being conducted.

2. Visited ATK-COI Ceramics, Inc. on March 30, 2004 and gave separate presentations summarizing work on (1) oxide/oxide exposures in the Keiser Rig, (2) high water-vapor pressure experiments in the Keiser Rig, and (3) microstructural evaluation of PIP-processed CFCCs.

3. Attended meeting at Solar Tubines, Inc. on March 31, 2004 (with UTRC) to discuss evaluation of CFCC/EBC combustor liners recently removed from engine tests at Chevron and Malden Mills.

4. Collaboration is ongoing with UTRC to expose BSAS, BAS, and SAS coupons and Si-based standards in the Keiser Rig at very high (~20 atm) water-vapor pressures to induce volatilization (see DE Quarterly Report for 10/03-12/03).

5. Study underway with Rishi Raj from the University of Colorado to expose candidate EBC compositions in the Keiser Rig at 1200°C and 10% H_2O. Pre- and post-exposure microstructural characterization is being conducted to evaluate stability of experimental coatings.

Problems Encountered

None

Publications/Presentations

1. P.F. Tortorelli and K.L. More, "Evaluation of EBCs in the Keiser Rig," presented at the DER EBC Workshop, Nashville, TN, Nov. 18-19, 2003.
2. K.L. More, E. Lara-Curzio, P.F. Tortorelli, A. Szweda, D. Carruthers, and M. Stewart, "Evaluating the High Temperature Stability of an Oxide/Oxide Composite Material at High Water-Vapor Pressures," presented at the 28th Annual Advanced Ceramics and Composites Conference, January 26-29, 2004, Cocoa Beach, FL.

DEVELOPMENT OF MONOLITHIC CERAMICS AND HIGH-TEMPERATURE COATINGS

Kennametal's Hot-Section Materials Development

R. Yeckley, J. R. Hellmann, K. M. Fox, D. J. Green, and E. C. Dickey
Kennametal Inc.
1600 Technology Way, P.O. Box 231, Latrobe, PA 156-0231
Phone: (724) 539-4822, E-mail: Russ.yeckley@kennametal.com

Objective

Determine potential of an existing structural SiAlON that is being manufactured for other applications that, commensurate with the requirements of advanced microturbines shows potential for strength, environmental stability, and manufacturability for complex shapes.

Highlights

Keiser rig tests are completed for two SiAlONs from the screening matrix. Both SiAlONs have the higher rare earth content. SiAlON ab832 performed poorly. The second SiAlON ab532 is comparable to silicon nitrides previously tested.

Technical Progress

Two SiAlONs from the screening matrix were sent to K. More at ORNL for corrosion testing in the Keiser Rig. The two SiAlONs are ab532 and ab832. Both have the higher rare earth content. The mechanical properties for these SiAlON are shown in Table 1. Samples from each SiAlON were run at 1200 C, 3 % H_2O and 1200 C with 20% H_2O. The SiAlON behaviors are quite different. SiAlON ab832 has a very high corrosion rate. SiAlON ab532's corrosion behavior is very similar to other silicon nitrides tested. The corrosion resistance may be related to the SiAlON solid solution. SiAlON ab532 with the better corrosion resistance and has greater substitution of Al, O in the β SiAlON and α SiAlON crystal structures. Weight loss and reaction layer thickness after 2000 hours are summarized Figure 1 and Figure 2 for the two SiAlONs. Weight loss with time is plotted in Figure 3 for ab532. Morphology of the corrosion layer is very similar to silicon nitride. The corrosion mechanism in water vapor appears to be the same for SiAlON as silicon nitride. Figures 4-7 are SEM photos depicting the corrosion layer observed on SiAlON ab532.

Table 1 SiAlON Properties

Composition ID	ab832	ab532
Hardness (GPa)	18.72±0.35	17.38±0.58
Fracture Toughness, K_{1C} (MPa√m)	7.36±0.22	5.73±0.16
Fracture Strength (MPa) at RT	783	651
Weibull Modulus at RT	6.06	5.92
Fracture Strength (MPa) 1204°C	540	393
Weibull Modulus at 1204°C	6.25	9.75
α-SiAlON Content (w/o)	44	35.8
α-SiAlON x'	0.248	0.40
ß-SiAlON z'	0.376	0.820

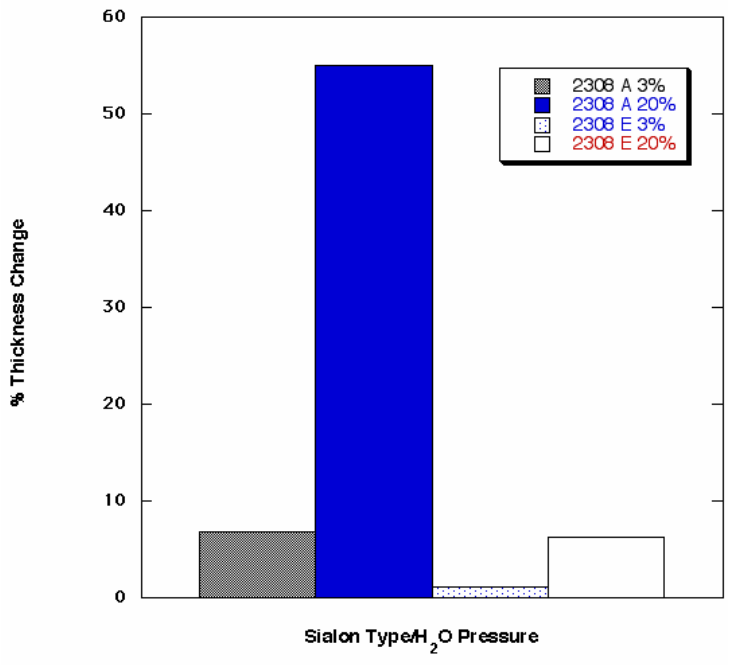

Figure 1. Thickness change after 2000 hours in Keiser Rig. In the legend, 2308A is ab832 and 2308E is ab532.

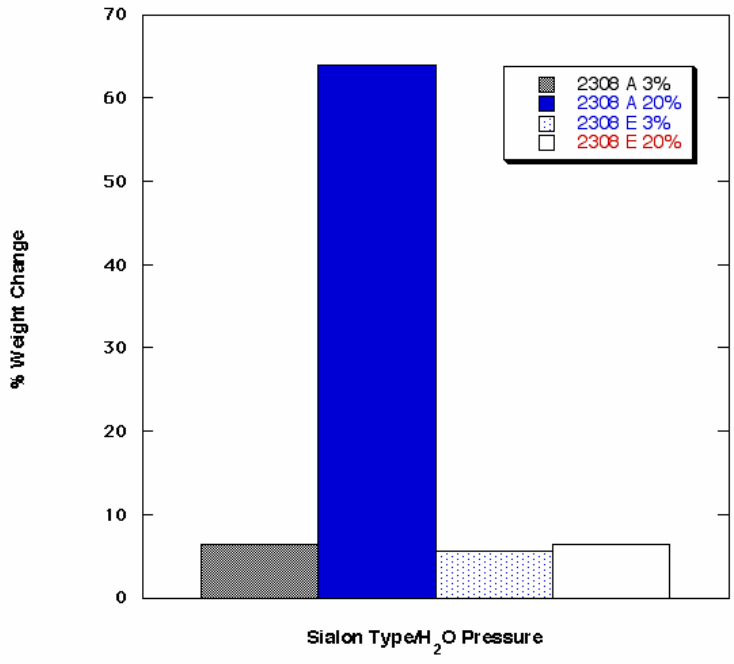

Figure 2. Weight change after 2000 hours in the Keiser Rig. In the legend, 2308A is ab832 and 2308E is ab532.

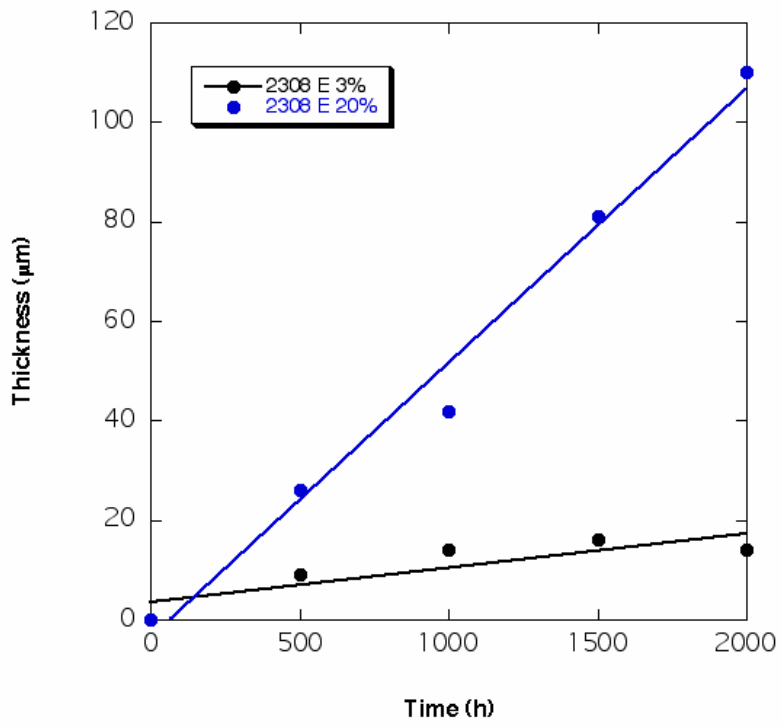

Figure 3. Thickness change with time for SiAlON ab532.

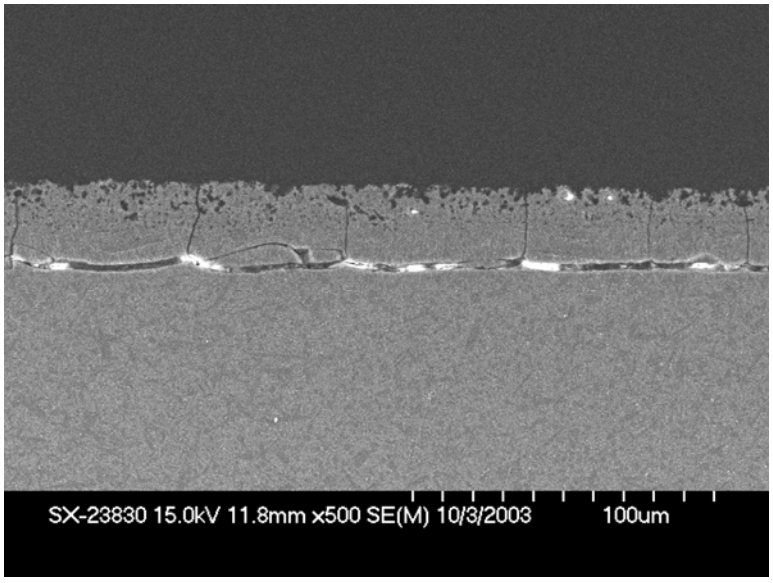

Figure 4. SEM micrograph showing corrosion layer after 500 hours in 20% water vapor for SiAlON ab532.

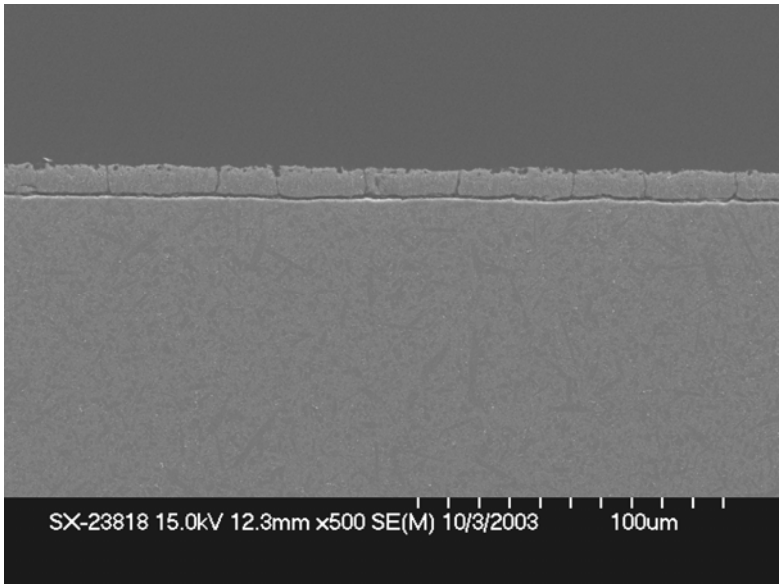

Figure 5. SEM micrograph showing corrosion layer after 500 hours in 3% water vapor for SiAlON ab532.

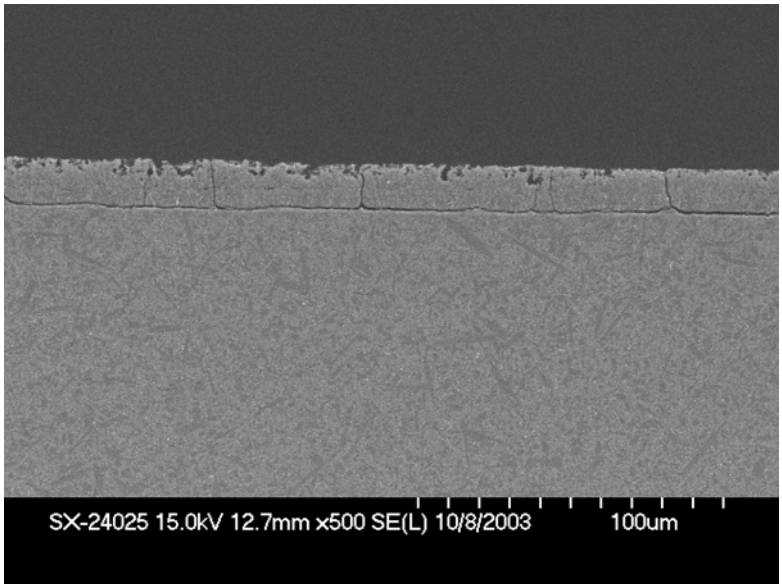

Figure 6. SEM micrograph showing corrosion layer after 1500 hours in 3% water vapor for SiAlON ab532.

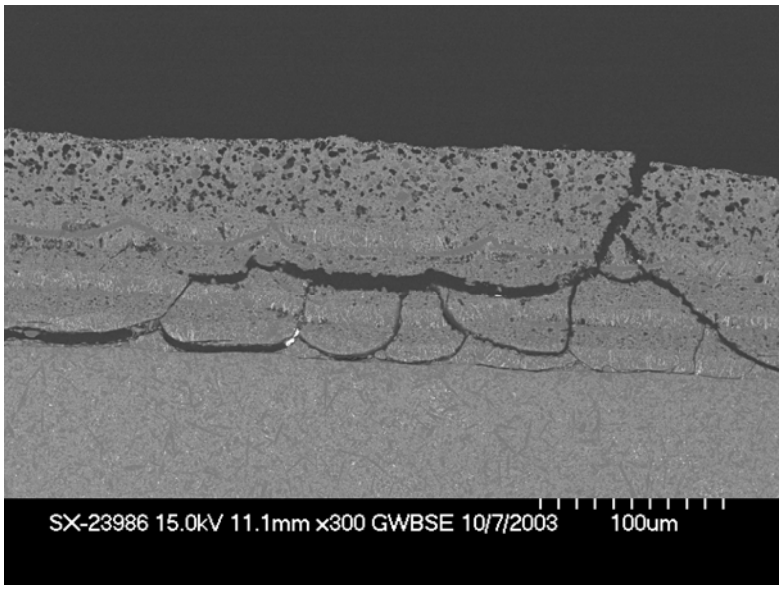

Figure 7. SEM micrograph showing corrosion layer after 1500 hours in 20% water vapor for SiAlON ab532.

Completion of the Keiser rig testing ends the work with the SiAlON screen matrix. SiAlON ab532 demonstrated that SiAlON could equal the corrosion performance of silicon nitride. Additional testing will be conducted on SiAlONs containing less rare earth additive.

Two SiAlONs from the matrix are selected for additional mechanical testing and environmental testing. The SiAlONs are ab831and ab531. These SiAlONs contain 30% less rare earth than the SiAlONs tested in the Keiser rig. Four tile of each SiAlON were sent for Keiser rig testing. Also, tiles are completed for flexure bar preparation. Strengths will be determined for the machined surface and as processed surface. Tensile rod blanks are completed and sintering will be completed in June.

The SiAlONs prepared in the screening matrix have β SiAlON z values ranging from 0.3 to 0.8. A similar range in β SiAlON z value exists between the two SiAlONs selected for continued evaluation. The SiAlON microstructure characteristics are similar at equivalent z values. The β SiAlON grains have a lower aspect ratio at higher z values. SEM images showed lower grain boundary volume with higher z SiAlONs. The grain boundaries were analyzed by TEM to determine whether a grain boundary film is present. The high z SiAlON ab582 has a high percentage of grain boundaries with no apparent amorphous film. A grain boundary is shown in Figure 8 with no amorphous film.

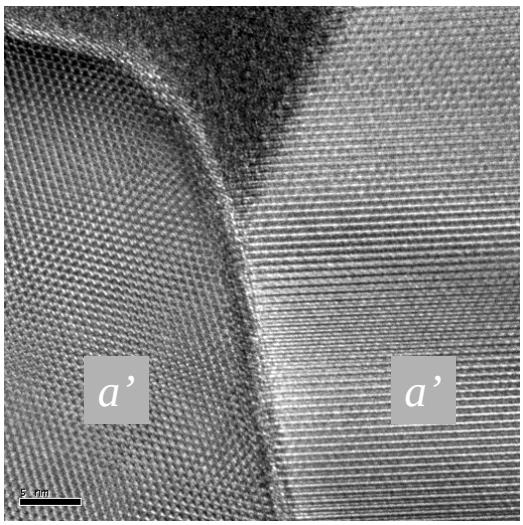

Figure 8. A grain boundary between α SiAlON grains. No amorphous film is apparent.

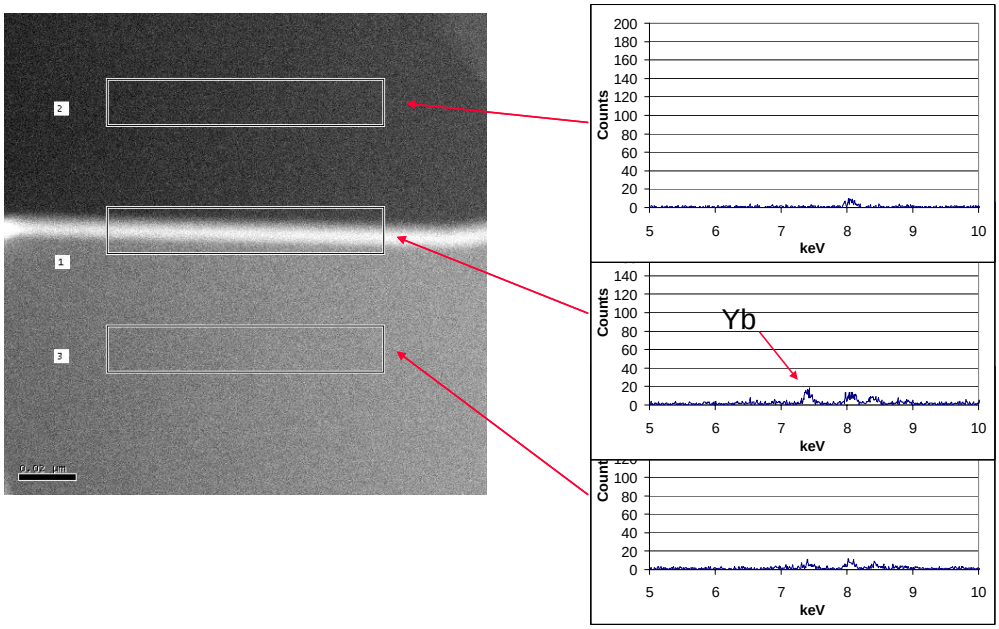

Figure 9. Amorphous film present in grain boundary between a β SiAlON and α SiAlON grain. Higher Yb is present in the grain boundary.

Many grain boundaries in the low z SiAlON, ab831, have a amorphous phase present as shown in Figure 9. Also grain boundaries with no amorphous phase were observed in ab831. Figure 10 is a grain boundary between α SiAlON grains. Figure 11 is a grain boundary between β SiAlON grains. EDS did not detect the presence of the rare earth at the grain boundary. The difference in Keiser Rig performance could be influenced by the grain boundary structure.

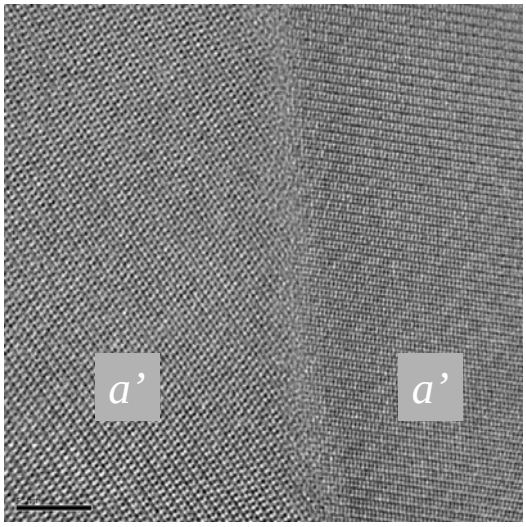

Figure 10. Grain boundary in SiAlON ab831.

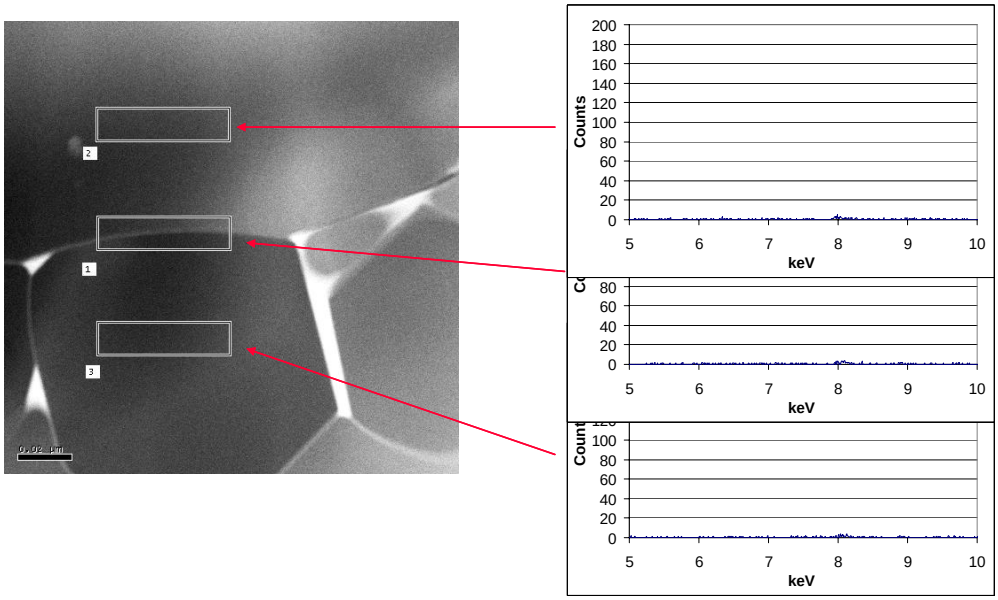

Figure 11. Grain boundary between β SiAlON grains. No Yb is observed at the interface suggesting there is not an amorphous film present.

The results from the first four hertzian creep tests are in Figure 12. The indenter is a 2mm diameter SiC cylinder. Profilometer trace of the impression shows that excellent alignment is achieved between the indenter and specimen surface. The creep tests are conducted on polished SiAlON surfaces. The creep rate differences between the two SiAlONs are interesting. SiAlON ab582 has 57 % α SiAlON and a small volume of grain boundary phase. SiAlON ab831 contains 31% α SiAlON and more grain boundary but exhibits lower creep. SiAlON ab582 microstructure is more equiaxed than ab831. SiAlON ab582 has a fracture toughness of 4.9 MPa $m^{1/2}$ compared to 6.9 MPa $m^{1/2}$ for ab831. The ab582's equiaxed structure may allow a greater grain boundary-sliding rate than ab831.

Temperature and stress will be varied in future creep experiments. ORNL provided NT154 for hertz creep testing as a comparison to the SiAlON. Also, ORNL will measure compressive creep of the SiAlONs for comparison with the hertzian creep tests.

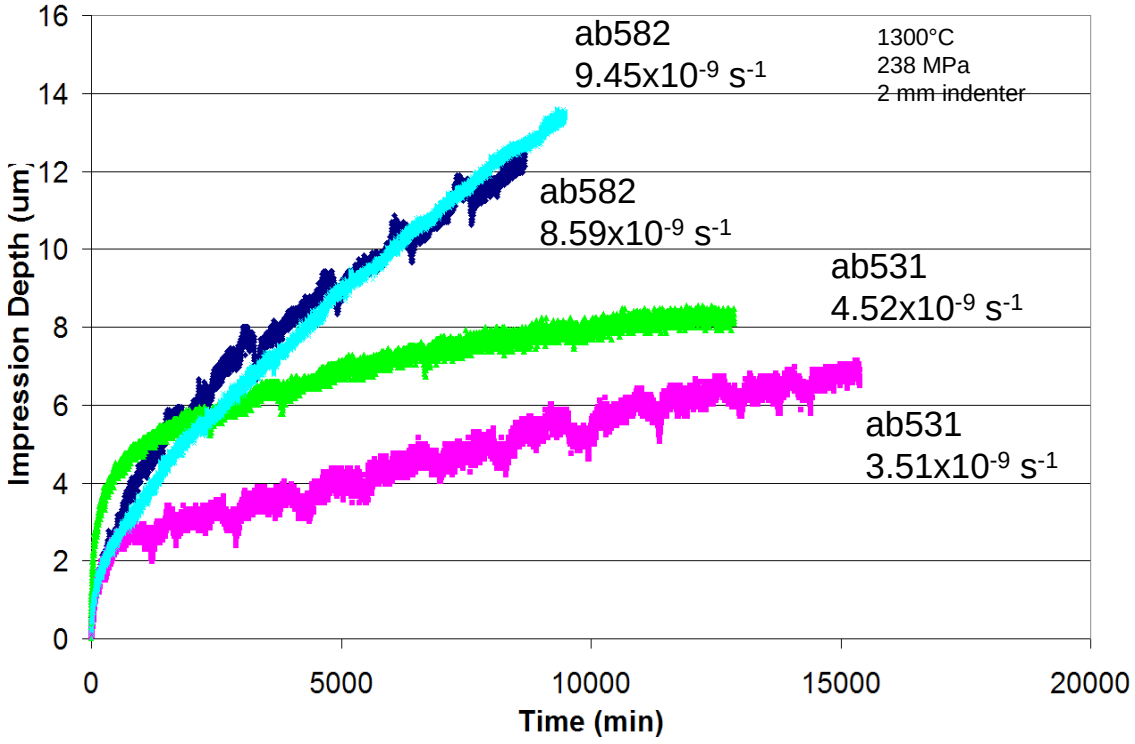

Figure 12. Deformations with time for the hertzian creep tests.

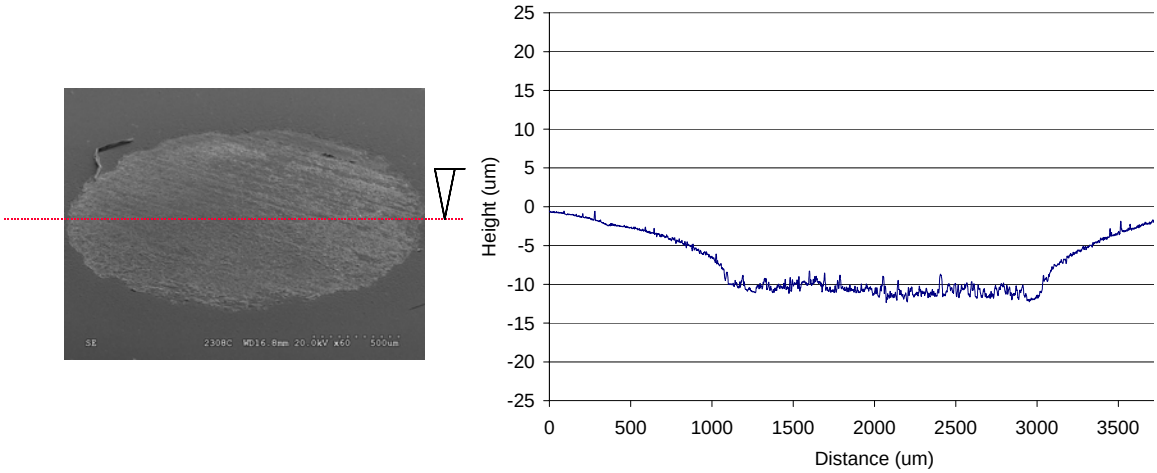

Figure 13. Excellent alignment is attained during creep tests as shown by the profilometer trace of the impression.

Status of Milestones

1) SiAlON compositional preliminary matrix - completed
2) Complete mechanical and microstructural characterization of initial SiAlON compositions.

Sept ‘04

a. Prepare flexure bars (ground and as processed surface) – Densification complete. Flexure bar finishing in process.
b. Tile for Keiser Rig testing – complete, sent to ORNL
c. Deliver tensile rods to ORNL – Densification scheduled for completion in June.

3) Colloidal Processing of Silicon Nitride Apr. ‘04

On schedule for completion in April. Final report and process transfer to Kennametal will occur in June.

4) Role of Microstructure and Crystalline Phase Evolution on Thermo-mechanical Properties of SiAlON Ceramics for Microturbine Applications Oct. ‘04

This effort is on schedule.

Problems Encountered

None

Publications/Presentations

Presented at the Amer. Cer. Society Annual Meeting: “Role of microstructure and crystalline phase evolution on thermomechanical properties of SiAlON ceramics for microturbine applications.” K. Fox, Prof. J Hellman and R Yeckley

Saint-Gobain Hot -Section Materials Development

R. H. Licht, Vimal K. Pujari, William T. Collins, James M. Garrett, Ara M. Vartabedian
Saint-Gobain Ceramics & Plastics, Inc.
Goodard Road, Northboro, MA 01532
Phone: (508) 351-7815, E-mail: Robert.h.licht@saint-gobain.com

Objective

The goal of this program is to develop and optimize a high temperature silicon nitride based ceramic material and process suitable for microturbine hot section component applications.

Highlights

The technical effort during this reporting period focused on a) the optimization of As-Processed (AP) surfaced properties of NT154 (PHASE 1) and b) to launch PHASE II program with activity leading to a recession resistant NT154 material and net-shape components.

Utilizing the proprietary new HIP process reported previously, the targeted AP strength of 700MPa was reproduced in the production HIP.

The Phase II effort to develop a robust solution for the "recession" of silicon nitride, in the gas turbine environment, was also launched. More specifically, the technical approach focused on two techniques to modify the silicon nitride surface. Namely, HEEPS (Hip Engineered Environmental Protection System) and Pack Cementation.

Technical Progress

The technical effort involves a two-pronged approach:

1. Material development
2. Net Shape Forming Development (NSFD)

1. MATERIAL DEVELOPMENT:

1.1 AP Strength Optimization

Optimization of the as-processed (AP) surface strength of NT154 using a larger, production HIP continued this period. As has been reported previously, a new proprietary HIP process, has been shown to reduce the reaction layer and the surface roughness of the dense NT154. The target AP strength of 700MPa, as reported previously using a smaller, laboratory-scale HIP furnace, has been duplicated in the production HIP. An excellent AP Strength of 717MPa was achieved. Based on the work to date, the desired conditions leading to target AP strength have been identified. We are working towards consistently reproducing the target AP strength.

1.2 Recession Mitigation

Material recession, due to volatilization in humid gas turbine environments, is an issue for silicon nitride and has been reported on in the literature. Phase II of the contract investigates recession resistant solutions for NT154. Two different approaches are currently being investigated internally:

a) HEEPS - HIP Engineered Environmental Protection Surface
b) Pack Cementation

1.2.1 HEEPS

Under the HEEPS approach, pre-sintered NT154 tiles were surface modified / dip coated with various suitable recession resistant compounds. Based on microprobe and micro-XRD analyses, the surface was not adequately modified. Some experiments are planned in an attempt to minimize the coating material migration and help develop the desired surface modification deemed to be suitable under a humid oxidative environment.

1.2.2 Pack Cementation

Some initial, scoping pack cementation experiments are underway. Dense NT154 tiles with AP and machined surfaces were embedding in various rare earth oxides at various temperatures and gaseous environments. SEM, EDS, and XRD were performed to characterize the modified surface layers. The analyses indicate the formation of rare-earth silicates up to depths of 8 m. Unfortunately, the rare-earth silicates have not formed a continuous layer to protect the base silicon nitride. Several pack cementation experiments are planned to investigate several parameters (time, temperature, environment, and powder bed). The goal is to change the surface of the silicon nitride to a continuous rare-earth silicate layer with sufficient depth. Pack cementation samples, along with the HEEPS specimens mentioned above, are being recession tested using a simplified screening test procedure developed at NRDC as described below.

Collaboration in this area, with Steve Nunn at ORNL, is also planned.

1.2.3 Recession Screening Test

A simple recession screening test has been developed at Northboro Research and Development Center (NRDC). The test will allow us to down select techniques and process parameters for further optimization. Suitable candidates will then be delivered to Karren More at ORNL for Keiser Rig Testing.

In the NRDC test, a controlled amount of humidified air is allowed to flow through a tube furnace which is maintained at a desired temperature. The test allows capability to control the $\%H_2O$ in the air, the flow rate, and the temperature in the furnace, with certain ranges. Preliminary tests conducted on baseline NT154, Pack Cemented and HEEPS specimens, as well as several only reference samples, show the evidence of recession. The results from a recent 72 hour test (temp=1200°C, $\%H_2O$=47%, flow rate=18cm/s) are shown in Table I, ranked from best to worst.

Table I: Internal Recession Test Results

Samples	Normalized mass change (mg/cm2/hour) Run #3
Y2O3 Sample	-4.9E-04
Al2O3 Sample	-1.5E-03
Yttria stabilized Zirconia Sample	-2.6E-03
NT154 Pack Cementation Sample #12	-3.1E-03
NT154 Pack Cementation Sample #8	-3.3E-03
NT154 Pack Cementation Sample #13	-3.4E-03
Baseline NT154	-3.8E-03
NT154 HEEPS #1	-3.9E-03
NT154 Pack Cementation Sample #6	-4.4E-03
NT154 Pack Cementation Sample #11	-4.7E-03
NT154 HEEPS #2	-5.1E-03
Fused Quartz	-5.5E-03

2. NET SHAPE FORMING DEVELOPMENT (NSFD):

Under this task, the optimized green machining procedure (described in the previous quarterly report) was employed to fabricate four rotors of an Ingersoll-Rand design. One of the rotors has been densified (Figure 1), utilizing the new HIP process for improved as-processed (AP) surfaces. The dense rotor has an excellent average surface roughness (R_a) of 34 in. Several dimensions and blade profiles were measured on the dense rotor, using CMM. The dimensions are consistently on the low side with a maximum deviation of 0.012" from nominal. Upon further investigation, it has been determined that the new HIP process has a slightly different shrinkage than the old HIP process. The IR rotors were green machined according to the shrinkage seen with the old HIP process.

The rotor has been delivered to HT Lin at ORNL for mechanical testing. Biaxial disks from both the airfoils and hub region will be machined for mechanical property evaluation.

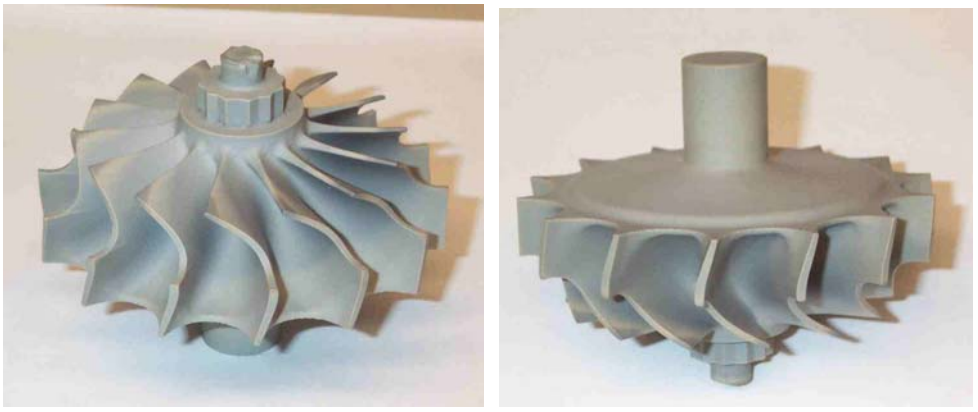

Figure 1: Dense NT154 Rotor of an Ingersoll-Rand Design

Status of Milestones

(1) Demonstrate a 40% improvement in the as-processed strength of Saint Gobain NT-154 silicon nitride (July 2004): ON SCHEDULE

Our baseline or starting average AP flexure strength for NT154 is 450-500 MPa, which we showed in Phase I and which is consistent with earlier ATTAP data. We are targeting a consistent improved AP strength of at least 650-700MPa, which would achieve the 40% DOE Milestone Goal.

We are encouraged that we can achieve the upper average 700 MPa goal and we have already achieved it on two occasions. We need to demonstrate it repeatable and are currently working to do so. We are in the process of demonstrating reliability and are currently making specimens for qualification at ORNL.

(2) Evaluate baseline recession resistance for uncoated and surface-modified NT154 (September 2004) and

(3) Develop a suitable surface modification procedure or EBC for test tiles and components to improve the recession resistance (December 2004): ON SCHEDULE

The development of an internal recession test will be instrumental in screening candidate solutions. The baseline NT154, as well as surface-modified NT154 from the initial experiments, has already been tested in the internal recession test. The results are shown above. Future samples will also be tested internally. Once a suitable sample has been produced, it will be forwarded to ORNL for Keiser Rig testing.

Industry Interactions

A visit to UTRC took place on March 15, 2004. Attendees included: Vimal K. Pujari, Oh-Hun Kwon, Ara Vartabedian, Bill Collins, Bob Licht and Bill Donahue. Discussions were held on our progress with the NT154 material and shape forming. Our most current material data base was provided to UTRC for rotor and vane life prediction calculations.

Problems Encountered

None

Publications/Presentations

"Reliable High Temperature Silicon Nitride and Components for Microturbine Applications", presented by Vimal K. Pujari at the 28th ACerS Cocoa Beach International Conference, January 29, 2004.

"Hot-Section Silicon Nitride Materials Development for Advanced Microturbines and Other Gas Turbine Component Applications", presented by Robert H. Licht at the 28th Annual Conference

on Composites, Materials and Structures, USACA ITAR Restricted Meeting, Cape Canaveral/Cocoa Beach, January 29, 2004.

Environmental Protection Systems for Ceramics in Microturbines and Industrial Gas Turbine Applications Part A: Conversion Coatings

S. D. Nunn and R. A. Lowden
Metals and Ceramics Division
Oak Ridge National Laboratory
P.O. Box 2008, Oak Ridge, TN 37831-6087
Phone: (865) 576-1668, E-mail: nunnsd@ornl.gov

Objective

Monolithic silicon nitride ceramics are currently the primary ceramic material being used in combustion engine environments and are under consideration as hot-section structural materials for microturbines as well as other advanced combustion systems. Under oxidizing conditions, silicon nitride will typically form a surface oxidation (silicate) layer. In a combustion environment, this silicate layer can undergo rapid degradation because of the corrosive and erosive effects of high temperature, high pressure, and the presence of water vapor. This degradation can severely limit the useful life of the ceramic in this environment. Thus, the development of an environmental protection system for the ceramic has become an essential goal for enabling the long-term utilization of these materials in advanced combustion engine applications.

One approach that is being pursued to produce an environmental protection system for silicon nitride is the formation of a surface conversion layer using the pack cementation process. Pack cementation has been used for many years to develop an oxidation protection coating on nickel-based superalloys that are used for hot-section components in gas turbine engines. A reactive gas atmosphere is used to change the composition and microstructure of the metal alloy at the surface of the component so that it will form a protective oxide film under normal operating conditions. The same approach can be used to form a modified surface region on silicon nitride ceramic components. By selecting an appropriate reactive atmosphere for the pack cementation process, the surface region can be modified to form ceramic compounds that may provide enhanced corrosion and erosion resistance in the combustion engine environment.

Highlights

Silicon nitride samples of Honeywell AS800, Kyocera SN281, and Saint Gobain NT154 were coated by pack cementation in air at 1400ºC. The coating packs contained the rare earth oxide Yb_2O_3, which had been identified in NASA and Kyocera studies as forming silicate compounds that are compatible with silicon nitride and stable in oxidizing environments. Silicon nitride samples that were coated in a powder pack of Yb_2O_3 alone formed surface layers containing mixtures of Yb_2SiO_5, $Yb2Si_2O_7$, SiO_2, and Yb_2O_3. When the powder pack consisted of Yb_2O_3 and Al_2O_3, the coated surfaces contained $YbAlO_3$, as well as $Yb_2Si_2O_7$ and some Al_2O_3 and mullite ($Al_6Si_2O_{13}$). These coated samples will be examined further for resistance to a moist, oxidizing environment.

Technical Progress

Initial tests were begun to evaluate the formation of ytterbium-containing coatings on silicon nitride substrates. Samples of Honeywell AS800, Kyocera SN281, and Saint Gobain NT154 silicon nitrides were heated in air to 1400ºC while embedded in powder packs containing Yb_2O_3. Two pack compositions were compared in the coating study: one contained only the rare earth oxide Yb_2O_3, the second consisted of a mixture of Yb_2O_3 and Al_2O_3. The processing variations and the coating phases that were formed are summarized in Table 1.

Table 1. Processing variations and coating phases identified by XRD.

Silicon Nitride Substrate	Pack Composition	X-ray Diffraction Phase Analysis
AS800	Yb_2O_3	Yb_2O_3, Yb_2SiO_5, $Yb_2Si_2O_7$
AS800	$Yb_2O_3 – Al_2O_3$	Al_2O_3, $Yb_2Si_2O_7$, Mullite, $YbAlO_3$
NT154	Yb_2O_3	Yb_2O_3, SiO_2, $Yb_2Si_2O_7$
NT154	$Yb_2O_3 – Al_2O_3$	$Yb_2Si_2O_7$, Al_2O_3, $YbAlO_3$, Mullite
SN281	Yb_2O_3	Yb_2O_3, $Yb_2Si_2O_7$, Yb_2SiO_5
SN281	$Yb_2O_3 – Al_2O_3$	$Yb_2Si_2O_7$, Al_2O_3, $YbAlO_3$, Mullite

The silicon nitride samples that were coated in a powder pack of Yb_2O_3 alone formed surface layers containing mixtures of Yb_2O_3, Yb_2SiO_5, and/or $Yb2Si_2O_7$. Some SiO_2 was observed in the NT154 sample coating. The ytterbium silicates have been identified in NASA and Kyocera studies as being compatible with the thermal expansion coefficient of silicon nitride and stable in oxidizing environments. When the powder pack consisted of Yb_2O_3 and Al_2O_3, the coated surfaces contained the aluminate compound $YbAlO_3$, as well as $Yb_2Si_2O_7$. There was also some Al_2O_3 and mullite ($Al_6Si_2O_{13}$) identified in these coatings. Additional variations of the coating process using Yb_2O_3 are planned to better refine and control the coating phases that are formed. The coatings will be examined further for resistance to the oxidizing and corrosive conditions of the high-temperature gas turbine engine environment.

A simple testing system is being prepared to allow evaluation of coated samples at elevated temperature in a high-moisture-content atmosphere. The setup will be similar in function to the rig being used by researchers at NASA. A laboratory steam generator has been ordered to be used with a tube furnace to provide an environment that simulates the gas turbine engine. Although the turbine engine pressure will not be simulated, the temperature and water vapor levels should provide a good screening mechanism for examining the durability and protective characteristics of the coatings produced on the various silicon nitride substrates.

Status of Milestones

Evaluate the corrosion resistance of strontium aluminate-type and ytterbium-containing surface conversion coatings on silicon nitride in a simulated combustion atmosphere. (Sept. 2004)

Industry Interactions

Obtained a sample of composite material from GE Aircraft Engines for evaluation of applying a protective coating by pack cementation.

Met with Kennametal to discuss status of SiAlON production and possible protective coating compounds.

Problems Encountered

None

Publications and Presentations

None

Polymer Derived EBC for Monolithic Silicon Nitride

Rishi Raj and Sudhir Brahmandam
University of Colorado
Boulder, Co
Phone: (303)492-1029, E-mail: Rishi.Raj@Colorado.EDU

Objective

The overall objective of this work is to develop novel EBCs for monolithic silicon nitride turbine blades from oxide/non-oxide based precursor derived ceramics, for example, ZrO_2-SiCN. The statement of work includes three tasks:

A. Thermodynamic and kinetic stability of oxides with SiCN in the temperature range of 1473 to 1673 K will be evaluated.
B. Oxidation kinetics of oxide-SiCN structures will be studied to discern if the interfacial bonding will avert formation of silica.
C. Structures prepared in 'B' will be tested in the Keiser Rig at ORNL.

Highlights

•Composites with SiCN content from 2 to 50 vol%, corresponding to SiCN interface thicknesses from 1 μm to 20 nm, have been prepared. These samples are being used to study the oxidation behavior by microstructural analysis (coating thickness and reactions at zirconia-SiCN interfaces. A second type of specimen geometry has been developed to study the oxidation behavior both microstructurally and by weight change. This geometry is in the form of fibers, which can be easily sectioned for microstructural information, and because of high surface to volume ratio can be studied by change in weight.

•Hydrothermal corrosion setup have been fabricated to study the oxidation and corrosion behavior of the composites in air and water vapor for temperatures up to 1673 K, at flow rates of up to 100 cm s^{-1}.

Technical Progress (Cumulative)

Review of the literature shows that dense SiCN samples could only be made when at least one dimension of the sample is < 500 μm. Further, there is no reported data on the processing of bulk SiCN based composites. Therefore, initial studies were aimed at developing a processing route to obtain dense zirconia – SiCN. These studies revealed that the presence of zirconia particles in the SiCN matrix can be hot-pressed to full density. The following samples have been made.

Samples made from Oxide Powders

Earlier work has focused on processing particulate composites made from SiCN and zirconia, and alumina. These composites are called Type I if SiCN phase is continuous and Type II if the SiCN phase is in particulate form. Table 1 lists the samples prepared and sent for Keiser Rig evaluation in Dec. 2003.

Table 1: Samples sent for Keiser Rig evaluation.

Sample	Composition	Oxide Particle Size (μm)	Microstructure Type$_2$	Preparation Method*	Comments
S1	ZrO_2-8v%SiCN	0.5	I	A	Nearly dense
S2	ZrO_2-15v%SiCN	0.5	II	B	Nearly dense
S3	ZrO_2-8v%Al_2O_3	0.5	I	A	Porous
S4	ZrO_2-15v%Al_2O_3	0.5	II	B	Porous

**Process A*: Mixing oxide powders in Ceraset. Cross-linking at 673 K. Warm pressing at 673 K and hot pressing at 1573 K. *Process B*: Mixing oxide and SiCN in powder form. Hot pressing at 1573 K.

Subsequent studies have shown that a modification of 'process A' gives nearly dense oxide-SiCN composites with Type I microstructures even with SiCN content as high as 50 vol%. Details for this process are given in the previous quarterly report. The BET surface area analysis indicated that the nano-porosity in these samples can range from 0.5 m^2/g to 4 m^2/g. We are pressing ahead to obtain as low porosity in our samples, reproducibly. Figure 1 shows the XRD data for these composites. The peaks correspond to cubic zirconia, indicating that the processing route did not cause an appreciable reaction between SiCN and zirconia.

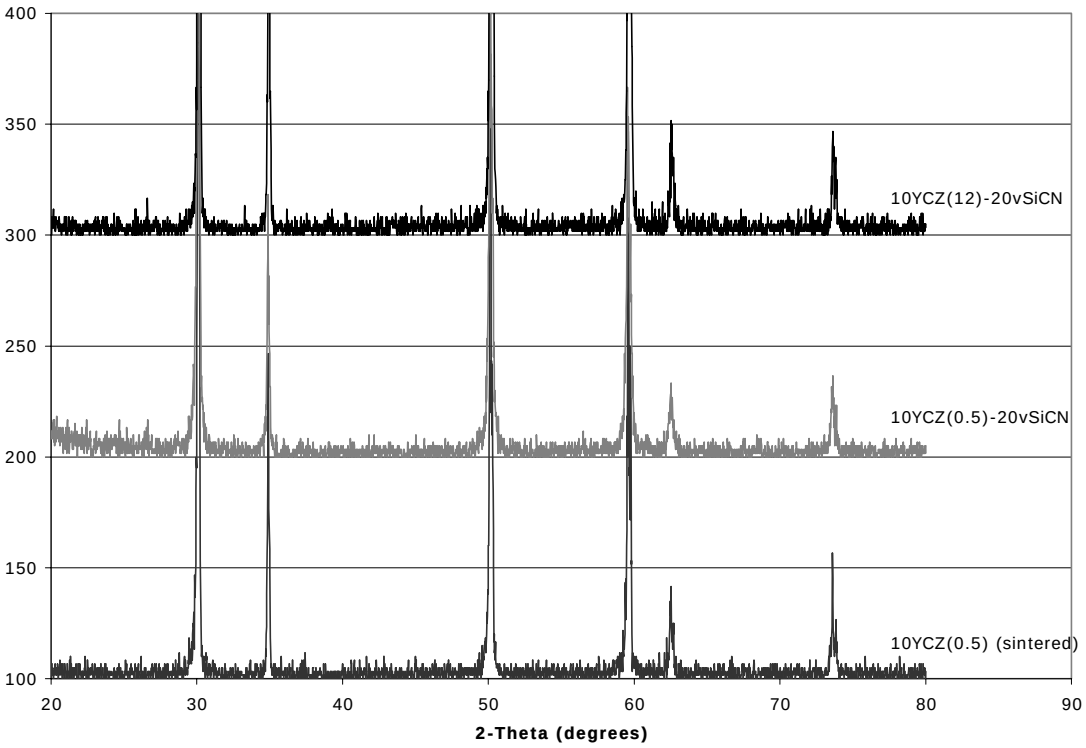

Figure 1: XRD data of zirconia – 20v%SiCN composites. Cubic zirconia data shown for comparison.

<u>High Surface area Samples</u> made from Polymer Precursors of Zirconia

Samples described under (1.) above are suitable for the study of oxidation by microstructural analysis, that is, by the study of the oxidation layer on the surface of the specimen and the reactions at SiCN-ZrO2 interfaces deep within the sample. These studies of oxidation behavior have begun.

A second method of studying oxidation is to measure the change in weight of the sample with oxidation. For this purpose high surface area samples are needed. In this task we are preparing these samples directly from the polymer route using organic precursors for both the oxide and the silicon carbonitride. The weight change results must be combined with microstructural analysis. The shape of a fiber enables both types of studies to be done easily. The microstructural evaluation can be done by sectioning the fiber, and the weight change study is possible because the fibers have a high surface to volume ratio. Fiber samples with 10-20 vol% ZrO_2 are now being prepared by adding Zr-n-propoxide to ceraset. These fibers have a diameter of 5-10 μm.

Design and Construction of a Set Up for First-Phase Oxidation Studies

In this study we are evaluating new materials. Different microstructures and sample geometries are being considered to understand the oxidation behavior of zirconia-silicon carbonitride materials. Therefore, there is a need to have a set-up that can provide first-phase information on the oxidation behavior of this new materials in humid environments before the samples are sent in for evaluation in the Keiser Rig. A setup has been fabricated to study the hydrothermal corrosion behavior in highly humid conditions with vapor flow rates of up to 100 $cm.s^{-1}$ and temperatures up to 1673 K. Figure 2 gives a schematic illustration of this unit.

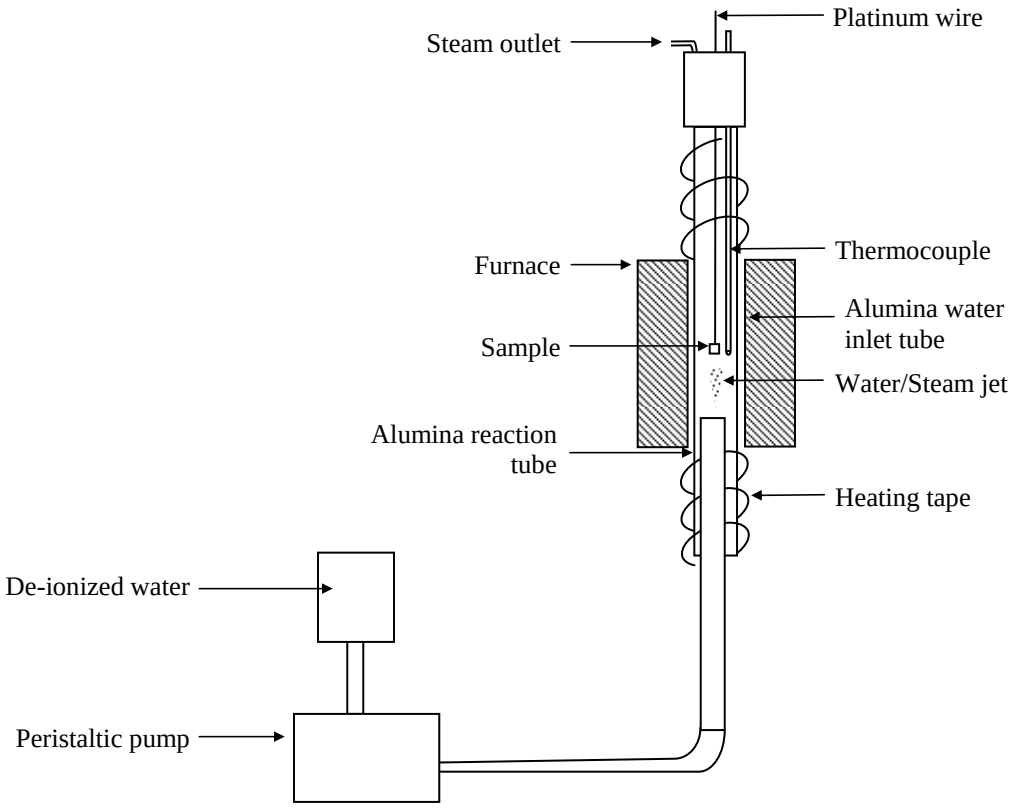

Figure 2: Hydrothermal corrosion testing unit

The hydrothermal setup consists of injecting a jet of water at a controlled flow rate into an alumina reaction tube that is heated to the testing temperature in a high temperature tube furnace. The exposed portions of the reaction tube are heated to > 400 K using heating tapes to prevent condensation of water inside the tube. The sample is suspended in the hot zone of the reaction tube using a platinum wire.

Status of Milestones

The following experiments are planned for the coming quarter:

Task A: Interfacial reactions in SiCN-ZrO_2 composites as a result of oxidation in humid environments.

Status: Good samples of the composites with Type I and Type II microstructures have now been prepared. They will be tested during this period. The hydrothermal oxidation unit will be calibrated with silicon nitride samples during the next quarter.

Task B: Phase stability of SiCN-ZrO_2 microstructures.

Status: Power samples for x-ray studies have been prepared and will be characterized next quarter.

Task C: Testing in the Keiser Rig

Status: Preliminary samples were sent to Karren More in December 2003. However, these samples were not dense and they may have cracked upon heating to the oxidation temperature. We are now preparing good samples, and studying them in Boulder to see if they are indeed promising. They will then be sent to ORNL in July 2004, so that the results from the Keiser testing can be reported in the EBC workshop in mid November.

Industry Interactions

There are on-going interactions with Honeywell, Inc. This work is presently concentrated on the development of processes to make multilayer coatings from SiCN and ZrO_2. After preliminary experiments at Boulder the coatings will be sent to Honeywell for evaluation.

Problems Encountered

Preparation of dense SiCN-ZrO2 samples has taken considerable development. Now, specimens with low porosity (0.5 m^2/g) are being prepared. This has caused some delay in meeting the milestones. However, this delay would be overcome in the coming quarter.

Publications and Presentations

None

Environmental Protection Systems for Ceramics in Microturbines and Industrial Gas Turbine Applications: Slurry Coatings

B. L. Armstrong, K. M. Cooley, and G. H. Kirby
Metals and Ceramics Division
Oak Ridge National Laboratory
P. O. Box 2008, Oak Ridge, Tennessee 37831-6063
Phone: (865) 241-5862, E-mail: armstrongbl@ornl.gov

Objectives

Silicon-based monolithic ceramics are candidate hot-section structural materials for microturbines and other combustion systems. The performance of silica-forming ceramic materials in combustion environments is, however, severely limited by rapid environmental attack caused by the combination of high temperature, high pressure, and the presence of water vapor. Thus, the development of environmental protection systems has become essential for enabling the long-term utilization of these materials in advanced combustion applications.

Similar to thermal barrier coatings for nickel-based super alloys that utilize a specialized oxide surface layer and a metallic bond coat, successful environmental protection systems for ceramics and ceramic composites will likely utilize multiple layers and complex combinations of materials. Most recent efforts have focused on the selection and deposition of the oxide surface layer, and due to numerous factors, the majority of the candidates have been from the aluminosilicate family of oxide ceramics. Stable rare-earth silicate deposits have been found on component surfaces after recent engine and rig tests, indicating there may be other stable oxide compositions that have not been fully investigated. Thin coatings of selected silicate compositions will be deposited on test coupons using a variety of techniques. The specimens will then be exposed to simulated high-pressure combustion environments and materials that demonstrate good potential will be investigated further

Highlights

Mullite coatings were formed by dipping SiC, Si_3N_4, and silicon substrates into concentrated, mullite suspensions of tailored rheological behavior. Dried coatings were crack-free and fully densified at 1350^{o}C, which is considerably below the temperature requirement for densification of mullite in bulk form (1600^{o}C).

Technical Progress

Optimization of Mullite-PEI Suspension Rheology

Work continued on the optimization of mullite (MULCR®, Baikowski International Corporation, Charlotte, NC) slurry rheology for a dip coating process. Mullite was used as a surrogate material for the yttrium disilicates in order to optimize general rheology and dip

conditions. A cationic polyelectrolyte (polyethylenimine or PEI, Polysciences, Warrington, PA), with a weight average molecular weight (M_w) of 10,000 g/mole and one amine group (NH) per monomer unit was implemented as a rheological modifier for this system. Concentrated mullite suspensions (45 vol% solids) were prepared at a constant pH of 7 and varying PEI concentration. The suspensions were ultrasonically treated for 5 min to break up weak agglomerates and mixed on a shaker table for 24 h to obtain equilibrium behavior. Rheological measurements were carried out using a controlled stress rheometer (Rheometric Scientific SR5, TA Instruments, New Castle, DE) in stress viscometry and oscillatory stress modes to measure the apparent viscosity and elastic modulus, respectively.

The apparent viscosity is plotted as a function of applied shear stress in Fig. 1 for suspensions of varying PEI concentration. The degree of shear-thinning decreased with increasing PEI concentration until nearly Newtonian flow behavior was obtained at a PEI concentration of 0.2 mg/m^2 mullite. These suspensions exhibited stable flow behavior over a 15 day time span, as shown by the data in Fig. 2. The elastic modulus is plotted as a function of applied shear stress in Fig. 3 for suspensions of varying PEI concentration. Solid-like behavior, indicative of colloidal gels, was observed for suspensions with PEI concentrations less than 0.2 mg/m^2 mullite. The linear elastic modulus and yield stress decreased with increasing PEI concentration until a transition from gel- to fluid-like behavior occurred at 0.2 mg/m^2 mullite.

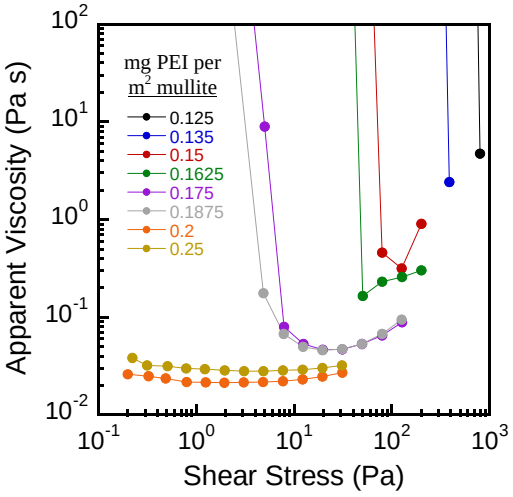

Fig. 1. Apparent viscosity as a function of shear stress for concentrated mullite suspensions (45 vol% solids) of varying PEI concentration. Note, the solid lines merely guide the eye.

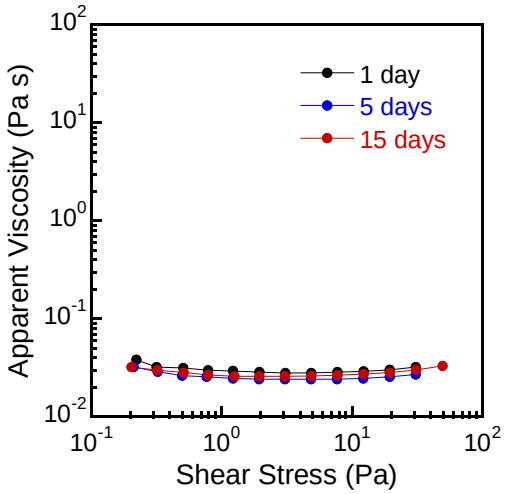

Fig. 2. Apparent viscosity as a function of shear stress for concentrated mullite suspensions (45 vol% solids, 25 mg PEI/m^2 mullite) aged for varying times.

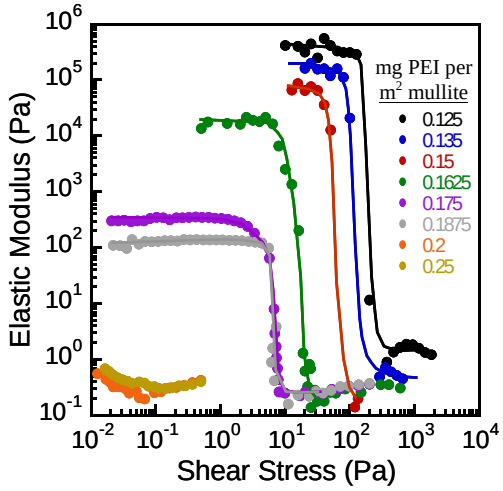

Fig. 3. Elastic modulus as a function of shear stress for concentrated mullite suspensions (45 vol% solids) of varying PEI concentration. Note, the solid lines merely guide the eye.

Slurry Coatings

Substrates of varying composition, including silicon carbide (Hexaloy, Carborundum Co., Niagara Falls, NY), silicon nitride (AS800, Honeywell Ceramic Components, Torrance, California), and metallic silicon, were dipped into concentrated mullite suspensions (45 vol%) of varying PEI concentration. The substrates were dipped at rate of 85.7 mm/min, submerged for 1 min, and withdrawn at a rate of 85.7 mm/min. Coated substrates were dried under ambient conditions and are displayed in the image gallery in Fig. 4. Excellent coatings were obtained from mullite suspensions with 0.1625 - 0.175 mg PEI/m^2 mullite surface. Mullite suspensions with less than 0.1625 mg PEI/m^2 mullite resulted in thick, uneven coatings. The quality of the coatings decreased with decreasing PEI concentration. These features result from a particle gel network that is too strong, i.e., when the linear elastic modulus is greater than ~ 10 kPa. Mullite suspensions with 0.1875 mg PEI/m^2 mullite or greater resulted in coatings with three types of defects: drying defects or "dimples", pores due to entrained air bubbles, and thickness gradients. All of these defects stem from a particle gel network that is too weak, i.e., when the linear elastic modulus is less than ~ 100 Pa. For example, drying defects arise from solvent wicking and particle migration from the center of each coated face to drying fronts that initiate, and converge inward from the corners and edges.[1] Pores arise from air bubbles that are entrained in the low viscosity suspensions and quickly migrate to the suspension/substrate interface during dipping. Thickness gradients result from dripping and beading of the suspensions at the bottom of the substrate surface.

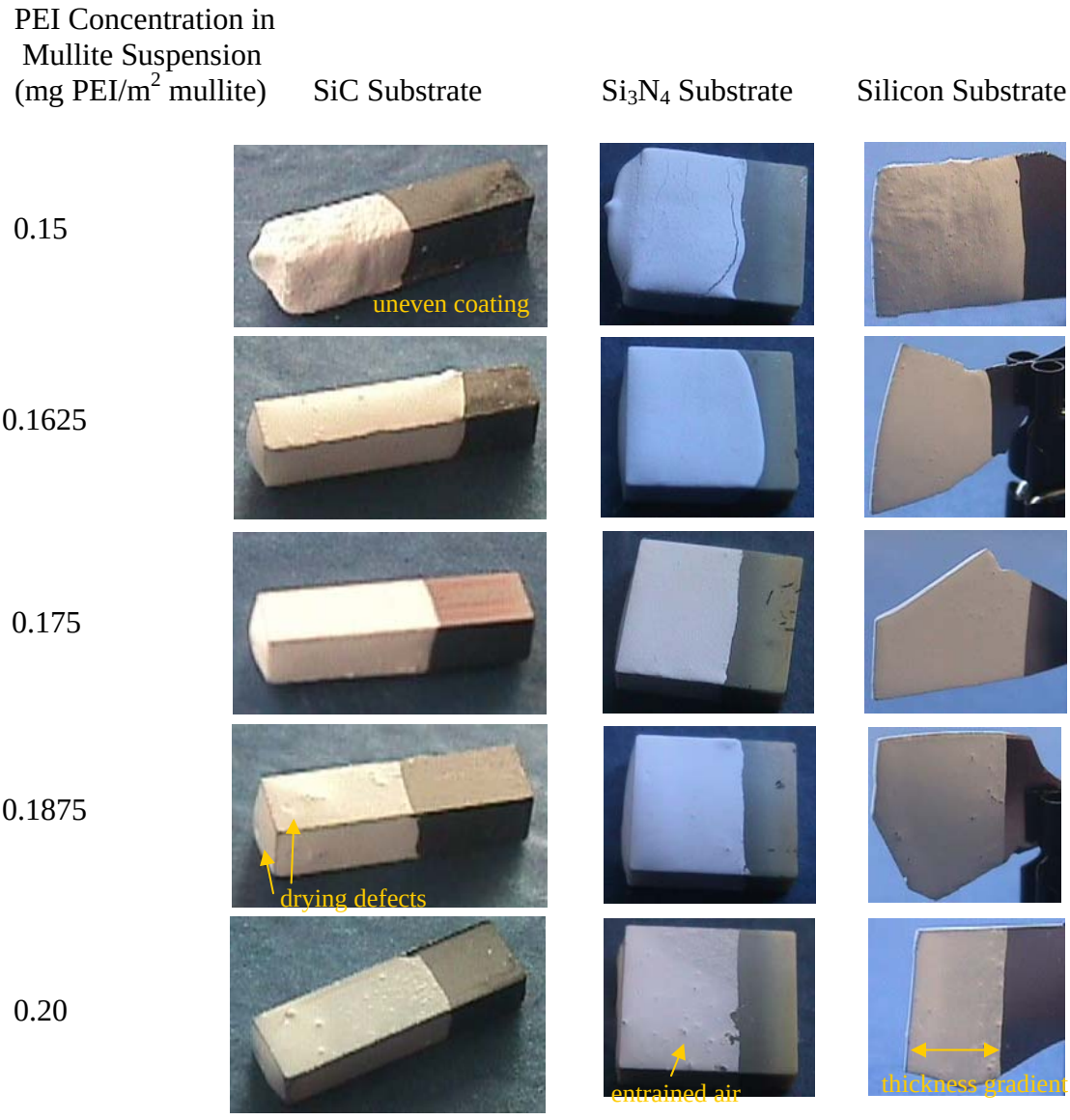

Sintering Behavior

Early results suggest that the sintering atmosphere plays an important role in obtaining adherent, dense coatings. Adherent coatings have been obtained in an oxygen atmosphere, but not in argon or nitrogen. It is believed that a thin, silica rich reaction layer may form to provide a bond coat in oxygen, but not in argon or nitrogen. Furthermore, the coatings likely react with nitrogen to form AlN, leading to a net volume expansion and spallation of the coating. Preliminary results show that dense coatings are achieved at 1350^{o}C, which is significantly lower than the temperature requirement for densification of mullite in bulk form (1600^{o}C). These results demonstrate the feasibility of dip coating and sintering environmental barrier coatings onto functional components. The effect of sintering temperature and atmosphere on coating properties after exposure to high temperature steam are in-process.

Development of a Sacrificial Coating

No work to report this quarter.

Status of Milestones

Evaluate the protective capacity yttrium disilicate deposited by a slurry-based process on silicon nitride in a simulated combustion environment. (September 2004)

Industry Interactions

Discussions with UTRC and GE have continued. This project has also collaborated with an ARTD Fossil Energy project on Corrosion Resistant Coatings.

Problems Encountered

None

Publications

None

References

1. C. J. Martinez, J. A. Lewis, "Rheological, Structural, and Stress Evolution of Aqueous Al_2O_3:Latex Tape-Cast Layers," *J. Am. Ceram. Soc.*, **85** [10] 2409-16 (2002).

Failure Mechanisms in Coatings

J. P. Singh, K. Sharma, and P. S. Shankar
Energy Technology Division
Argonne National Laboratory
Argonne, IL 60439
Phone: (630) 252-5123, E-mail: jpsingh@anl.gov

Objective

The purpose of this proposed research is to identify failure mode(s), understand and evaluate failure mechanisms, and develop appropriate test methods and protocols to characterize the integrity and predict failure of environmental and thermal barrier coatings for advanced turbine applications.

Technical Highlights

Four-point flexure strength of AS800 silicon nitride (Si_3N_4) specimens coated with different compositions of tantalum oxide (Ta_2O_5) based environmental barrier coating (EBC) has been evaluated. The measured strength of AS800 specimens coated with Ta_2O_5 + 3wt.% Al_2O_3 + 3wt.% La_2O_3-EBC (543±6 MPa) was higher than that of the specimens coated with Ta_2O_5 (458±20 MPa) or Ta_2O_5 + 3wt.% Al_2O_3-EBC (351±2 MPa). On the other hand the strength of these coated specimens was lower than that of the uncoated specimens (709±58 MPa). Fractographic analysis indicated that failure occurs at the EBC/substrate interface, which is associated with pores/voids, and microstructural discontinuities.

Technical Progress

Effort this quarter concentrated on evaluating the four-point flexure strength of AS800 Si_3N_4 specimens coated with different compositions of Ta_2O_5-EBC. AS800 substrates (50 mm x 26 mm x 4 mm) coated with Ta_2O_5 + 3wt.% Al_2O_3, and Ta_2O_5 + 3wt.% Al_2O_3 + 3wt.% La_2O_3 EBCs were received from Northwestern University/Honeywell. The EBCs had been deposited using small particle plasma spray process [1] on the substrates, which had been preheated to 450°C following a 1250°C soak. Four-point flexure bar specimens of dimension 26 mm x 2 mm x 1.5 mm were machined from the coated substrates using diamond saw. Four bars for each composition were tested according to the ASTM C1161-94 specification (Configuration A) with the coating side loaded in tension.

Figure 1 shows the measured four-point flexure strength of AS800 specimens coated with different compositions of the Ta_2O_5 based EBCs. For comparison, the measured strength of uncoated AS800 specimens (Quarterly Report July-September 2003) is also shown in the figure. The strength evaluation of the coated specimens was based on the analysis of a composite beam in bending. For the strength calculations, elastic modulus of EBC was taken as 90 GPa for all the EBC compositions. It can be clearly seen from Figure 1 that the flexure strength (543±6 MPa) of AS800 coated with Ta_2O_5 + 3wt.% Al_2O_3 + 3wt.% La_2O_3 EBC is the highest among the three EBC compositions. However, all the three sets of EBC-coated AS800 specimens have a

lower strength than the uncoated AS800 specimens. The observed decrease in strength for the EBC-coated AS800 specimens may be related to the presence of residual stresses at the interface arising from thermal expansion mismatch between the AS800 substrate and the EBC.

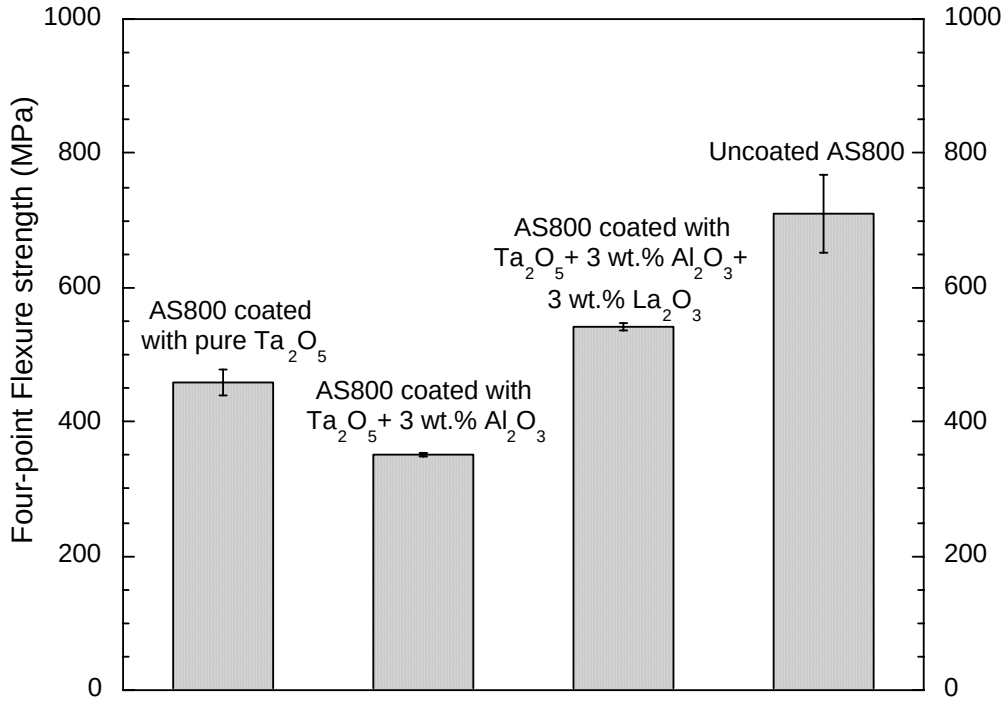

Figure 1. Four-point flexure strength of AS800 Si_3N_4 specimens coated with different compositions of Ta_2O_5 based EBC. The flexure strength of uncoated AS800 is also shown.

Fractographic evaluation of failed four-point flexure bars was performed to identify failure origin and characterize critical flaws. Figure 2 shows the fracture surface and a critical flaw (voids/pores) in an AS800 flexure bar specimen coated with Ta_2O_5 + 3wt.% Al_2O_3 + 3wt.% La_2O_3-EBC. Similar fracture morphology and critical flaws were observed in all the specimens of this composition. As shown in Figure 3, failure in EBC specimens with Ta_2O_5 + 3wt.% Al_2O_3 composition primarily initiated at the EBC/substrate interface, apparently from microstructural discontinuities. Currently, effort is in progress to understand the effect of compositional variations in Ta_2O_5 based EBCs on the flexural response of EBC-coated AS800 Si_3N_4 specimens. Furthermore, microindentation testing and stress analysis at the EBC/substrate interface are in progress to understand the observed strength degradation of the coated AS800 specimens as compared with the uncoated specimens.

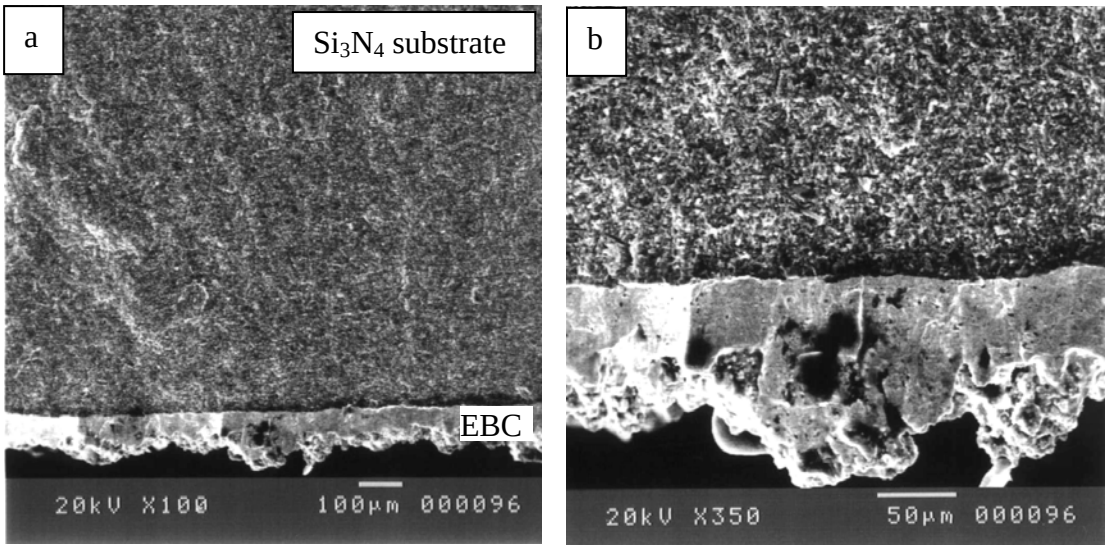

Figure 2. Fracture surface of AS800 coated with Ta_2O_5 + 3wt.% Al_2O_3 + 3wt.% La_2O_3. (a) Fracture markings at the failure origin, and (b) higher magnification image showing critical flaw (voids/pores) at the failure/origin.

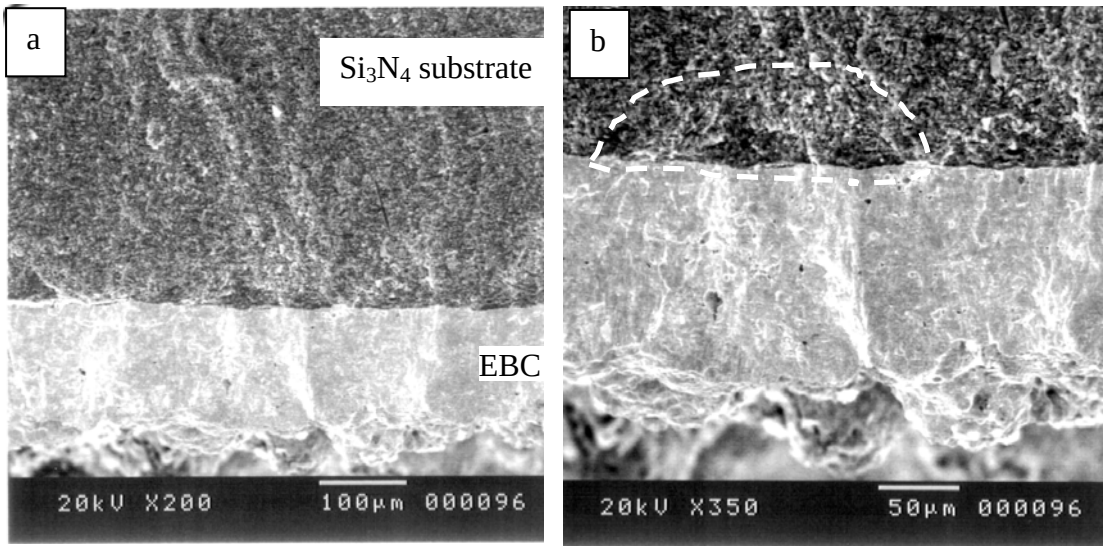

Figure 3. Fracture surface of AS800 coated with Ta_2O_5 + 3wt.% Al_2O_3, showing the (a) fracture markings, and (b) location of failure initiation at the EBC/substrate interface.

Status of Milestones

Complete evaluation of the effects of compositional variation in Ta_2O_5-based EBCs on mechanical behavior of coated Si_3N_4 (AS800) substrates that are being developed at Northwestern University/Honeywell. September 2004. On Schedule.

Industry Interactions

Discussion on the results of mechanical and microstructural evaluation of Ta_2O_5-coated AS800 Si_3N_4 specimens was continued with Northwestern University/Honeywell.

Problems Encountered

None

Publications/Presentations

K. Sharma, P. S. Shankar, and J. P. Singh, "Mechanical and Fractographic Evaluations of Si_3N_4 substrates with Environmental Barrier Coatings," presented at the 106th American Ceramic Society Annual Meeting and Exposition, Indianapolis, IN, Apr 18-21, 2004.

Reference

1. M. Moldovan, C. M. Weyant, D. L. Johnson, and K. T. Faber, "Tantalum Oxide Coatings as Candidate Environmental Barriers," J. Thermal Spray Technology 13 (1) 51-56 (2004).

High-Temperature Diffusion Barriers for Ni-Base Superalloys

B. A. Pint, K. M. Cooley and J. A. Haynes
Metals and Ceramics Division
Oak Ridge National Laboratory
Oak Ridge, TN 37831-6156
Phone: (865) 576-2897, E-mail: pintba@ornl.gov

Objective

Nickel-base superalloys require coatings to improve their high temperature oxidation resistance, particularly when a thermal barrier coating is employed. The underlying oxidation-resistant metallic coating or bond coat is degraded by the loss of Al due to oxidation, but much more Al is lost due to interdiffusion with the superalloy. Loss of Al causes diffusion aluminide coatings to undergo phase transformations, which likely cause deformation of the bond coat surface and subsequent loss of the protective alumina scale and the overlying thermal protection layer. The goal of this program is to fabricate and assess potential compounds for use as high-temperature diffusion barriers between coating and substrate. Ideally, the barrier would act to reduce the inward diffusion of Al, as well as the outward diffusion of substrate elements (such as Cr, Re, Ta, W), which generally degrade the oxidation resistance of the coating. The work is motivated by previous experimental results which suggested some compositions that exhibited diffusion-barrier capabilities. A secondary objective is to demonstrate routes to fabricating diffusion aluminide coatings incorporating a diffusion barrier using chemical vapor deposition (CVD).

Highlights

Electron microprobe analysis of Pt-Hf coatings revealed that although a layer with composition similar to the target phase of $HfPt_3$ (Engel-Brewer compound) formed during heat-treatment of Pt-Hf thin films below 1000°C, this phase was not stable. The $HfPt_3$-like phase either completely dissolved during short-term CVD aluminizing at 1100°C or else began to be diluted by the interdiffusion processes. Subsequent experiments heat treated Pt-Hf thin films at temperatures higher than 1000°C, the temperature at which a rapid exothermic reaction between Pt-Hf is reported to occur. Again, the Pt-Hf rich phase was observed to be unstable after CVD aluminizing at 1100°C.

Technical Progress

Electron Microprobe Analysis of Pt-Hf Coatings

The deposition of Pt and Hf layers on low sulfur René N5 substrates was described in prior reports. Specimens with Pt-Hf thin films were characterized by electron microprobe analysis (EPMA) for determination of the composition of the coatings after heat-treatment and after aluminizing. Specimens were heat treated for 1h at 500°C in order to relieve stress in the sputtered thin films, and then at higher temperatures to promote interdiffusion between the deposited Hf and Pt layers and the substrate. The temperature 900°C was initially selected since it is below the temperature at which a rapid exothermic reaction is reported to occur between Pt and Hf (1000°C). However, subsequent work looked at higher temperatures. The heat treated coatings were then aluminized. In order to compare specimens as accurately as possible, each specimen disc was first heat treated and then 30% of the specimen was cut off with a diamond saw and mounted for metallographic preparation. The remaining specimen was then aluminized via a low activity CVD process described in previous reports.

Two sets of samples were examined with a 900°C heat treatment for 2h: PHA5 has 3μm of Pt and

1µm of Hf and PHB5 has 5µm of Pt and 1µm of Hf. Figure 1 shows the cross-section and composition profile of PHA5 after both heat treatments but before aluminizing. A three-layer structure was present above the superalloy. The porous, outer layer of the coating was about 3 µm thick. It was Pt-rich but contained significant amounts of Ni and smaller amounts of Al, Hf, Co and Cr. The center layer was mostly dense, with a composition 69.5 Pt-20.9Hf-6.2 Ni-1.6 Al (at%) at approximately 4 µm below the surface. This layer had a composition similar to $HfPt_3$, although Pt-rich. The EPMA profile shows a minimum in both the Al and Ni contents within this phase. This result suggests a low solubility of Al and Ni in the Hf-Pt phase, which would be a positive characteristic for a diffusion barrier. The innermost layer of the coating was rich in Ni, Pt and Al.

Figure 2 shows similar results for the specimen after CVD aluminizing for 1h at 1100°C. Again three layers are visible. The outer layer is the typical dense, β-NiAl expected after CVD aluminizing. The outer surface of this layer had very high Al (47.2 at%) and Ni (40.4 at%) contents, with a significant amount of Pt (8.3 at%) present. The composition of the thin central layer showed a minimum in Al and Ni content, but there was only a slight peak in Pt and Hf. This central layer appears to be the remnant of the $HfPt_3$ layer after significant dissolution. The thicker innermost layer is the typical interdiffusion zone present in a CVD aluminide coating.

The second set of samples had a thicker initial Pt layer. Figure 3 shows the composition and cross-section after heat treatment of PHB5. A similar three-layer coating was observed in this case. Figure 3a shows that there was a Pt-Hf peak at approximately 4µm, similar to Figure 1a. The composition was similar to $HfPt_3$, but was again Pt rich. The surface composition of the outer layer was approximately 70 at% Pt, 19 at% Ni, 4 at% Al, 2.6 at% Co. The most obvious microstructural difference in Figs. 1b and 3b is the thinner interior layer in the latter case. The reason for this difference is not apparent. There do appear to be more voids in Figure 3b. These may have inhibited interdiffusion. Also, the thicker Pt layer may have had a higher residual stress, which could degrade adhesion with the inner Hf layer.

Figure 4 shows the cross-section and composition profile for PHB5 after aluminizing for 1h at 1100°C. The higher Pt content had a significant effect on the aluminized composition. The Pt-Hf

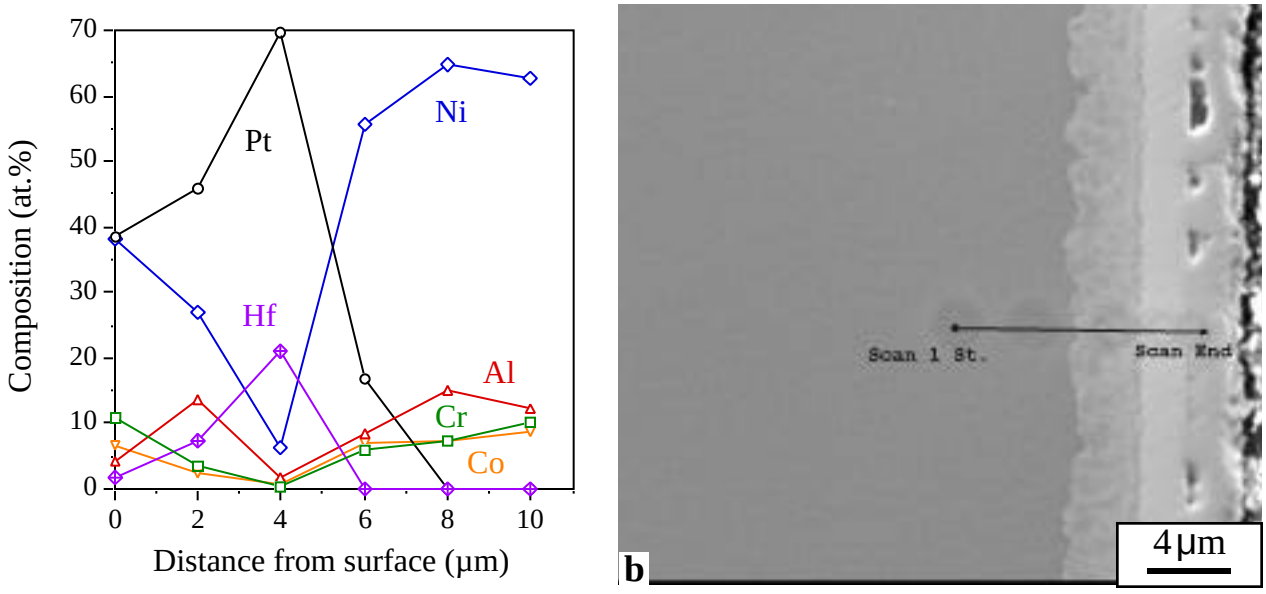

Figure 1. (a) EPMA profile of PHA5 after heat treatment. (b) micrograph of region analyzed.

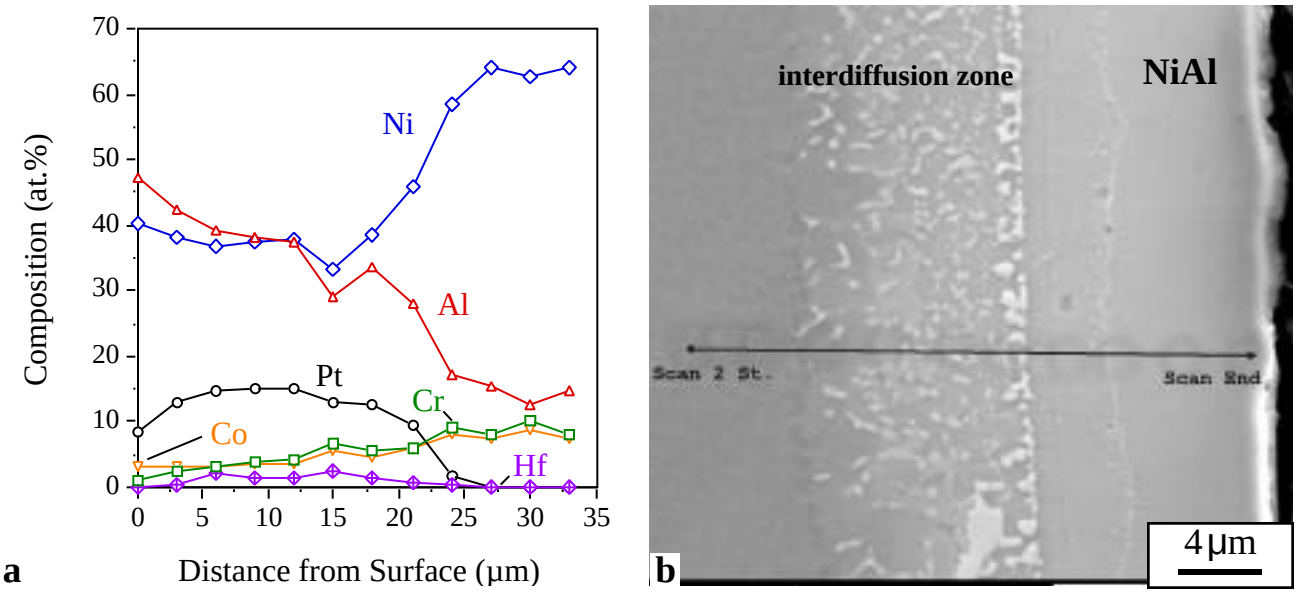

Figure 2. (a) EPMA profile of PHA5 after heat treatment and aluminizing. (b) micrograph of region analyzed.

layer is more evident in this case and the Al content of the coating is much lower. However, the Al content at the surface is very high (55%). The Hf content in the outer layer is much higher than in the other aluminized coating, suggesting that there may have been a slightly thicker Hf layer in this case. While these results are promising, it is worth noting that dilution of the Hf-Pt layer has already begun to occur on a limited basis after 1h of aluminization and will likely continue for longer aluminizing times.

Heat treatments above 1000°C

Since the 900°C heat treatment did not result in a stable $HfPt_3$ phase, a higher temperature anneal was tried. An exothermic reaction between Hf-Pt was reported in the literature above 1000°C and there

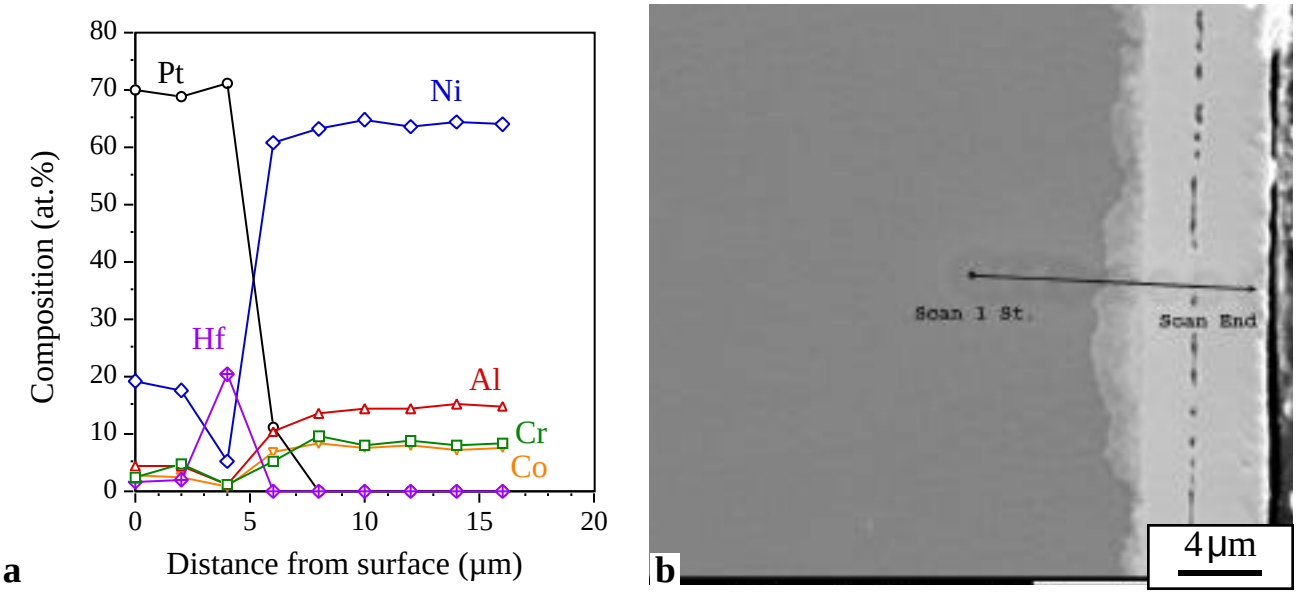

Figure 3. (a) EPMA profile of PHB5 after heat treatment. (b) micrograph of region analyzed.

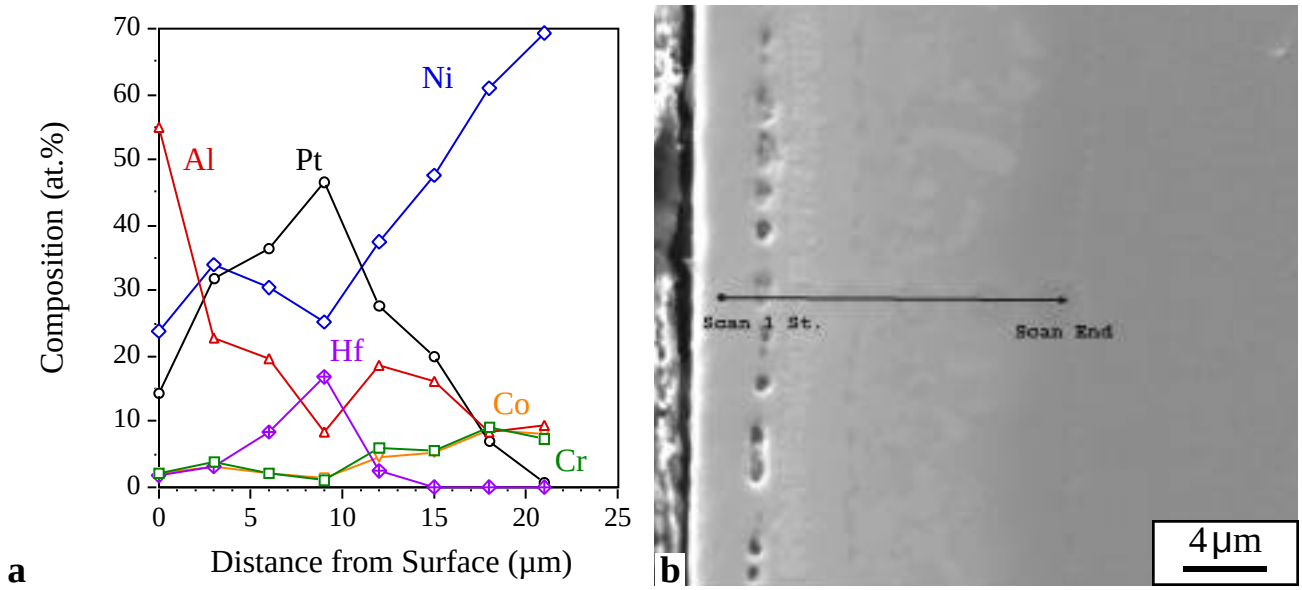

Figure 4. (a) EPMA profile of PHB5 after heat treatment and aluminizing. (b) micrograph of region analyzed.

was concern that this reaction could disrupt the coating. However, heat treatments at 1050° and 1100°C did not show any unusual behavior. Figure 5a shows the cross-section of a specimen with a 5μm Pt/1μm Hf coating after a heat treatment of 2h at 1100°C. A similar layered structure forms but much larger voids were observed after the higher temperature anneal. Figure 5b shows the same specimen after CVD aluminizing for 3h at 1100°C. The Pt-Hf layer is no longer distinctly visible although chemical analysis has not been completed at this time. These preliminary results indicate that higher temperature annealing does not appear to be beneficial.

Status of Milestones

FY 2004
Complete characterization and testing of the first batch of precious metal-based diffusion barriers and report disclosable findings in an open literature publication.
(September 2004)

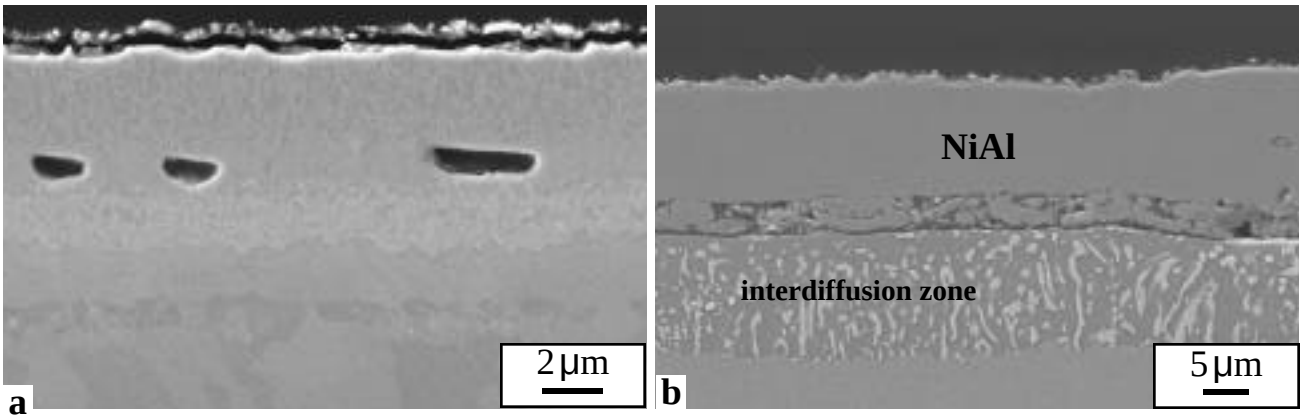

Figure 5. Specimen PHB8 after (a) heat treatment at 500°C for 1h and 1100°C for 2 h, (b) heat treatment plus 3 h CVD aluminizing at 1100°C.

Industry Interactions

Pre-oxidized superalloys were sent to Tom Houvouras of Huntington Plating Inc (Huntington, WV) for Ni-plating of additional pre-oxidized superalloys.

Problems Encountered

None

Publications

None

POWER ELECTRONICS

High Temperature Heat Exchanger

E. Lara-Curzio, J. G. Hemrick, A. Zaltash, N.C. Gallego, C.A. Walls
Metals and Ceramics Division
Oak Ridge National Laboratory
P.O. Box 2008, Oak Ridge, TN 37831-6069
Phone: (865) 574-1749, E-mail: laracurzioe@ornl.gov
B.E. Thompson
University of Western Ontario

Objective

As part of a collaborative effort between ORNL and the University of Western Ontario, graphite-based heat exchangers will be designed and evaluated for heat recovery systems in microturbine applications. In particular, it is desired to improve the efficiency of heat recovery systems based on aluminum fin heat exchangers that are currently being used in commercial units. In coordination with modeling efforts, the microstructure of graphite-based heat exchangers will be designed in order to maximize heat transfer while minimizing pressure drop. The efficiency of the new designs will be compared against currently used aluminum fin heat exchangers and eventually evaluated using a Unifin Microgen heat recovery unit couple to a Capstone C60 microturbine.

Work will be supplemented with experiments to gain a better understanding of the effect of heat exchanger material microstructure on gas flow penetration, pressure drop, and mechanical strength.

Technical Progress

Upon consideration of the costs and labor associated with connection of the Unifin Microgen heat exchanger to the 60 kW Capstone microturbine, discussion was held regarding the feasibility of using the current microturbine/heat exchanger system already in place at the ORNL Cooling, Heating, and Power Facility (bldg. 3115). This option would utilize the already existing infrastructure and instrumentation, while allowing alteration to the current equipment to facilitate the testing of new heat exchanger concepts.

Efforts to fabricate a “miniature wind tunnel” device were combined with expertise at the University of Western Ontario. Carbon foam samples with varying densities were prepared at ORNL and supplied to Materials Resources International for S-bond joining to aluminum plates. These joined samples will be provided to the University of Western Ontario for testing in their existing wind tunnel facility. Information on the depth of gas penetration in these systems is important to optimize material usage.

Development and implementation of a method to evaluate and compare the mechanical properties of individual foam ligaments using X-ray tomography and rapid prototyping techniques has been continued. Low spatial resolution (28μm) CT scans were performed at Argonne National Laboratory. High spatial resolution (3μm) CT scans were performed at the

Japan Fine Ceramics Center in Nagoya, Japan. Estimates are still being sought for file conversion and rapid prototyping services.

High thermal conductivity graphite fiber samples have been obtained. Lower thermal conductivity/lower modulus fiber materials have also been identified and samples have been obtained. A commercial company (3-Tex, Inc. of Cary, NC) has been identified as a partner in the project. They have a unique weaving process (3-Weave) which is capable of producing 3-dimensional fiber preforms. A visit was made to 3-Tex and possible preform weaving techniques and designs were discussed. Out of the meeting, it was decided that a series of preforms would be woven with and without metallic tubing incorporated in the structure. Initial weavings will use 50 msi/lower thermal conductivity fibers. Subsequent weavings will be attempted with higher modulus/higher thermal conductivity fibers. Fiber has been ordered for the initial weavings and production time is being scheduled at the 3-Tex Rutherfordton, NC facility.

Brian Thompson and Qijun Yu, from the University of Western Ontario, visited ORNL in early May. Both presented seminars outlining their work and progress in regard to the modeling of carbon foam and the design of alternative carbon foam heat exchangers. The design of microturbine/heat exchanger experiments, the base-line performance of the current Unifin heat exchanger, and the cooling of power electronics were also discussed.

A test rig has been designed and constructed to evaluate heat transfer, permeability, and pressure drops associated with experimental graphite foams and woven fiber preform structures. Results will be used to optimize the pore structures of foams and fiber preforms to maximize performance and to verify model predictions.

Status of Milestones

In Progress

- Fabrication and joining of samples for wind tunnel analysis at University of Western Ontario. Eight samples have been provided for analysis and additional samples are in preparation (July 2004)
- Alteration of current equipment in place at the ORNL Cooling, Heating, and Power Facility (bldg. 3115) to facilitate the testing of new heat exchanger concepts. (August 2004)
- Development and implementation of a method to evaluate and compare the mechanical properties of individual foam ligaments using X-ray tomography and rapid prototyping techniques. (August 2004)
- Testing of carbon foam and fiber performs in test rig. (August 2004)
- Fabrication of carbon-fiber preform prototypes. (September 2004)

Problems Encountered

None

Publications/Inventions/Meetings

Visit to 3-Tex, Inc., Cary, NC to discuss 3-dimensional weaving process (4/04)

Visit by Brian Thompson and Qijun Yu, from the University of Western Ontario (5/04)

Industrial Interactions

Technical discussions have been held with the following organizations:
Albany International Techniweave Inc.
Cytec Carbon Fibers
Ford Motor Company
Javelin
Nippon Graphite Fibers
3-Tex, Inc.
Unifin

Heat Exchange Concepts Utilizing Porous Carbon Foam

B. E. Thompson and A. G. Straatman
Faculty of Engineering
The University of Western Ontario
London, Ontario, Canada N6G 4K1
Phone: (519)850-2530, E-mail: Thompson@eng.uwo.ca

Objective

There is a need to produce engineering models for design of heat exchangers made from emerging porous carbon-foam materials. Knowledge and understanding of the effects of carbon foam on convective heat transfer is crucial to the development of appropriate engineering approximations for these design models. The overall objective is to explore new ideas for heat-exchanger configurations, especially for situations in which current technology is marginally cost effective. A thermo-economic model and a strategic design study are planned to provide new understanding for assessment in a stage-gate approach to further prototype development.

Highlights

Alternative designs of air-cooled heat exchangers for electronics and of water-cooled for inverters on hybrid electric automobiles have been generated using carbon foam as the primary heat transfer surface. Engineering analysis is being performed to down selecting the most promising configurations. A model of the structure of carbon foam has been formulated in order to calculate physical characteristics of importance to thermal modeling. Comparisons with ORNL measurements are being done to validate the model. The design of experiments to assess the interstitial flow under the porous surface has been completed and the test apparatus is under construction.

Technical Progress

A computational model has been developed both for the pressure drop and heat transfer rate in porous carbon foam because, in part, high heat transfer with minimal pressure drop are the motivations in heat exchanger design. The pressure-drop component of the model was formulated based on the Darcy-Forchheimer equation because of its validity in low to intermediate Reynolds number flows, specifically those in the aforementioned applications. A constant Nusselt number correlation was derived for the prediction of heat transfer coefficients based on slug flow in a channel with one wall at constant temperature and the others adiabatic. The computational modeling approximations required validation and this was done with data taken from experiments performed at Oak Ridge National Laboratory in which a heater was attached to the top of a block of carbon foam that was mounted in a channel in such a way that the fluid passing through the channel was forced convection cooling the foam. Calculations were compared to measured bulk outlet temperatures and pressure drop in the ranges of flow rates from 25

to 45 USgpm and heater power from 300 to 600 W. For test conditions of 25 USgpm and 300 W, the calculated pressure drop was 6.700 kPa and compared a measured value of 6.895 kPa; the measured outlet bulk temperature was about 3% more than predicted, and the calculated and measured temperature distributions across the outlet agreed within 0.8%. For flow rates of 45 USgpm and heater power in the range 300 to 600 W, agreement between measured and calculated pressure drop and outlet bulk temperature were within 12% and 0.5%, with the latter being within experimental uncertainty and perhaps somewhat fortuitous. Although the computational model was developed with simple geometries, it could be applied to complex geometries for design purposes.

Status of Milestones

The next milestones are the validation of the computational model, selection of the most promising heat exchanger concepts made from carbon foam, and the set up of the windtunnel for experiments to quantify heat transfer from the surface of carbon foam.

Industry Interactions

Unifin continues to support Western efforts to obtain better understanding of heat-exchanger performance and selection issues for microturbine applications. Ford Motor Company has interacted with students, of course, while under the supervision of Professor Albert Shih at the University of Michigan.

Problems Encountered

Professor Thompson will relocate to become the Dean of Engineering at the University of Ottawa on July 1st.

Publications/Presentations

Thompson, B.E. and Yu, Q.: Development of an ultra-efficient air to water heat exchanger using carbon foam. DOE/CETC Conference on Microturbine Applications, Los Angeles, CA, January 20-23, 2004.

Hemrick, J. G., Lara-Curzio, E., Zaltash, A., Gallego, N. C., Walls, C. A., Thompson, B. E.: Evaluation and Application of High Thermal Conductivity Materials for Microturbine Heat transfer Systems. DOE/CETC Conference on Microturbine Applications, Los Angeles, CA, January 20-23, 2004.

Yu, Q. and Thompson, B. E: Thermal engineering model of a heat exchanger with finned tubes made from porous carbon foam. CSME Forum 2004, June 1-4, 2004. University of Western Ontario, London, Canada.

MATERIALS FOR ADVANCED RECIPROCATING ENGINES

Spark Plug Erosion and Failure

H. T. Lin and M. P. Brady
Oak Ridge National Laboratory
Oak Ridge, TN 37831-6068
Phone: (865) 576-8857, E-mail: linh@ornl.gov

Objective

This subtask focuses on two parallel efforts. The first task will characterize the electrode near-surface region microstructure in spark plugs before and after engine testing to understand corrosion/erosion mechanisms as a function of engine condition (environment) and time in determining the lifetime limiting processes. The information gained from the first task will feed into an exploratory alloy development effort for electrode materials with improved corrosion/erosion resistance to extend the long-term durability and lifetime performance of spark plugs for advanced reciprocating engines.

Highlights

Setup of a bench type electrode material screening test rig has been completed during this reporting period (Fig. 1). The test rig will provide a cost-effect approach to screening the oxidation/erosion resistance of developmental of alloys. Also, results would provide guidelines for alloy design to improve the oxidation/erosion resistance. The Pt alloy would be used as a reference for comparison.

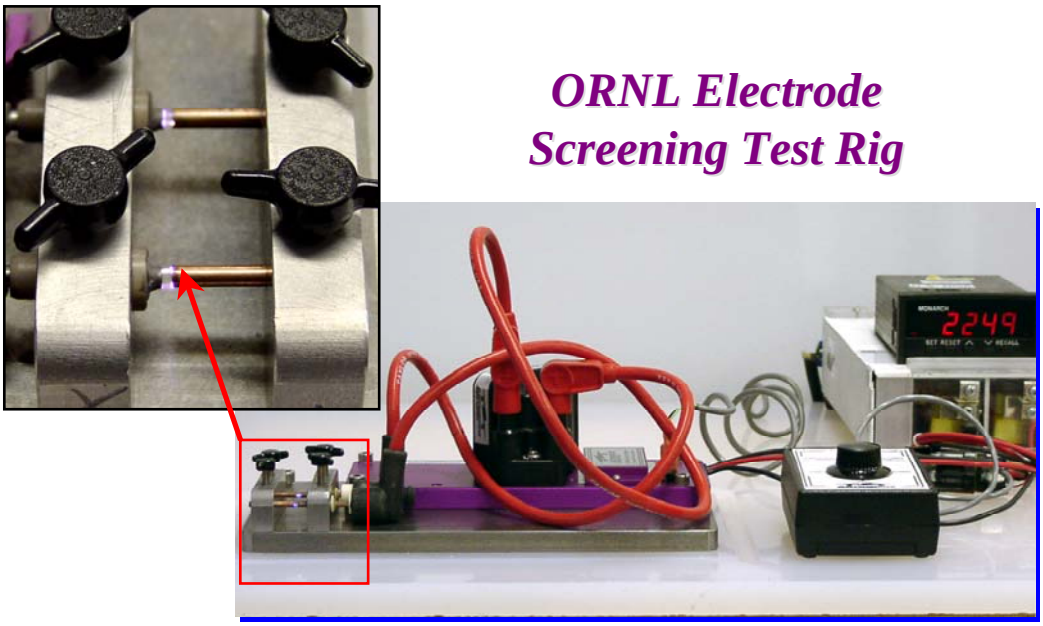

Figure 1. Photo shows the bench type electrode material screening test rig.

Technical Progress

Quantitative compositional analysis was performed on the polished cross-sections of as-received and field-tested spark plugs by electron probe microanalysis (EPMA) using pure element standards. These as-received and field-tested spark plugs with operating times of 4,386h, manufactured by Champion, Federal Mogul Corp., were acquired from Caterpillar Inc. The purpose of these quantitative analyses was to confirm and characterize the size of interdiffusion zone between Ni-base alloy electrode and Pt-W alloy and Ir tip insert if they existed after the joining process. Results of EPMA showed that there existed a significant interdiffusion zone of Pt-W tip insert with the Ni-base electrode (Fig. 2). The size of interdiffusion zone ranged from 250 to 300 µm. On the other hand, no apparent interdiffusion zone was observed between Ni-base electrode and Ir tip insert, as shown in Fig. 3. Note that similar compositional profiles were also obtained for tested plugs. The formation of this interdiffusion zone between Ni-base alloy electrode and Pt-W alloy insert occurred during joining process. The Ni-Pt solid solution zone, which exhibits a high oxidation susceptibility, would readily oxidize at temperatures of 800-1000°C and form Ni-Pt-O compounds. The dominant crack could readily initiate at the interface corner of oxidized interdiffusion zone (Ni-Pt-O), which is brittle in nature, when subjected to thermomechanical stress during operation. Note that an oxidized interdiffusion zone with an extensive crack generation along the interface between Ni alloy electrode and Pt-W tip insert was consistently observed for all tested plugs (Fig. 4). When the crack reached a critical size and completely separated the Pt-W insert from the Ni-base ground electrode, it could have a significant impact on the long-term durability and lifetime of spark plugs.

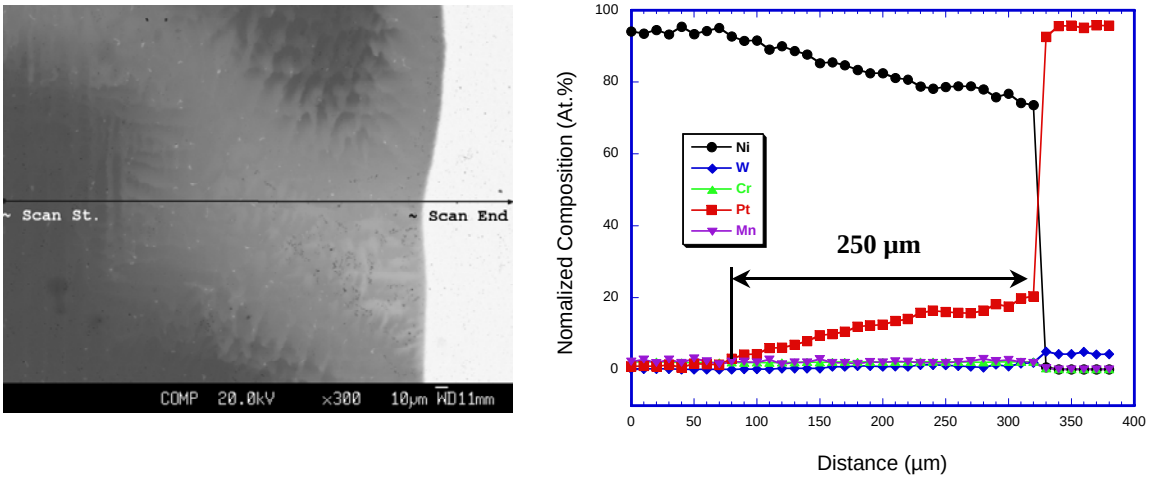

Figure 2. Quantitative compositional profile across the Ni-base electrode and Pt-W alloy tip insert interface.

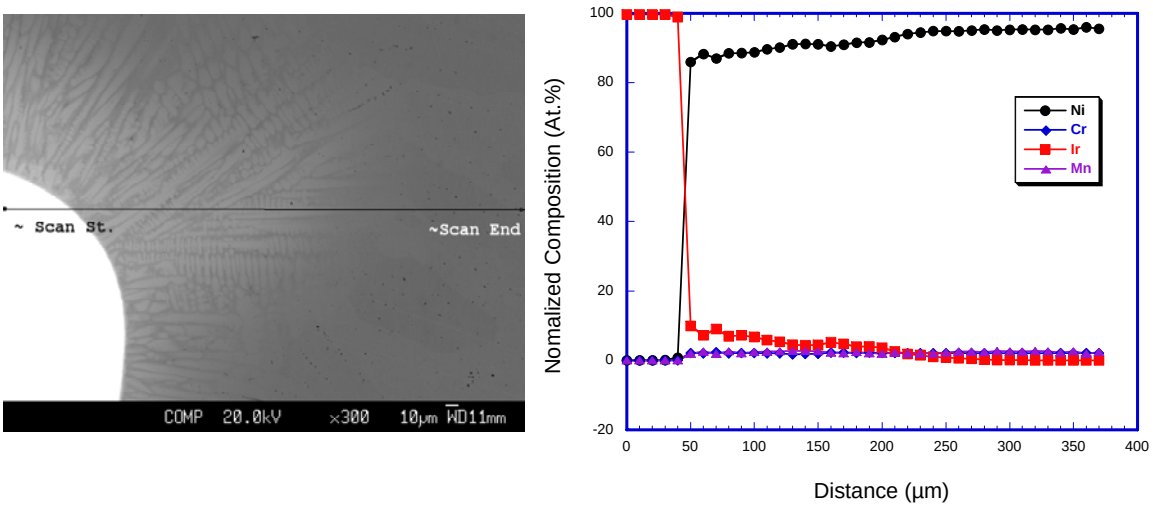

Figure 3. Quantitative compositional profile across the Ni-base electrode and Ir tip insert interface.

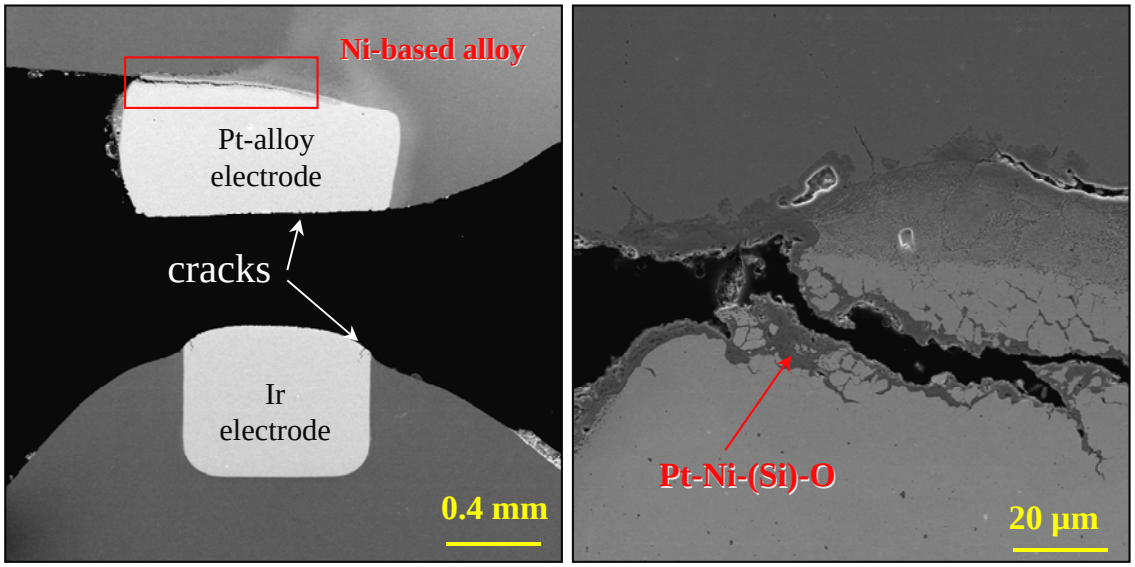

Figure 4. SEM micrographs show an extensive crack generation along the Ni-base alloy electrode and Pt-W ally tip insert after field service.

Based on initial observations of cracking and corrosion issues in the Pt and Ir electrode insert tips from worn natural gas engine spark plugs, two developmental Cr-base alloys were designed and manufactured for testing. These two Cr-base alloys were designed with melting points in excess of 1800°C and oxide additions to improve ductility. The high levels of Cr are expected to impart excellent corrosion resistance, and resist the cracking phenomena observed. The alloys were hot-pressed for consolidation, and then EDM machined to make 1/8" diameter rods for initial evaluation for sparking resistance. This testing will be initiated in the next quarter.

Status of Milestones

Establish test protocol for rapidly screening developmental alloys for resistance to spark erosion and complete initial assessment of 1 material class/protection phenomenon for improved erosion resistance. September 2004. On schedule.

Industry Interactions

Drs. Rangarajan and Derra from Waukesha Engine visited ORNL and NTRC on March 30th to discuss the spark plug and ignition system issues and potential collaborative research area.

Drs. Benson and Tozzi from Woodward visited ORNL and NTRC on March 30th to discuss the ignition system and spark plug issues and potential collaborative research area.

Communication with Caterpillar on the microstructure characterization results for spark plugs after 4,386h field service.

Problems Encountered

None

Publications/Presentations

R. K. Richards, H. T. Lin, and M. P. Brady, "Characterization of Erosion Mechanisms of Natural Gas Engine Spark Plugs" has been submitted for presentation and publication at ASME International Combustion Engine Division, 2004 Fall Technical Conference, Long Beach, CA, October 24-27, 2004.

Advanced Materials for Exhaust Components of Reciprocating Engines

P. J. Maziasz, N. D. Evans, J. J. Truhan, and K. L. More
Metals and Ceramics Division
Oak Ridge National Laboratory
P.O. Box 2008, Oak Ridge, TN 37831-6115
Phone: (865) 574-5082, E-mail: maziaszpj@ornl.gov

Objective

This program is expanding to consider limitations of various critical in-cylinder and exhaust system components due to performance, temperature capability, and tribology for advanced natural gas reciprocating engine systems (ARES). While initial efforts focused on exhaust valves, recent input from engine manufactures has expanded the scope to include intake and exhaust valves and seats, as well as other exhaust components. The program is engaged in active dialog to define the long-term needs and priorities of engine makers.

Highlights

ORNL microcharacterization of a Ni-based superalloy exhaust valve (Pyromet 31V) after moderate engine service was completed last quarter. Engine service produces additional precipitates within grains and along grain boundaries, in addition to coarsening the γ' that hardens the matrix. Fatigue resistance is summarized for a new CF8C-Plus cast austenitic stainless steel, developed for exhaust component applications, that is now being commercialized. New discussions of materials R&D needs began with Waukesha Engine Division, Dresser Industries this quarter, and they visited ORNL at the end of the quarter.

Technical Progress

Microcharacterization of exhaust valves of Pyromet 31V (Ni-22Cr-15Fe alloy with Ti and Al for γ' precipitation hardening), provided by Waukesha Engine Division, Dresser Industries, Inc. was completed last quarter. Microcharacterization of the valves in the middle of the combustion face, comparing fresh and engine tested valves, showed that aging during engine service produced significant changes in microstructure, causing additional precipitation in the matrix and along grain boundaries. The γ ' phase particles that harden the matrix after the initial heat-treatment, coarsen after moderate service at less than 700^{o}C.

Last year, ORNL and Caterpillar developed a new cast austenitic stainless steel, CF8C-Plus, that has the potential for use as exhaust component applications in advanced diesel engines. Typical exhaust manifolds and turbocharger housings are made from SiMo cast iron, which has poor strength above 550-600^{o}C, and can be susceptible to thermal fatigue cracking during severe cycling after prolonged use. Standard CF8C steel (Fe-19Cr-9Ni-

0.7Nb-0.07C), has good castability and sufficient strength up to about 600-625^{o}C, but is not strong enough at higher temperatures. CF8C steel contains a large amount (20-25 vol.%) of δ-ferrite, which then transforms into σ-phase during aging at 600^{o}C and above, and severely reduces ductility. CF8C-Plus steel was developed to be stronger and much more fatigue and thermal fatigue resistant for use in severe thermal cycling conditions. CF8C-Plus has an "engineered microstructure" that contains no δ-ferrite in the as-cast microstructure, and hence no σ-phase forms during aging.

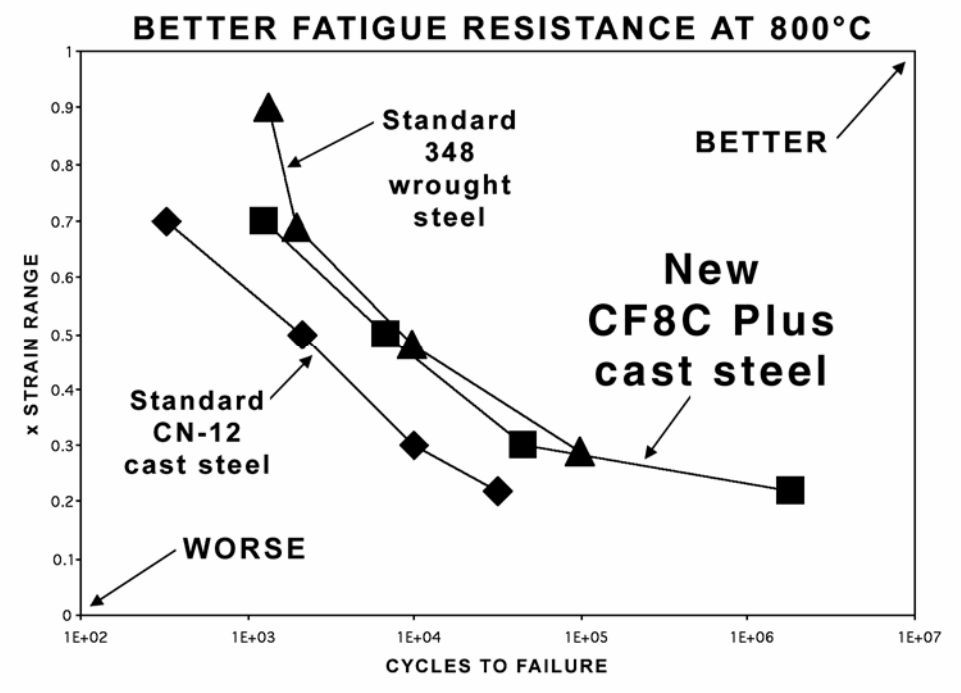

Figure 1. Isothermal fatigue testing of commercial standard CN12 and new CF8C-Plus stainless steels at 800^{o}C. The CF8C-Plus has significantly better fatigue cracking resistance than standard CN12 steel, and both are much better than SiMo cast iron at these conditions.

The isothermal fatigue resistance of a new commercial heat of the CF8C-Plus steel at 800^{o}C is much better than standard, commercial CN-12 steel (Fig. 1). Both stainless steels are much better than SiMo cast iron at these conditions. The new CF8C-Plus steel is currently being commercialized, and may be applicable for exhaust components of advanced ARES engines.

This quarter discussions began with Waukesha Engine Division to expand the materials needs for in-cylinder and exhaust component applications. Discussions included valve seats and guides as well as valves for both intake and exhaust valves, and included bulk metallurgical properties as well as surface behavior (corrosion, tribology). The discussions led to a visit by Waukesha managers to ORNL at the end of the quarter (March 30, 2004).

Status of Milestones

FY 2004 – Complete characterization Ni-based superalloy (Pyromet 31V) valves to define aging effect during engine service. Define aging effects at weld overlay and coating bond regions (December 2003) – completed.

Industry Interactions

New discussions with Waukesha Engine Dresser, Inc. (Jim Drees, Joe Derra, Roger Rangarajan, and others) about materials needs and interests for advanced ARES engines with ORNL (Tom King, Tim Theiss, Phil Maziasz and John Truhan) began this quarter, and will continue next quarter.

Problems Encountered

None

Publications/Presentations

None

Development of Catalytically Selective Electrodes for NOx and Ammonia Sensors

T. Armstrong, F. Montgomery, and D. West
Oak Ridge National Laboratory
P.O. Box 2008, Oak Ridge, TN 37831-6084
Phone: (865) 574-7996, E-mail: armstrongt@ornl.gov

Objective

To develop non-catalytic and catalytically selective electrodes for use in NOx and ammonia sensors and to build and test sensors using the materials and technology developed

Technical Highlights (NO Selective Sensor Development)

1. New electrode geometries investigated this quarter (use two materials, same number as "original" design).
2. NO response (w/o bias) tends to be stronger than "original design", although still much less than NO_2 response.
3. Semicircular and interdigitated geometries appear to offer enhanced recovery time (in mixed-potential mode) when compared to original design (operating without bias).
4. Response/recovery time not a strong function of geometry for semicircular and interdigitated geometries.
5. New element geometries (semicircular and interdigitated) exhibited "NO-selective" behavior when current biased.

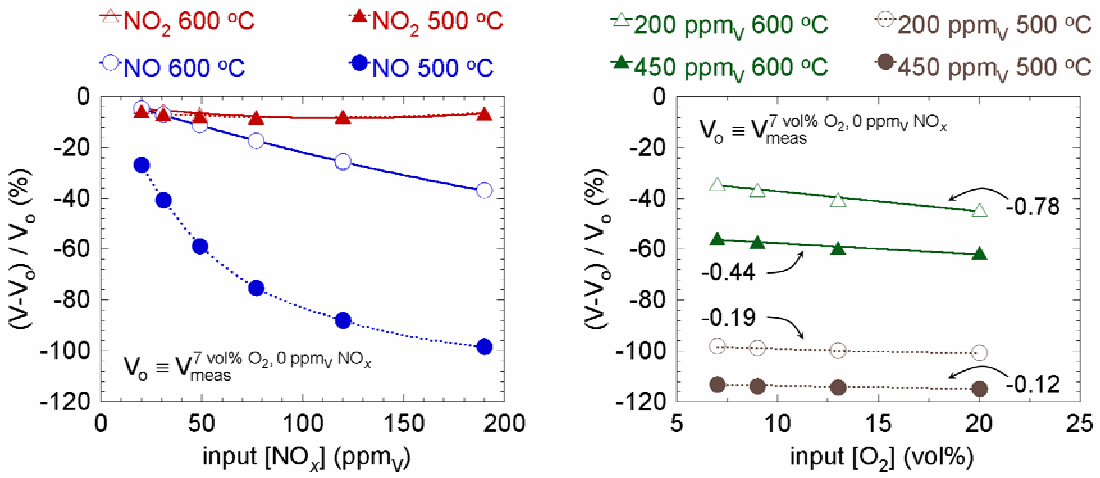

Figure 1. NO_x sensing performance of the semicircular element with current bias. For the graph on the right, the input NO_x was NO and the numbers are the slope of a linear fit to $(V-V_o) / V_o$ vs. $[O_2]$.

Status of Milestones

1. Determine kinetics of NO reaction on electrode as a function of temperature and environment.
   This is ongoing and will continue as new electrode materials are developed and tested as well as new sensor designs.

2. Fabricate and test a prototype NOx sensor (09/03)
   We are focusing on refining the NO and total NOx sensors. Testing of these sensors is ongoing.

Communications/Visits/Travel

Cummings has expressed interest in our program and discussions are being initiated to brief them on our progress.

Problems Encountered

None

Publications

Electrically Biased NO_x Sensing Elements with Co-Planar,Multi-Layered Electrodes submitted to Journal of the Electrochemical Society.

Presentations

Electrically Biased NO_x Sensing Elements with Co-Planar, Multi-Layered Electrodes presented at the Electrochemical Society Meeting, San Antonio, TX May 2004.

Internal Distribution

B. L. Armstrong, 4515, MS-6063, armstrongbl@ornl.gov
T. R. Armstrong, 4508, MS-6084, armstrongt@ornl.gov
P. F. Becher, 4515, MS-6068, becherpf@ornl.gov
T. M. Besmann, 4515, MS-6063, besmanntm@ornl.gov
C. A. Blue, 4508, MS-6083, blueca@ornl.gov
M. P. Brady, 4500S, MS-6115, bradymp@ornl.gov
M. A. Brown, 4500N, MS-6186, brownma@ornl.gov
M. K. Ferber, 4515, MS-6069, ferbermk@ornl.gov
J. A. Haynes, 4515, MS-6063, haynesa@ornl.gov
D. R. Johnson, 4515, MS-6066, johnsondr@ornl.gov
M. A. Karnitz, 4500N, MS-6186, karnitzma@ornl.gov
J. O. Kiggans, 4508, MS-6087, kiggansjojr@ornl.gov
T. J. King, 4515, MS-6065, kingtjjr@ornl.gov
J. W. Klett, 4508, MS-6087, klettjw@ornl.gov
E. Lara-Curzio, 4515, MS-6069, laracurzioe@ornl.gov
H. T. Lin, 4515, MS-6068, linh@ornl.gov
R. A. Lowden, 4515, MS-6063, lowdenra@ornl.gov
P. J. Maziasz, 4500S, MS-6115, maziaszpj@ornl.gov
K. L. More, 4515, MS-6064, morekl1@ornl.gov
R. D. Ott, 4515, MS-6083, ottr@ornl.gov
S. D. Nunn, 4508, MS-6087, nunnsd@ornl.gov
B. A. Pint, 4500S, MS-6156, pintba@ornl.gov
D. T. Rizy, 3147, MS-6070, rizydt@ornl.gov
D. P. Stinton, 4515, MS-6063, stintondp@ornl.gov
R. W. Swindeman, 4500S, MS-6155, swindemanrw@ornl.gov
T. N. Tiegs, 4508, MS-6087, tiegstn@ornl.gov
P. F. Tortorelli, 4500S, MS-6156, tortorellipf@ornl.gov
I. G. Wright, 4500S, MS-6157, wrightig@ornl.gov
A. Zaltash, 3147, MS-6070, zaltasha@ornl.gov

External Distribution

ALLISON ADVANCED DEVELOPMENT CO., 1100 Wilson Blvd., Suite 1450, Arlington, VA 22209
J. Miles, r.jeffrey.miles@allison.com

ALM SYSTEMS, INC, 1920 N Street, NW, Suite 750, Washington, DC 20036
M. Kalin, mkalin@ibek.com

ARGONNE NATIONAL LABORATORY, 9700 S. Cass Ave., Argonne, IL 60439-4838
W. Ellingson, ellingson@anl.gov
J. P. Singh, jpsingh@anl.gov

BATTELLE MEMORIAL INSTITUTE, 505 King Avenue, Columbus, OH 43201
D. Anson, ansond@battelle.org

BAYSIDE MATERIALS TECHNOLOGY, 21150 New Hampshire Ave., Brookville, MD 20833
D. Freitag, dfreitag@ix.netcom.com

BCS, INC., 5550 Sterrett Place, Suite 216, Columbia, MD 21044
D. Bartley, dbartley@bcs-hq.com

BOWMAN POWER, 20501 Ventura Boulevard #285, Woodland Hills, CA 91364
T. Davies, tdavies@bowmanpower.co.uk
T. Hynes, ahynes.bowmanpower@att.net
D. Flaxington, dflaxington@bowmanpower.co.uk

CALIFORNIA ENERGY COMMISSION
A. Soinski, asoinski@energy.state.ca.us

CANNON-MUSKEGON CORP., Box 506, Muskegon, MI 49443-0506
J. Wahl, jwahl@canmkg.com

CAPSTONE TURBINE CORP., 6430 Independence Ave., Woodland Hills, CA 91367
P. Chancellor, pchancellor@capstoneturbine.com
K. Duggan, kduggan@capstoneturbine.com
M. Stewart, mstewart@capstoneturbine.com
J. Willis, jwillis@capstoneturbine.com
M. Rodrigues, mrodrigues@capstoneturbine.com
B. Treece, btreece@capstoneturbine.com

CERAMATEC INC., 2425 South 900 West, Salt Lake City, UT 84119
C. Lewinsohn, clewinsohn@ceramatec.com
B. Nair, bnair@ceramatec.com

CLEMSON UNIVERSITY, South Carolina Institute for Energy Studies, 386-2, Clemson, SC 29634-5180
L. Golan, glawren@clemson.edu
R. Wenglarz, rwnglrz@clemson.edu
J. Hinson, jhinson@clemson.edu

CONNECTICUT RESERVE TECHNOLOGIES, 2997 Sussex Ct., Stow, OH 44224
E. Baker, baker@crtechnologies.com
S. Duffy, sduffy@crtechnologies.com
J. Palko, jpalko@crtechnologies.com

DTE ENERGY, 37849 Interchange Dr., Suite 100, Farmington Hills, MI 48335
M. Davis, davism@dteenergy.com

ELECTRIC POWER RESEARCH INSTITUTE, 3412 Hillview Ave., Palo Alto, CA 94303
J. Stringer, jstringe@epri.com

ELGILOY SPECIALTY METALS, 1565 Fleetwood Drive, Elgin, IL 60123

T. Bartel, terryb@elgiloy.com

ELLIOTT ENERGY SYSTEMS, 2901 S.E. Monroe Street, Stuart, FL 34997
D. Burnham, dburnham@elliott-turbo.com
D. Dewis, ddewis@elliott-turbo.com

ENERGETICS, INC., 501 School St., SW, Suite 500, Washington, DC 20024
R. Scheer, rscheer@energeticsinc.com

ENERGY TECHNOLOGIES APPLICATIONS, 5064 Camino Vista Lujo, San Diego, CA 92130-2849
T. Bornemisza, borneger@ix.netcom.com

GAS TURBINE ASSOCIATION, 1050 Thomas Jefferson St., NW, 5th Fl, Washington, DC 20007
J. Abboud, abboud@advocatesinc.com

GENERAL ELECTRIC (GE) CR&D, 1 Research Circle, Building K1-RM 3B4, Niskayuna, NY 12309
S. Correa, correa@crd.ge.com
K. Luthra, luthra@crd.ge.com
M. VanDerwerken, vanderwerken@crd.ge.com
C. Johnson, johnsonca@crd.ge.com

GENERAL ELECTRIC AIRCRAFT ENGINES, One Neumann Way, Mail Drop M89, Cincinnati, OH 45215-1988
R. Darolia, ram.darolia@ae.ge.com

GENERAL ELECTRIC POWER SYSTEMS, One River Rd., 55-127, Schenectady, NY 12345
R. Orenstein, robert.orenstein@ps.ge.com

GENERAL ELECTRIC POWER SYSTEMS, Gas Technology Center, 300 Garlington Road, Greenville, SC 29615
P. Monaghan, philip.monagham@ps.ge.com

HAYNES INTERNATIONAL, INC., 1020 W. Park Avenue, P.O. Box 9013, Kokomo, IN 46904-9013
V. Ishwar, vishwar@haynesintl.com
D. Klarstrom, dklarstrom@haynesintl.com

HONEYWELL CERAMIC COMPONENTS, 2525 W. 190th St., Torrance, CA 90504
D. Foley, dan.foley@honeywell.com
C. Li, chien-wei.li@honeywell.com
D. Newson, danielle.newson@honeywell.com
M. Savitz, MaxineSavitz@aol.com
J. Wimmer, jim.wimmer@honeywell.com
M. Mitchell, michele.mitchell@honeywell.com

HONEYWELL COMPOSITES, 1300 Marrows Rd., PO Box 9559, Newark, DE 19714-9559
L. Connelly, liz.connolly@ps.ge.com
P. Gray, paul1.gray@ps.ge.com
D. Landini, dennis.landini@ps.ge.com

HONEYWELL ENGINES, SYSTEMS, & SERVICES 2739 E. Washington St., PO Box 5227, Phoenix, AZ 85010
B. Schenk, bjoern.schenk@honeywell.com
HONEYWELL POWER SYSTEMS, 8725 Pan American Freeway NE, Albuquerque, NM 87113
S. Wright, e.scott.wright@honeywell.com

HOWMET RESEARCH CORP., 1500 South Warner St., Operhall Research Center, Whitehall, MI 49461-1895
B. Mueller, bmueller@howmet.com
R. Thompson, rthompson@howmet.com

INGERSOLL-RAND ENERGY SYSTEMS, 32 Exeter St., Portsmouth, NH 03801
A. Kaplau-Colan, alex_haplau-colan@ingersoll-rand.com
M. Krieger, michael_krieger@irco.com
J. Johnson, jay_johnson@ingersoll-rand.com
J. Kesseli, jim_kesseli@ingersoll-rand.com
J. Nash, jim_nash@ingersoll-rand.com

KENNAMETAL INC. 1600 Technology Way, P.O. Box 231, Latrobe, PA 15650-0231
R. Yeckley, Russ.yeckley@kennametal.com

KINECTRICS NORTH AMERICA, 124 Balch Springs Circle, SW, Leesburg, VA 20175
B. Morrison, blake.Morrison@kinectrics.com

KRUPP VDM TECHNOLOGIES CORP., 11210 Steeplecrest, Suite #120, Houston, TX 77065-4939
D. Agarwal, dcagarwal@pdq.net

NASA GLENN RESEARCH CENTER, 21000 Brookpark Rd., MS 49-7, Cleveland, OH 44135
D. Brewer, david.n.brewer@grc.nasa.gov
J. Gykenyesi, john.p.gyekenyesi@lerc.nasa.gov
S. Levine, stanley.r.levine@lerc.nasa.gov
N. Nemeth, noel.n.nemeth@grc.nasa.gov
B. Opila, opila@grc.nasa.gov

NATIONAL RURAL ELECTRIC COOPERATIVE ASSOC., 4301 Wilson Blvd., SS9-204, Arlington, VA 22203-1860
E. Torrero, ed.torrero@nreca.org

NATURAL RESOURCES CANADA, 1 Haanel Drive, Nepean, Ontario, Canada K1A 1M1
R. Brandon, rbrandon@nrcan.gc.ca

PCC AIRFOILS, INC., 25201 Chagrin Blvd., Suite 290, Beachwood, OH 44122
C. Kortovich, ckortovich@pccairfoils.com

PENN STATE UNIVERSITY, Applied Research Laboratory, PO Box 30, State College, PA 16823
J. Singh, jxs46@psu.edu

RICHERSON AND ASSOC., 2093 E. Delmont Dr., Salt Lake City, UT 84117
D. Richerson, richersond@aol.com

ROLLS-ROYCE ALLISON, 2925 W. Minnesota St., PO Box 420, Indianapolis, IN 46241
S. Berenyi, steve.g.berenyi@allison.com
P. Heitman, peter.w.heitman@allison.com
F. Macri, francis.g.macri@allison.com
J. Oswald, jim.oswald@rolls-royce.com

SAINT-GOBAIN CERAMICS & PLASTICS, INC., Goddard Road, Northboro, MA 01532
B. LaCourse, Brian.C.LaCourse@saint-gobain.com
R. Licht, robert.h.licht@saint-gobain.com
M. Abouaf, Marc.Abouaf@saint-gobain.com
V. Pujari, Vimal.K.Pujari@saint-gobain.com
A. Vartabedian, Ara.M.Vartabedian@saint-gobain.com

SEBESTYEN, T., Consultant, 6550 Mission Ridge, Traverse City, MI 49686-6123
T. Sebestyen, sebestyen@chartermi.net

SIEMENS WESTINGHOUSE POWER CORP., 1310 Beulah Rd., Pittsburgh, PA 15235-5098
M. Burke, michael.burke@swpc.siemens.com
C. Forbes, christian.forbes@swpc.siemens.com

SOLAR TURBINES, INC., TurboFab Facility, 16504 DeZavala Rd., Channelview, TX 77530
B. Harkins, harkins_bruce_d@solarturbines.com

SOLAR TURBINES INC., 818 Connecticut Ave., NW, Suite 600, Washington, DC 20006-2702
R. Brent, solardc@bellatlantic.net

SOLAR TURBINES, INC., 2200 Pacific Highway, PO Box 85376, MZ R, San Diego, CA 92186-5376
P. Browning, browning_paul_f@solarturbines.com
M. Fitzpatrick, fitzpatrick_mike_d@solarturbines.com
P. Montague, montague_preston_j@solarturbines.com
M Van Roode, van_roode_mark_x@solarturbines.com
M. Ward, ward_mike_e@solarturbines.com
J. Price, jeffprice@solarturbines.com

SOUTHERN CALIFORNIA EDISON COMPANY, 2244 Walnut Grove Avenue, Rosemead, CA 91770

S. Hamilton, hamiltsl@sce.com

SOUTHERN COMPANY, 600 N. 18th Street, 14N-8195, P.O. Box 2641, Birmingham, AL 35291

S. Wilson

STEVEN I. FREEDMAN, Engineering Consultant, 410 Carlisle Ave., Deerfield, IL 60015

S. Freedman, sifreedman@aol.com

STAMBLER ASSOCIATES, 205 South Beverly Drive, Suite 208, Beverly Hills, California 90212

I. Stambler

THE BOEING COMPANY, Rocketdyne Propulsion & Power, 6633 Canoga Avenue
MC: GB-19, P.O. Box 7922, Canoga Park, CA 91309-7922

G. Pelletier, gerard.pelletier@west.boeing.com

TELEDYNE CONTINENTAL MOTORS, 1330 W. Laskey Rd., PO Box 6971, Toledo, OH 43612-0971

J. T. Exley, texley@teledyne.com

TURBEC

L. Malmrup, lars.malmrup@turbec.com

UCI COMBUSTION LABORATORY, U. of CA, Irvine, Irvine, CA 92697-3550

V. McDonell, mcdonell@ucic1.uci.edu

UDRI, Ceramic & Glass Laboratories, 300 College Park Ave., Dayton, OH 45469-0172

A. Crasto, allan.crasto@udri.udayton.edu
G. Graves, gravesga@udri.udayton.edu
N. Osborne, osborne@udri.udayton.edu
R. Wills, roger.wills@udri.udayton.edu

UNITED TECHNOLOGIES RESEARCH CENTER, 411 Silver Lane MS 129-24, East Hartford, CT 06108

H. Eaton, eatonhe@utrc.utc.com
J. Holowczak, holowcje@utrc.utc.com
T. Rosfjord, rosfjotj@utrc.utc.com
J. Smeggil, smeggijg@utrc.utc.com
G. Linsey, linseygd@utrc.utc.com
J. Shi, shij@utrc.utc.com
E. Sun, suney@utrc.utc.com
D. Mosher, mosherda@utrc.utc.com

UNIVERSITY OF CALIFORNIA, Department of Mechanical Engineering, Berkeley, CA 94720
R. Dibble, rdibble@newton.berkeley.edu

UNIVERSITY OF COLORADO, Department of Mechanical Engineering, Boulder, CO 80309-0427
R. Raj, rishi.raj@Colorado.edu

UNIVERSITY OF MARYLAND, Department of Mechanical Engineering, College Park, MD 20742-3035
R. Radermacher, rader@eng.umd.edu

UNIVERSITY OF WESTERN ONTARIO, Faculty of Engineering, London, Ontario, Canada N6G 4K1
B. E. Thompson, Thompson@eng.uwo.ca
A. G. Straatman, astraat@engga.uwo.ca

US DOE-NETL, P. O. Box 880, MSO-D01, 3610 Collins Ferry Rd., Morgantown, WV 26507-0880
C. Alsup, Jr., charles.alsup@netl.doe.gov
A. Layne, abbie.layne@netl.doe.gov
L. Wilson, lane.wilson@netl.doe.gov

US DOE-NETL, PO Box 10940, Pittsburgh, PA 15236
N. Holcombe, norman.holcombe@netl.doe.gov
U. Rao, rao@netl.doe.gov

US DOE CHICAGO OPERATIONS OFFICE, 9800 S. Cass Ave., Argonne, IL 60439
J. Jonkouski, jill.jonkouski@ch.doe.gov
J. Mavec, joseph.mavec@ch.doe.gov
J. Livengood, joanna.livengood@ch.doe.gov
S. Waslo, stephen.waslo@ch.doe.gov

US DOE-HQ, 1000 Independence Ave., S.W., Washington DC 20585
R. Fiskum, ronald.fiskum@ee.doe.gov
D. Haught, debbie.haught@ee.doe.gov
P. Hoffman, patricia.hoffman@ee.doe.gov
W. Parks, william.parks@ee.doe.gov
M. Smith, merrill.smith@ee.doe.gov
C. Sorrell, charles.sorrell@ee.doe.gov

WILLIAMS INTERNATIONAL, 2280 West Maple Rd., PO Box 200, Walled Lake, MI 48390-0200
G. Cruzen, g.cruzen@williams-int.com
W. Fohey, w.fohey@williams-int.com
C. Schiller, cschiller@williams-int.com

WRIGHT PATTERSON AIRFORCE BASE,

R. Sikorski, ruth.sikorski@wpafb.af.mil